Institutt for den faste jords fysikk
Institute of Solid Earth Physics

Crustal structure and seismicity of Cuba and Web-based applications for earthquake analysis

by

Bladimir Moreno Toirán

Submitted as a Dr. Scient Thesis

Institute of Solid Earth Physics
University of Bergen

September 2002

Abstract

This thesis comprises six papers divided into two parts. Part I consist of four papers in which a study of the crust and seismicity of Cuba is presented. The main achievements in this part are: (1) A new P-wave velocity model for earthquake location using travel time inversion; (2) Crustal structure at seismic stations using Receiver Function Method; (3) A new attenuation relation for the frequency-dependent quality factor Q using Coda-Q and spectral ratio method; (4) Estimation of the near-surface attenuation factor kappa; (5) A new local and coda magnitude scales; (6) Characterization of the seismicity and kinematics; and (7) Orientation of the principal stress axes using stress-inversion from earthquake focal-mechanisms. Most of these results are new for the region and offer a unique opportunity to develop new insight into the tectonic and kinematic regime along the southern Cuban margin. Part II includes two papers dealing with the design and implementation of Web-based applications in seismology. The first paper (Paper 5) proposes a Graphical User Interface (GUI) for retrieving and processing parametric and waveforms earthquake data through Internet. Here some aspects of the design are discussed like server-side and client-side processing, GUI and data-transfer speed. The second paper (Paper 6) proposes a relational Java database and a GUI for diagnosing active faults also through Internet. The system is based on distributed database technology, which means that the database can be distributed in several Internet-servers.

Preface

I would like to use this preface to mention the circumstance under which I got the opportunity to study seismology in Norway and also state chronically the main events that took place during the development of my thesis.

I became familiar with earthquake seismology in 1992, when I started working at the National Centre of Seismological Researches (CENAIS) in Santiago de Cuba. Since my first degree is Computer Sciences, I was mainly involved in the development of software for earthquake analysis. The need for good understanding of the problem increased my interest in seismology day after day. I was really fascinated with the subject, so I started to follow several seismological courses. It was then when I met my supervisor Jens Havskov during the GFZ / UNESCO Training Course on "Seismology, Seismic Hazard Assessment and Risk Mitigation" held in Nicaragua in 1995.

During a short visit of Jens Havskov to Cuba, we agreed to collaborate in the portability of the SEISAN software to other operating system like LINUX and Windows and also the possibility to be enrolled for a Master degree in Seismology at Bergen. In January 1998 I was accepted in the Master of Philosophy program at the Institute of Solid Earth Physic, University of Bergen. After one year of studies I got my Master degree, then I was encouraged to continue as a doctor grad student for three more years. The proposal of my thesis consisted mainly of Web-based applications for earthquake analysis. In addition, taking into account the recent change of the old visual recordings for digital recordings in the Cuban seismograph network, basic seismological research was also proposed.

The first paper "SEISWEB", which is presented as number 5 in my thesis, took me more time that it was planned. It was a joint effort of several people who spent months of programming and technicalities that cannot be reflected in an academic paper. This paper was the subject of my oral presentation during the first IAGA-IASPEI joint scientific assembly 2001, held in Hanoi, Vietnam. During my second year of study I travelled for one month to The University of West Indies, Jamaica. At that time I was spending one semester in Cuba collecting and converting the Cuban earthquake data into SEISAN format. With the collaboration of Margaret Grandison at the Earthquake Unit of Jamaica, the Cuban and Jamaican earthquake catalogues were merged. The new data was used to obtain a one-dimensional P-wave velocity model along the southern Cuban margin. This result is presented in the first paper of my thesis.

The installation of broadband seismic stations in Cuba in 1998 gave me the opportunity to use teleseismic recordings for estimating the structure of the crust beneath the stations with the Receiver function method. Afterward, I developed a new coda and local magnitude scales for eastern Cuba as well a new attenuation relation for Q. Making use of the result obtained in previous works I wrote an article about the new Cuban Seismograph network. My last paper fall within the same topic that the first one. It is a multidisciplinary effort in which a Web-based tool for diagnosing active faults is being

created. The system is being developed within the framework of the European project SAFE (Slow Active Faults in Europe) under the supervision of Kuvvet Atakan. The need for gathering and parameterize the data gave me the opportunity to get in contact with several people at different institution in Europe. I spent several days at the Institut de Physique du Globe, Strasbourg and the Royal Observatory of Belgium. The project has one more year of duration until December 2003; therefore the final version of the software is not finish yet. What we described in the paper is the database design and the graphical user interface.

Acknowledgements

Contents

Part I: Crustal structure and seismicity of Cuba

Paper 1: Crustal velocity model along the southern Cuban margin: Implications for the tectonic regime at an active plate boundary.

Paper 2: The crustal structure of Cuba derived from Receiver Function Analysis.

Paper 3: New magnitude scales and attenuation relation for eastern Cuba.

Paper 4: The new Cuban seismograph network.

Part II: Web-based applications for earthquake analysis

Paper 5: *SeisWeb*: A client-server-architecture-based interactive processing tool for earthquake analysis.

Paper 6: Database design and Graphical User Interface for diagnosing active faults.

Annexes

I. SeisWeb commands running on the server side

   http://www.ifjf.uib.no/seismo/seisweb/commands.html

II. List of tables defined in the database for diagnosing active faults

   http://www.ifjf.uib.no/seismo/safe-t/tables.html

III. Examples of XML files mapping the database for diagnosing active faults

   http://www.ifjf.uib.no/seismo/safe-t/XMLFiles.html

List of papers

Part I: Crustal structure and seismicity of Cuba

Paper 1: Moreno, B., Grandison, M., and Atakan, 2002, Crustal velocity model along the southern Cuban margin: Implications for the tectonic regime at an active plate boundary, *Geophys. J. Int.* **151**, 632-645

Paper 2: Moreno, B., 2002, The crustal structure of Cuba derived from Receiver Function Analysis, submitted to *Journal of Seismology*.

Paper 3: Moreno, B., 2002, New magnitude scales and attenuation relation for eastern Cuba, submitted to *Journal of Seismology*.

Paper 4: Moreno, B., 2002, The new Cuban seismograph network, *Seis. Res. Lett.*, **73**, 504-517

Part II: Web-based applications for earthquake analysis

Paper 5: Moreno, B., Ottemöller, L., Havskov J. and Olsen, K. A., 2002, *SeisWeb*: A client-server-architecture-based interactive processing tool for earthquake analysis, *Seis. Res. Lett.*, **73**, 84-89

Paper 6: Moreno, B., Atakan, K., Furuløkken, K. A., Temel, S., and Berland, O. J., 2002, Database design and Graphical User Interface for diagnosing active faults, submitted to *Seis. Res. Lett.*

Summary

Introduction

Seismology in Cuba started with the Russian cooperation at the beginning of the sixties. Several seismic stations were installed along the Island particularly in eastern Cuba, the most seismogenic active area of the country. The earthquake data recorded by these stations were used mainly in seismicity studies and seismic hazard analysis. Most of seismic studies and geophysical investigations were published in journals and reports that are not very accessible outside the country. Few Russian papers have been translated to English and published in international journals, most of them published 20 years ago. Other studies like waveform modelling and seismic tomography were impractical since the seismographs were analogue and the timing at each station was unstable. The change of the old technology of visual recordings by digital recording in 1998 opened new opportunities for seismological studies that were not feasible to perform before.

In the first part of this thesis the new earthquake data has been used to obtain basic results that are necessary for other research applications. The locations of the earthquakes were greatly improved with a new P-wave velocity model (Paper 1), which was obtained combining the Cuban and Jamaican earthquake data. Moho depth at Cuban seismic stations was estimated using Receiver Function Technique (Paper 2) and a new attenuation relation for the frequency-dependent quality factor Q was obtained (Paper 3). Paper 3 also propose a new local and coda magnitude scales. The results obtained in Paper 1 and Paper 3 were used for a seismicity and kinematic analysis in eastern Cuba (Paper 4 and part of Paper 1). Principal stress axes were also determined for this region from stress-inversion of focal mechanisms (Paper 1). Most of these results are new for Cuba and can be used as reliable constraints for the seismotectonic interpretations in the area.

The second part of the thesis deals with the development of Web-based applications for earthquake analysis. With the ongoing expansion of the Internet, the World Wide Web (WWW) has become an enormous source of information for people all over the globe. Seismologists use the Internet extensively for many purposes: data exchange, data transfer from the field to the central recording site, dissemination of information on recent earthquakes, and educational information. Several interactive tools for access to seismological, geological and geophysical data have been developed by different institutions. At present most of these tools are data retrieval tools, but the development of tools for processing geospatial data across the Web has begun. Here two papers are included. The first paper (Paper 5) propose a Graphical User Interface (GUI) for retrieving and processing parametric and waveforms seismic data through Internet. The second paper (Paper 6), which hereby will be referenced as Safe-T, proposes a relational Java database and a GUI for

diagnosing active faults. In both papers we make references to Web pages that, given the limited space of the journals, were not possible to be included for publication. These Web pages are attached to the thesis as annexes. The annexes have in the first page the corresponding Internet-URL address.

Part I: Crustal structure and seismicity of Cuba

Tectonic setting

The island of Cuba is situated in the Caribbean region within the Antilles island arc. It is located in the southern margin of the North America plate in direct contact with the Caribbean plate, where a mechanism of strike-slip deformation dominates (Fig. 1). Much of this deformation is concentrated
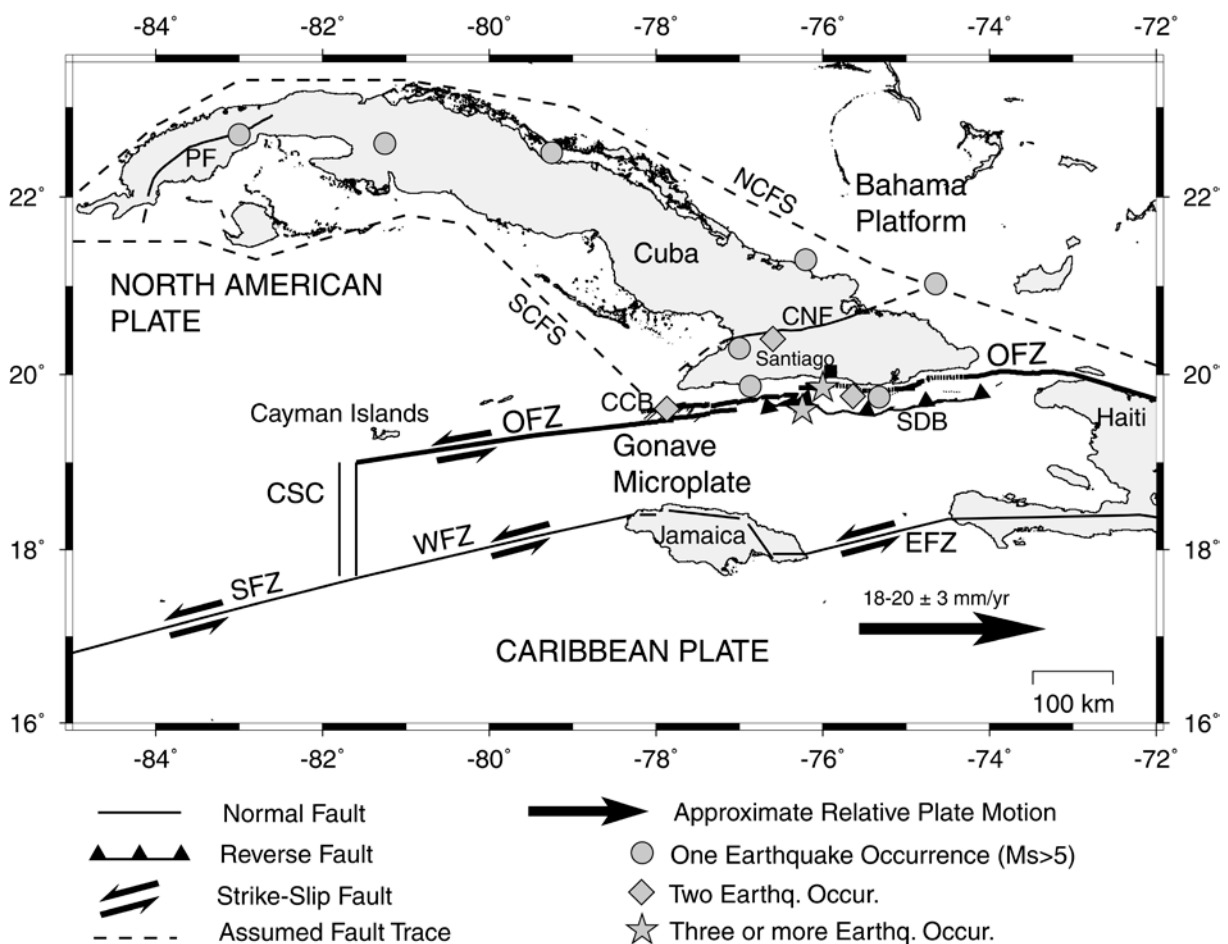
Figure 1. Kinematic framework along the southern Cuban margin. OFZ- Oriente Fault Zone; WFZ – Walton Fault Zone; EFZ – Enriquillo Fault Zone, SFZ- Swan Fracture Zone; CSC - Cayman Spreading Centre; CCB – Cabo Cruz Basin; SDB – Santiago Deformed Belt; CNF – Cauto Nipe Fault; PF – Pinar Fault; NCFS – Nortecubana Fault System; SCFS – Surcubana Fault System. The mapped OFZ trace, including CCB and SDB is taken from Calais and Mercier de Lépinay (1990, 1991). The PF and CNF traces are taken from Draper and Barros (1994).

Summary

along the releasing and restraining bends of the Oriente Fault Zone (OFZ) such as the Cabo Cruz Basin (CCB) and Santiago Deformed Belt (SDB). The OFZ extends over 900 km from the Cayman Spreading Center (CSC) to the central Dominican Republic. This major transform fault, which marks part of the boundary between the Caribbean and North American plates, is responsible for more than 90% of the seismicity and the largest earthquakes observed along the southern Cuban margin. According to Iturralde (1977) the island of Cuba can be considered as a block, a tectonic unit separating the quiescent Bahama platform from the seismically active Cayman trough. The Cuban block is limited to the north by Nortecubana fault system (NCFS) and to the south by OFZ and Surcubana fault system (SCFS) (Fig. 1). The Caribbean Plate is moving eastward relative to the North American Plate (NAP) an average of 18-20 ± 3 mm/yr with 18 ± 2 mm/yr of boundary-parallel slip and 3 ± 3 mm/yr of boundary-normal convergence south of eastern Cuba (DeMets et al., 2000). This eastward motion of the Caribbean plate produces left-lateral slip along the Enriquillo (EFZ) and Walton Fault Zones (WFZ), and left-lateral strike-slip deformation along the OFZ (Fig. 1).

One-dimensional P-wave velocity model

The area where earthquake activity is concentrated has a rather complex crustal structure. Previous studies have shown lateral variations in seismic wave velocity and irregular thickness of the crust (Case et al., 1990; Ewing et al., 1960). In order to establish a one-dimensional velocity model used in the hypocenter determination we merged the Cuban and Jamaican catalogues. We gathered 99 events from two years of earthquake activity (Fig. 2a). The inversion process was achieved with the program VELEST (Kissling et al., 1995). The coupled hypocentre-velocity model problem was solved performing the Joint-Hypocentre-Determination (JHD) using both P and S arrival times. The solution was obtained by a trial and error process with various initial velocity models and with different combinations of damping factors (Kissling1988; Kissling et al., 1994).

    To test the variability of the convergence of the solution with respect to the input model, we ran VELEST with several input models having different layer thickness and velocities (Fig. 2b). The set of solutions shows similar geometry but indicates large variability in the velocity range for the upper layers (Fig. 2c). The topmost layers did not converge very well due to the small number of earthquakes with depths less than 7 km; most of the earthquakes are generated at more than 5 km below the sea floor. The thinness and poor resolution of the topmost layers made the convergence of the inversion difficult. Bottom layers show a tendency to converge within a very small velocity range. These results indicate that the inversion problem has a solution space with several local minima.

    Since the range of velocities obtained from the simultaneous inversion for the near-surface layer was wide, we used forward modelling to get a suitable solution. According to the result of the inversion process and previous studies of seismic refraction, we defined a range of velocities for each

layer to be tested. The velocity models were tested using the HYPOCENTER program (Lienert and Havskov, 1995) and the model with the overall lowest RMS misfit was selected (Fig. 2d).
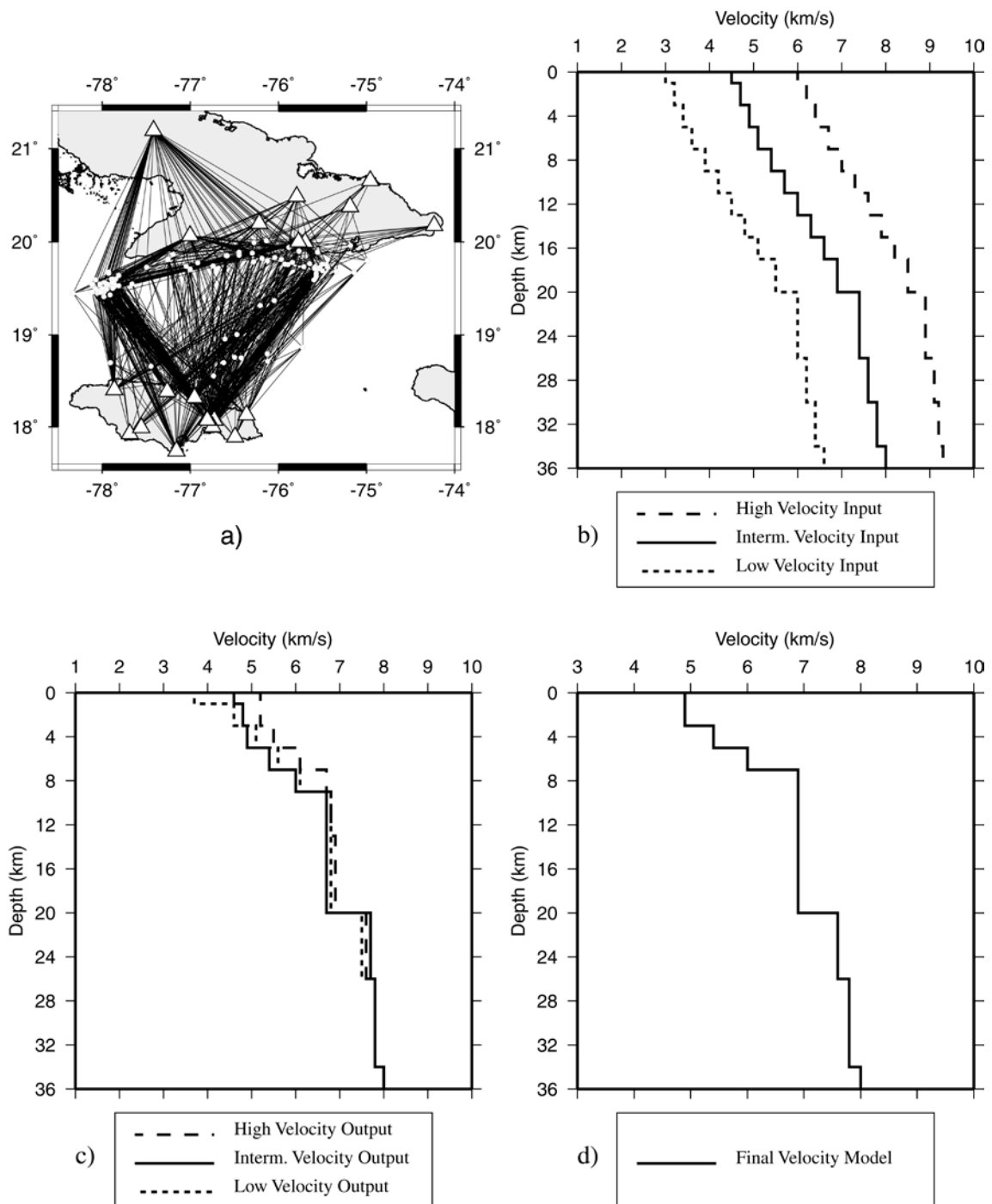

Figure 2. (a) - Area where inversion process was applied (station-hypocentre ray path); (b) Input models used in the inversion process for testing the stability (convergence) of the solution; (c) Output models of the inversion associated with the input models shown in (b); (d) Final model obtained from forward modelling.

Summary

Significant improvement in the earthquake location was obtained using the new velocity model. The relocation process defined very well the tectonic features in the area and the epicentre errors less than 10 km were increased from 22% to 33% for the entire catalogue.

Crustal structure beneath seismic stations

The characterization of the Cuban crust presented in previous studies was mainly based on seismic refraction methods combined with gravimetric data, deep drilling and satellite photographs (Shcherbakova et al., 1977, 1978; Bovenko et al., 1980, 1982; Bush and Shcherbakova, 1986). In this study we use the receiver function method (Langston's, 1979; Ammon, 1991) to determine first-order
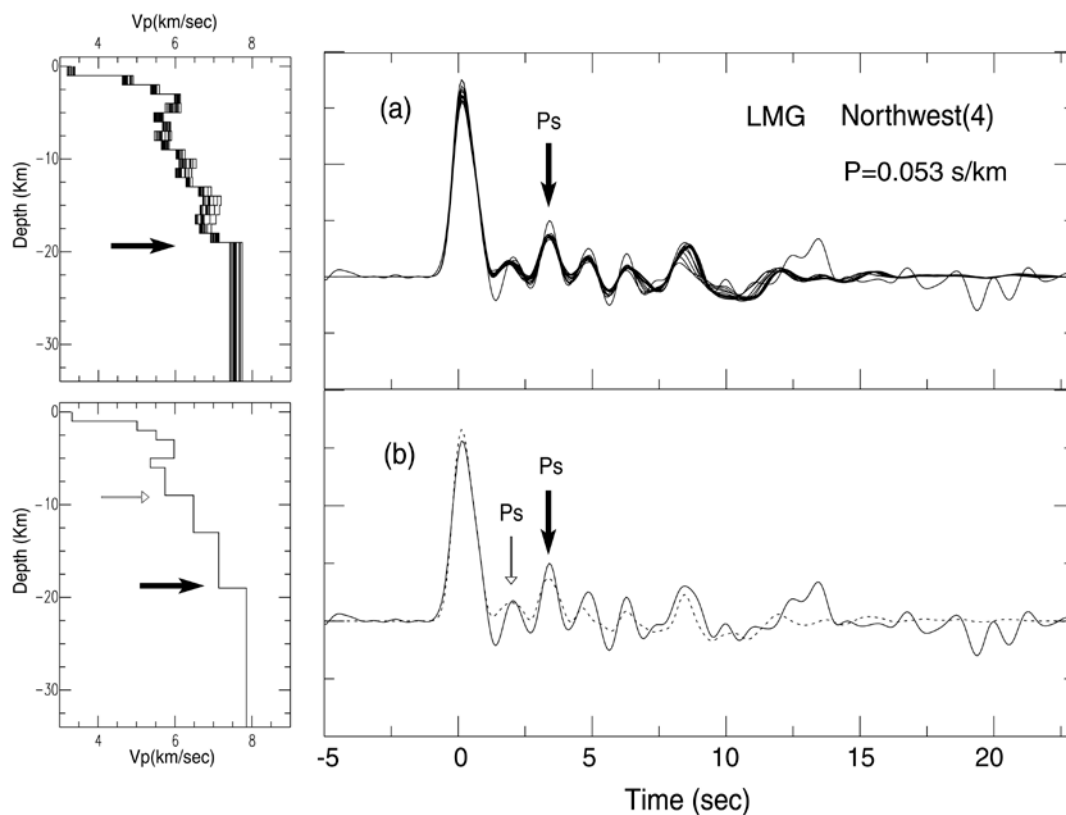
Figure 3. (a) - Output models and its corresponding synthetics radial receiver functions of LMG obtained from the inversion. The synthetic radial receiver functions overlap in a solid black line the observed radial receiver function. Black arrows indicate the Moho interface. Only models that fit the observed radial receiver function relatively well are shown. (b) - Simplified output model derived from the output models shown in (b) and its corresponding synthetic radial receiver function (dashed line). White arrows indicate interfaces within the crust. The number of receiver functions stacked is shown in parentheses. P indicates the ray parameter.

discontinuities or transition zones below the seismic stations from teleseismic recordings. The basic principle behind the method is that P to S conversion at interfaces below the seismic receiver has much stronger amplitude on the horizontal components than on the vertical component. By deconvolving the vertical component signal from the horizontal components, the effects of the source

function, propagation path and instrument response can be removed, leaving a signal composed of primarily S-wave conversions and reverberations below the seismic station.

The receiver functions were computed at 7 sites of the Island using 17 teleseismic earthquakes recorded by broadband seismic stations. The receiver-function inversion was based on a linearized-iterative inversion of a specified waveform by minimizing the misfit residual vector between the observed and synthetic receiver function (Ammon et al., 1990). Figure 3a shows the stacked radial receiver-functions of LMG overlapped by several synthetic radial receiver functions, which correspond to the P-wave velocity models (1 km thick layers) on the left. The output model with the best fit was simplified over several inversions by joining layers with similar velocities (Fig. 3b). Two clear P-S conversions (Ps) arrivals are identified. The earlier peak at about 2 sec is consistent with a Ps converted wave at 9 km and the next peak at about 3 sec is interpreted as a Ps phase generated at a Moho interface of 19 km.

The Moho interfaces revealed from this method suggest both oceanic and continental crust in Cuba. The results were consistent with previous studies at most sites, with the exception of MOA where was obtained a Moho depth of 29 km. According to Otero et al. (1998), MOA is located on oceanic crust with thickness lower than 20 km. However, there is no seismic profile close to this area to verify this. Their result is based on extrapolation. The crust at MOA seems to be much thicker than oceanic-crust type. It is located on the north coast, near to the contact zone between the Bahama platform and the Cuban block. There is a compressional deformation along this contact zone (Moreno, 2002), which could generate crustal thickening in this area.

Attenuation relation and magnitude scales

There are not any previous crustal attenuation studies for Cuba. For the first time, the frequency-dependent quality factor Q and the near-surface attenuation factor kappa have been estimated. The quality factor Q was computed following two distinct procedures: (1) Coda Q (Aki and Chouet, 1975; Rautian and Khalturin, 1978) and (2) Spectral ratio between two stations. The first method assumes that coda waves are S to S backscattered waves (Aki, 1981), which is consistent with the observation of equivalence between coda Q and Q of direct shear waves (Aki, 1980). The second method is based on the principle that if the seismic waves are recorded at two different stations at different distances, the difference in amplitude, at a given frequency, is due to attenuation and geometrical spreading (Campillo et al., 1985; Kvamme and Havskov, 1989). Figure 4 shows the results of the Q values represented by the relationship $Q(f) = Q_0 f^\alpha$ using the coda Q (Figure 4A) and the average spectral differences of 8 displacements spectral (Figure 4B). The results overlap within 1 standard deviation, which indicate that the quality factor obtained from coda Q analysis is quite representative for the region and equivalent to the Q of direct S waves.
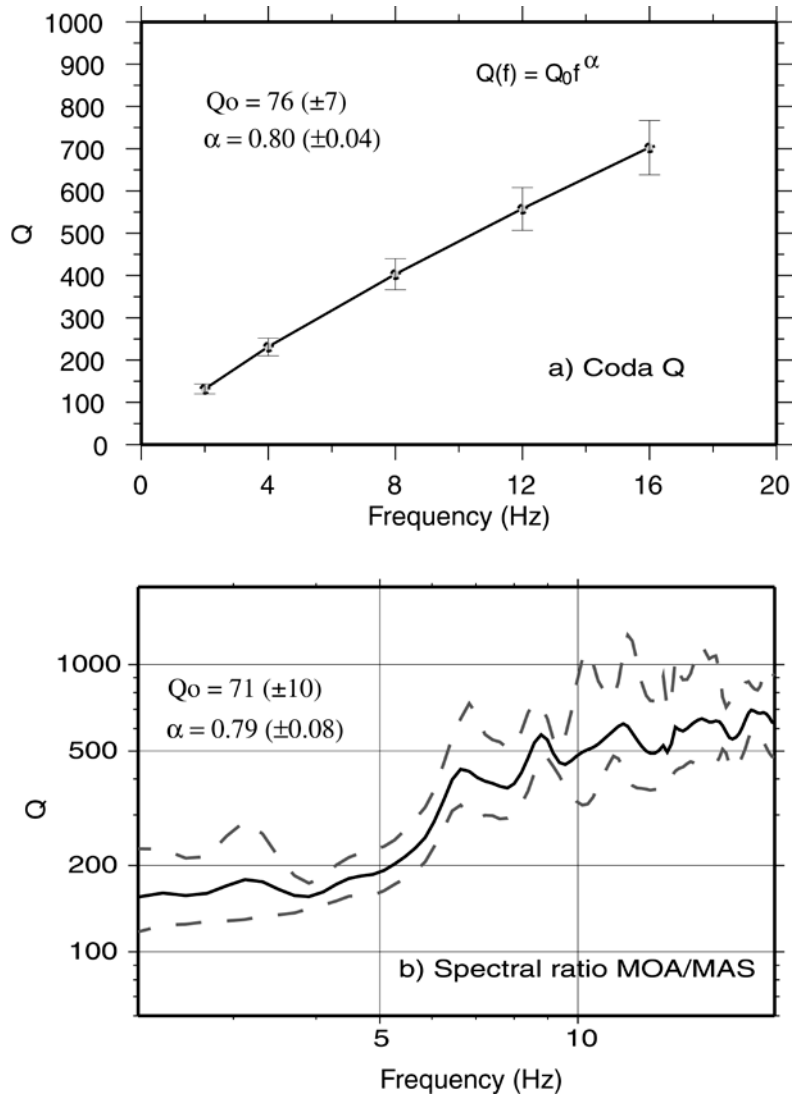
Figure 4. Result of the quality factor Q with the corresponding standard deviations (dashed line). (a) - Coda Q; (b) - Average of 8 displacement spectral ratio.

The new frequency-dependent quality-factor Q was used to calculate the moment magnitudes (Kanamori, 1977) for the same dataset used in the local magnitude scale determination, which is explained below.

Following Hutton and Boore (1987), the local magnitude scale can be written as

$$Ml = \log_{10}(A) + \alpha\Delta + \beta\log_{10}\Delta + K + Cs \quad (1)$$

where A is the maximum amplitude in millimeters of the Wood-Anderson instrument, Δ is the hypocentral distance, α and β are coefficients for the attenuation and geometrical spreading respectively and K is a constant which allows to fit the magnitude scale to an established scale. The Cs term is the station correction factor. The absolute value of the scale is defined so that an amplitude of

8

Summary

one millimeter on the seismogram at a distance of 100 km gives a magnitude of 3, which is represented as

$$-\log_{10}(\frac{1000000}{2050}) = \alpha 100 + \beta \log_{10}(100) - 3 \qquad (2)$$

where 2050 is the magnification of the Wood-Anderson instrument (Hutton and Boore, 1987).

The coefficients α and β, earthquake magnitudes (Ml) and station corrections (Cs) were determined from regression analysis using equation (3), which was obtained combining (1) with the constrained (2)

$$-\log_{10}(A_{ij}) - 3 + \log_{10}(488) = \alpha(\Delta_{ij} - 100) + \beta \log_{10}(\frac{\Delta_{ij}}{100}) - Ml_j + Cs_i \qquad (3)$$

where i goes from 1 to the number of stations (N) and j goes from 1 to the number of earthquakes (M). The system represents an over-determined inverse problem with N + M + 2 unknowns. The inverse problem can be solved through the least squares method subjected to the constraint that the sum of the station corrections must be zero. The constant 488 is the result of converting one millimiter amplitude on the Wood-Anderson trace to nanometers. The new Cuban local magnitude scale is determined as

$$Ml = \log_{10}(A) + 0.8889 \log_{10}(\Delta) + 0.0031\Delta - 1.804 \qquad (4)$$

The coda-length magnitude scale was also calculated from regression analysis using the moment magnitude values. The new Cuban coda magnitude scale is determined as

$$Mc = 1.89 \log_{10}(t) + 0.0017\Delta - 0.98 \qquad (5)$$

The frequency-dependent quality factor Q and the attenuation function obtained in the local magnitude scale both suggest high attenuation in eastern Cuba. The station corrections for the local magnitude values suggest strong attenuation-ray-path dependency, which can be associated with tectonic features in the area.

Seismicity

Earthquake activity in Cuba is not restricted to interplate seismicity, as small and moderate intraplate events are occurring throughout the country. The intraplate seismicity seems to be localized along the

pre-existing zones of crustal weakness (Cotilla, 1998). Since most of those intraplate events are very small, and their locations are in many cases constrained by only one or two seismic stations using azimuth determined from 3 components, there is not a good correlation of their locations with individual faults.

Figure 5 shows the seismic activity from March 1998 to December 1999. The solid-grey line at –79° of longitude separates two regions. In eastern Cuba, earthquakes located with three or more stations are shown. In many cases (106 events) more than 3 Jamaican seismic stations were used, which improved the location error along the OFZ. On the left side in western Cuba, earthquake locations are poorly resolved, with locations determined from analysis of 3-component data from one or two stations.

There are four clusters of seismic events label as A,B,C and D in the lower map of Figure 5. Cluster A is correlated with CCB (Fig. 1), a pull-apart zone characterized with shallow seismicity (depths less than 20 km). This zone is well defined by earthquake activity and was responsible for the 6.9 Ms Cabo Cruz earthquake on May 25th, 1992. Cluster B corresponds to the SDB (Fig. 1). Both, shallow and relatively deep earthquakes (depth greater than 30 km) are observed in this area. Shallow seismicity in the SDB might be generated by the thrust and reverse faults mapped by Calais and Mercier de Lépinay (1990,1991). On the other hand, it is unlikely to have earthquakes with focal depth below 30 km in oceanic crust, where the thickness of the crust barely reaches 20 km (Ewing et al., 1960; Edgar et al., 1971; Case et al., 1990). Another process, perhaps oblique subduction could be taking place (see "Kinematics").

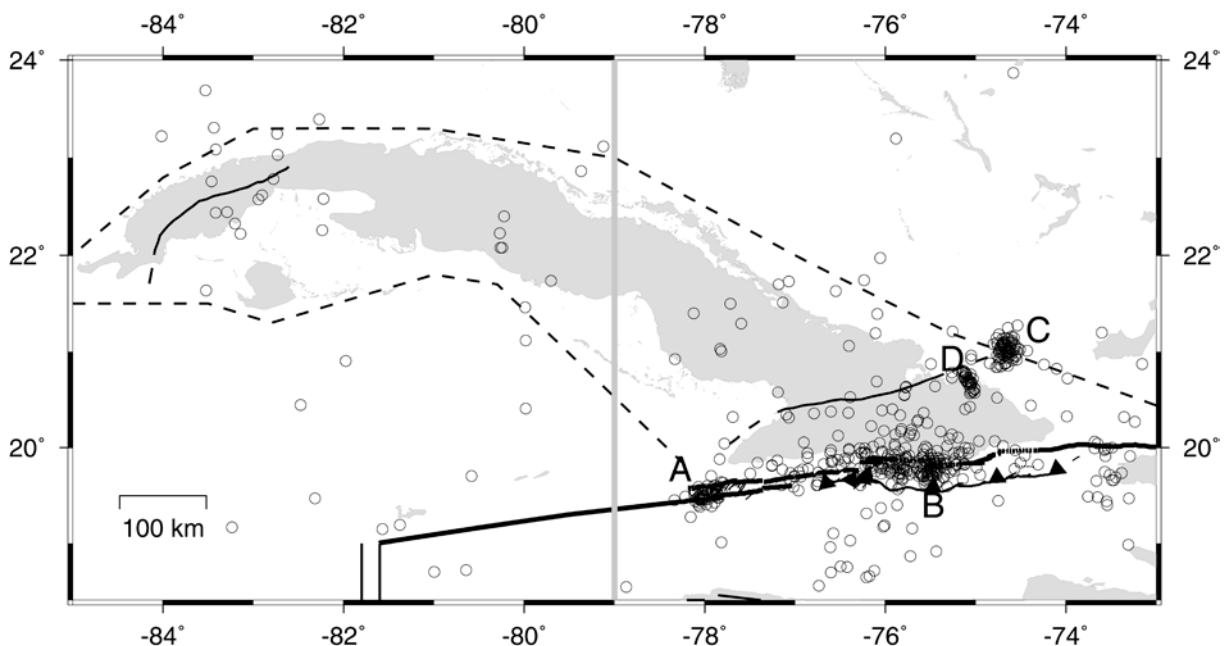Figure 5. Earthquakes recorded by the new Cuban Seismograph Network (CSN) from March 1998 to December 1999. The area at the right side of the solid-grey line (eastern Cuba) shows earthquakes located with three or more stations. On the left side (western Cuba) the earthquakes are poorly resolved with less than three stations by using three components analysis. Clusters of earthquakes explained in the main text.

Cluster C includes aftershocks of Mw=5.6 earthquake on December 28ᵗʰ 1998, the largest seismic event ever recorded in this area. About 116 events were registered during the month after the main shock. The main shock seems to have been generated by the NCFS. The hypocentral errors in this area are large because earthquakes are outside of the Cuban Seismograph Network (CSN) but our solution, including both focal depth (15 km) and epicentre, are very close to the NEIC solution. The last cluster (D) corresponds to an earthquake swarm during July 1999. The swarm could have been triggered by stress transfer following the December 28ᵗʰ (Mw=5.6) earthquake. A fault correlated with this swarm is not clearly identifiable. The swarm could be associated with the trace of Cauto Nipe fault (CNF) mapped in Figure 1, but also with NW-SE oriented faults, which have been identified from geomorphological data.

Kinematics

There are two important local structures affecting the tectonic regime along the southern Cuban margin: (1) the CCB and (2) the SDB (Fig. 1). The CCB is a narrow E-W trending depression, bordered on the north and south by two segments of the Oriente Fault and divided by normal faults into a series of oblique horsts and grabens (Calais and Mercier de Lépinay, 1991). The SDB is a narrow submarine mountain range extending over 300 km along the OFZ with folds and thrust faults showing clear evidence of transpressional deformation (Calais & Mercier de Lépinay, 1990, 1991; Calais et al., 1998). Another important seismogenic structure is the NCFS (Fig. 1). This structure seems to undergoing compressive deformation probably as result of the contact zone between the Bahama platform and the Cuban block.

   Figure 6 shows a number of earthquake focal-mechanisms determined using P-wave first -motion polarities from the Cuban and Jamaican seismic stations. The solutions are divided into three groups: (1) those associated with CCB; (2) those associated with SDB; and (3) events associated with NCFS. The rose diagram in the upper-left corner shows the maximum horizontal compressive stress (σ_h) for the first group (P1, 5, 2, 4, 10, 9, 3, 18). The event labelled as P1 is the 1992 Cabo Cruz earthquake (Perrot et al., 1997). The σ_h values are determined from the T (tensional) and P (compressional) axes, according to the method of Zoback (1992). Two clear dominant σ_h orientations are found for the CCB events. The axis with azimuth N10°-20°E correlates with the normal NE-SW faults mapped in the basin, such as faults associated with events 10, 9 and 3. This σ_h orientation is consistent with the expected W-E horizontal extension in this pull-apart zone. The second axis, oriented N40°-50°E, corresponds to W-E segments of the OFZ, which generated events 4 and 18. This stress orientation is in agreement to a regional σ_h (Zoback, 1992) driving left-lateral strike slip along the OFZ.

Summary
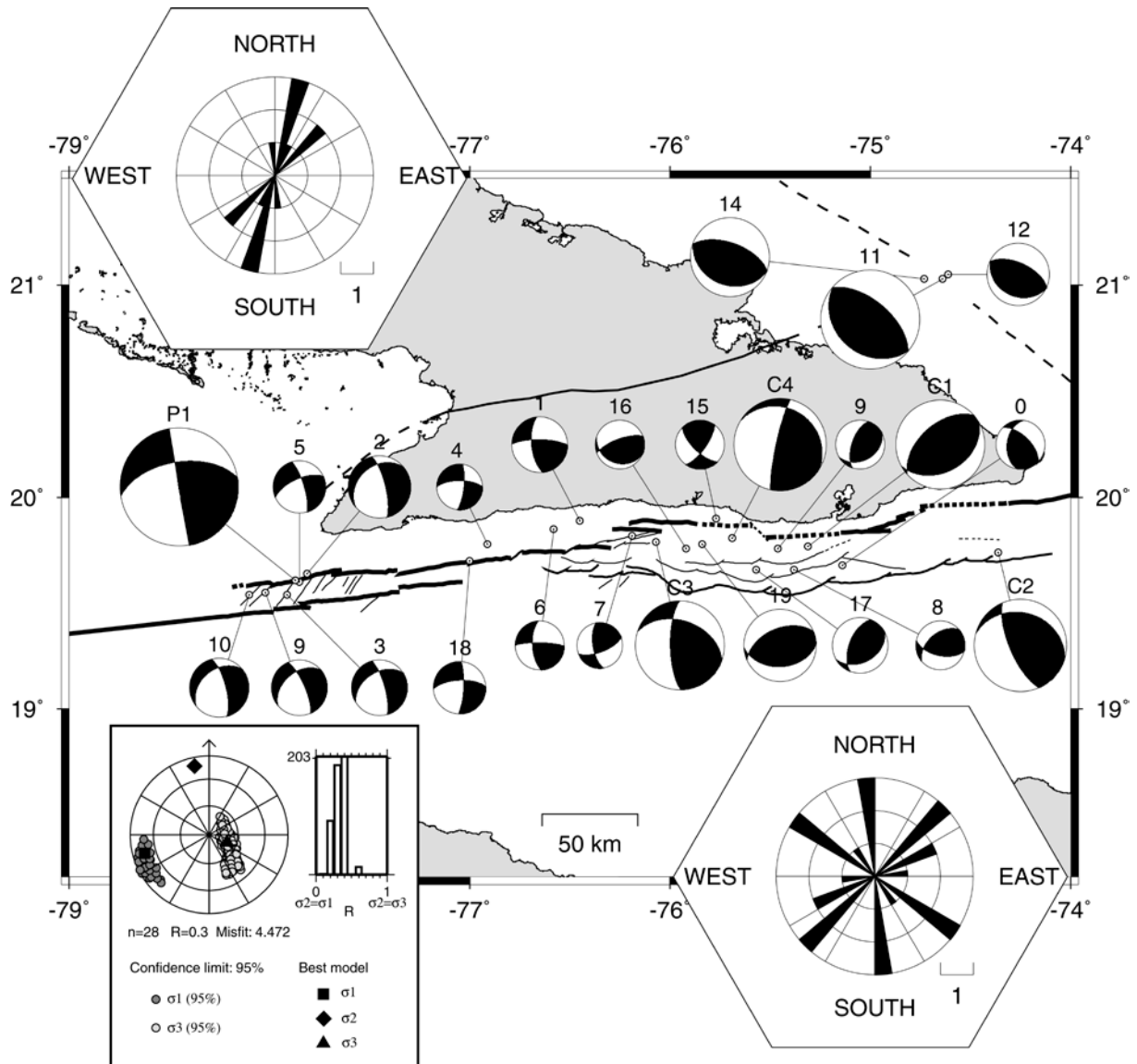
Figure 6. Earthquake focal mechanisms along the most active seismogenic sources in Cuba. Data from Jamaican Seismograph Network is used. Insets explained in the main text.

The σ_h orientations for the second group (1, 16, 15, 9, 0, 6, 7, 19, 17, 8, C1, C2, C3, C4) are shown by the rose diagram in the lower right corner of Figure 6. The events labelled as C1, C2, C3, C4 are taken from the Harvard CMT catalogue. The stress orientation for this group shows rather complex σ_h patterns and variable fault plane solutions. This is not unexpected considering the non-uniform orientation of the thrust faults in SDB. The area is dominated by reverse faulting with a few strike-slip faults that can be correlated with W-E segments of the OFZ. Some earthquakes show compressive deformation at relatively deep focal depths (below 30 km). Those earthquakes are located in oceanic crust, where the Moho is at about 18-20 km (Case et al., 1990). It is evident that the shallow thrust faults of SDB cannot generate earthquakes at such depths. Their solutions support what has been suggested in previous studies, that the Gonave Microplate is underthrusting beneath the Cuban block (Enman et al., 1997), probably causing crustal thickening in SDB area. The third group has no rose

diagram, but the stress orientations (N20°-40°E) are consistent with the regional σ_h, which may cause thrust faulting in NW-SE oriented structures. The fault plane solutions correlate with the NCFS, a NW-SE structure, which defines the external northern limit of the Cuban block. The inset in the lower left corner shows the principal stress axes along the southern Cuban margin obtained from stress-inversion of focal mechanisms. The near-horizontal σ_1 with near-vertical σ_3 suggest that the plate boundary along the OFZ enters into a thrust faulting regime within the SDB, showing that this area is undergoing active transpressional deformation along a major transcurrent fault. The orientation of the principal stress axes seems to be induced by an oblique WSW-ENE convergence of the Gonave Microplate with the North American Plate.

Part II: Web-based applications for earthquake analysis

To investigate the feasibility of interactive analysis and remote access to geosciences-related databases through the Internet, we developed two Web-based applications: SeisWeb and Safe-T. The systems are platform independent since they were written in Java programming language (Weber, 1998). Both tools are based on client-server architecture using the Internet's transfer protocol TCP/IP where most of the processing is performed on the server side (Fig. 7). In the case of SeisWeb, the server-side applications consist of Common Gateway Interface (CGI) (Gundavaram, 1996). Safe-T, on the other hand, use Enterprise Java Beans (EJB), Servlet and Java Server Page (JSP) (Monson-Haefel, 2000; Hall, 2002). In both cases, the client-side interface includes Java Applets and HTML forms (Fig. 8) (Powell, 2000).
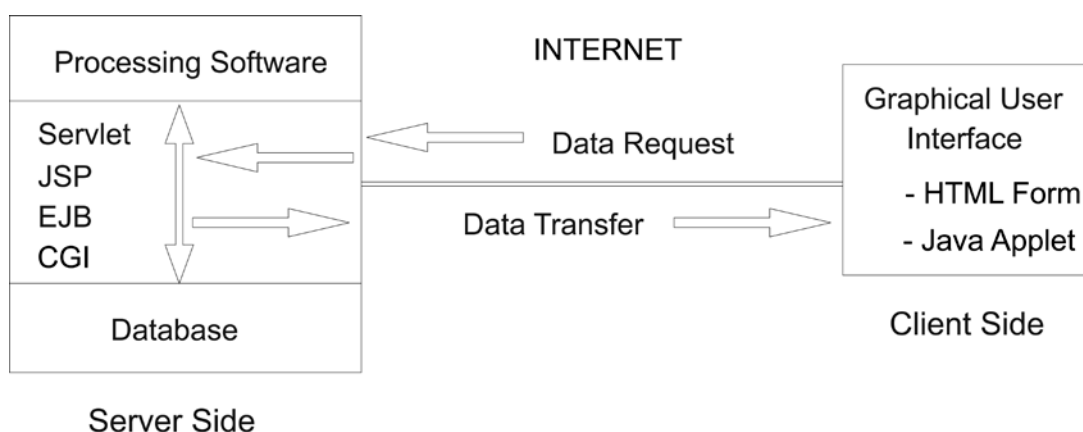
Figure 7. Client-Server architecture

Several aspects about SeisWeb design are discussed, like client-side and server-side processing, communication speed and Graphical User Interface (GUI). The GUI was designed to be independent of the database structure and processing software. The main functions supported in SeisWeb are:

13
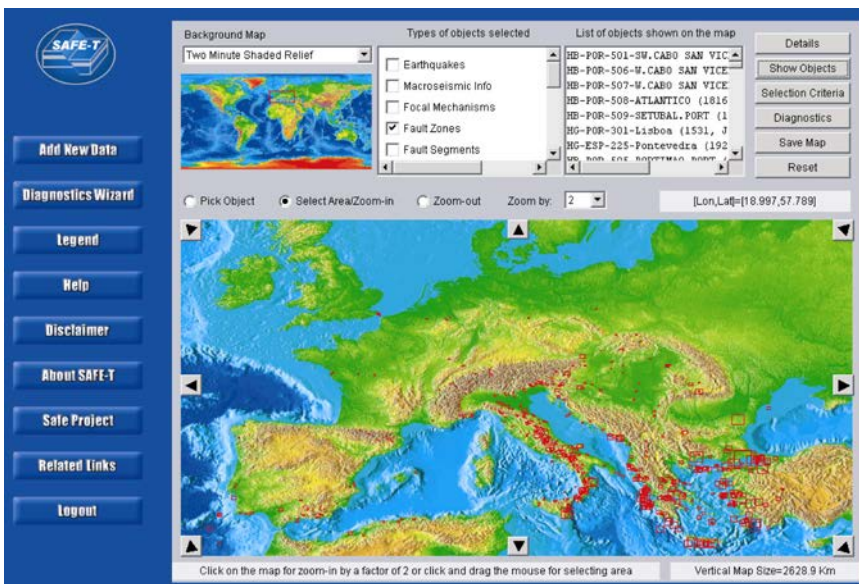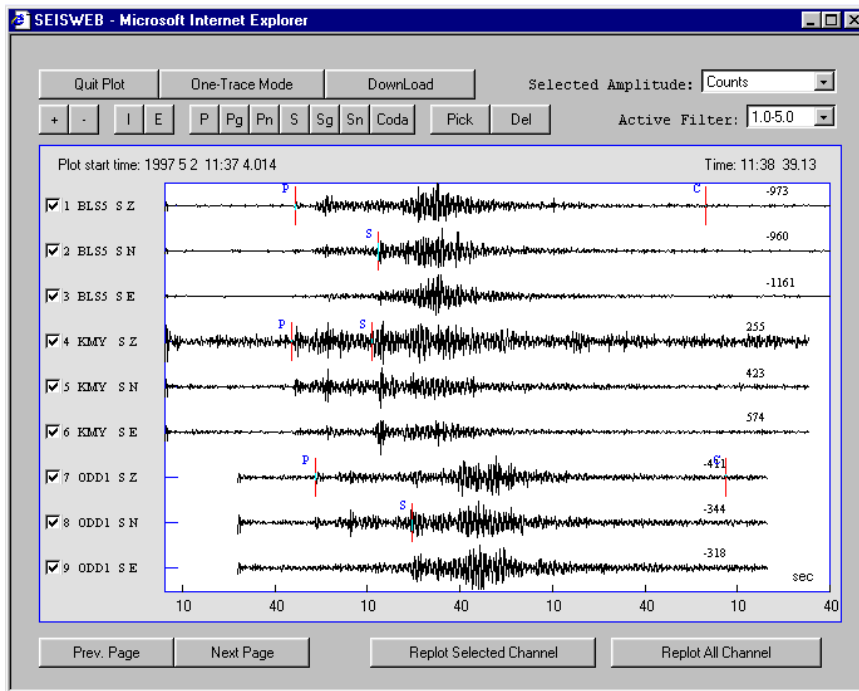
Figure 8. Examples of SeisWeb (upper) and Safe-T (lower) Graphical User Interfaces (GUI).

- display parametric data such as earthquake location, origin time, source parameters and phase readings
- search the database
- extract parametric information
- locate earthquakes
- produce epicenter maps
- extract waveform data (raw and processed)
- display seismic traces in single- or multi-trace mode

14

Summary

- basic processing of the seismograms (filtering, instrument correction, phase picking, amplitude reading)
- update database on the server side (login and password needed)

The main achievement of Safe-T lies in the database design. The data for diagnosing slow active faults was parameterized and stored in a relational Java database (Mukhar et al., 2001). The information was categorized into six main groups: (1) Seismologic, (2) Paleoseismic, (3) Geophysical, (4) Geological, (5) Geochemical and (6) Geomorphic data. These data are stored in tables with some logical relationship (Fig. 9). Four main tables are identified: (1) Earthquakes, (2) Maps, (3) Faults and (4) Cross-sections. These tables are considered as "parent" tables with a set of sub-tables describing particular cases within the corresponding type of data.
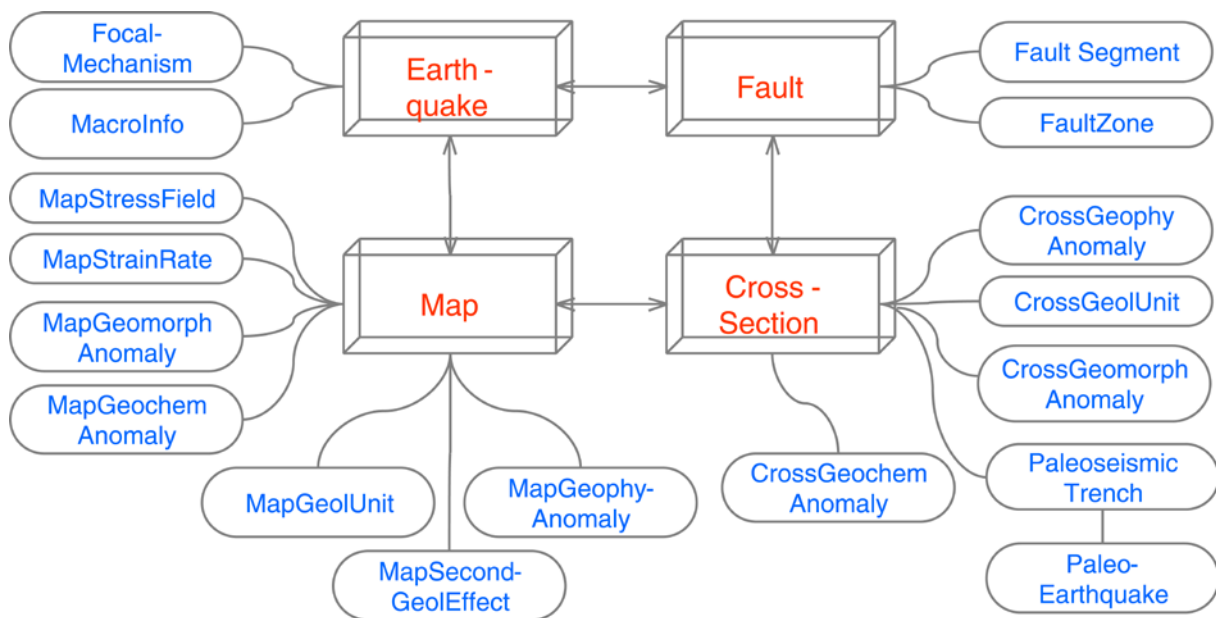
Figure 9. Information included into the database

The data or objects are geographically referenced as a point (e.g. earthquakes), as a poly-line (e.g. fault segments, cross-sections) and as a polygon (e.g. fault zones, geological units). Maps are stored as images and cannot be used by the processing-logic. However, the components of the maps can be parameterized and stored in the database in order to be used in a meaningful way. For example, the stress field has not a particular location on the map but what it is stored in the database is the region (polygon) in which the stress field is applicable and the corresponding parameters describing the stress. The database can be populated through Internet using HTML forms or submitting XML files (White et al., 2001).

Another relevant aspect on Safe-T design is that it is based on distributed database technology (Birnam, 2001). The database can be located in several computer servers, which are connected by

Internet. This allows more flexibility on maintenance and administration of the database and therefore easy upgrade of the information.

The graphical user interface includes a navigation map (lower graph in Fig. 8) where users can zoom-in, pick objects, see object details, selects an area for processing and more. The objects are plotted on a map with background information like country boundaries, topography, shaded relief, etc. The background maps are created dynamically by Web-Map-Servers and transmitted as images over Internet.

Conclusion

The conclusion of the study developed in the first part of the thesis can be summarized in the following points:

1. The combined Cuban and Jamaican catalogues over a period of two years allowed us to obtain for the first time a one-dimensional P-wave velocity model based on local seismic data. The model represents a significant improvement in the earthquake locations and can be used as an initial reference model for 3-D seismic tomography.

2. The crustal structure at seismic stations obtained from Receiver Function analysis suggests the existence of both oceanic and continental crust in Cuba. The oceanic crust is found in the extreme southeastern coast, whereas part of the north coast seems to be characterized by a continental crust.

3. For the first time a moment magnitude and a more reliable coda and local magnitudes can be reported in the Cuban catalogue.

4. Both the frequency-dependent quality factor Q and the attenuation relationship for the local magnitude scale indicate high crustal attenuation for eastern Cuba.

5. The station-corrections of the local magnitude values suggest that the attenuation seems to have strong ray-path dependence caused by the complex crustal structure along the boundary of the Caribbean and North American plates.

6. The more active structures along the OFZ are the CCB and the SDB. The CCB is characterized by shallow seismicity with normal faulting (small strike-slip component) and the SDB experiences shallow and relatively deep seismicity dominated by thrust faulting.

7. The earthquake focal mechanisms along CCB and SDB show evidences that transtension and transpression are occurring at the same time and at short distances along a major transcurrent fault, the OFZ.

8. Compressive deformation at relatively deep depths in SDB area supports a previous suggestion (Enman et al., 1997) that the Gonave Microplate is underthrusting the Cuban block, probably causing crustal thickening in this area.

9. The stress field along the southern Cuban margin is suggested to be transpressional, which is in agreement with the dominant structural trend associated with the SDB. The orientation of the principal stress axes seems to be induced by an oblique WSW-ENE convergence of the Gonave Microplate with the North American Plate.

As result of the second part of this thesis we found that

1. With the current transfer rates and computer systems, client-server-based processing across the Internet is already feasible.

2. The simple graphical user interface developed and easy access could make seismology more accessible to the public, increasing both interest and understanding.

3. Considering the large number of geosciences-related databases that could be accessed through the Internet, there is a large potential to make these data available for interactive use to professional seismologists and to non-experts.

References

Aki, K., 1980, Attenuation of shear waves in the lithosphere for frequencies from 0.05 to 25 Hz, *Phys. Earth Planet. Interiors* **74**, 615-631.

Aki, K., 1981, Attenuation and scattering of short-period seismic waves in the lithosphere, *in Identification of Seismic Sources - Earthquakes or Underground Explosions*, ed. Husebye, E. S. and Mykkeltveit, S., D. Reidel Publishing Co., Dordrecht, The Netherlands.

Aki, K. and Chouet B., 1975, Origin of coda waves: source, attenuation and scattering effects, *J. Geophys. Res.*, **80**, 3322-3342.

Ammon, C.J., Randall, G.E., and Zandt, G., 1990, On the nonuniqueness of receiver function inversions, *J. Geophys. Res.* **95**, 15303-15318.

Ammon, C.J., 1991, The isolation of receiver effects from teleseismic P wave fronts, *Bull. Seism. Soc. Am.* **81**, 2504-2510.

Birnam S., 2001, *Distributed Java platform Database Development*, Java Series, Sun Microsystems Press

Bovenko, V.G., Shcherbakova, B.E., and Hernández, H., 1980,1982, Novyye geofizicheskiye dannyye o glubinnour stroyenii vostochnoy kuby (New geophysical data on the deep structure of eastern Cuba), *Sovetskaya Geologiya* **9**, 101-109; translation in International *Geology Review* **24**, 1155-1162.

Bush, V.A., and Shcherbakova I.N., 1986, New Data on the Deep Tectonics of Cuba, *Geotectonics* **20**, 192-203.

Calais, E., Perrot, J., & Mercier de Lépinay, B., 1998. Strike-slip tectonics and seismicity along the Northern Caribbean plate boundary from Cuba to Hispaniola, *in Active strike-slip and collisional tectonics of the northern Caribbean Plate boundary zone*, Vol. 326, pp. 125-142, ed. Dolan, J.F. & Mann, P., Geol. Soc. of Amer. Special Paper, Boulder, CO, United States.

Calais, E., and Mercier de Lépinay, B., 1991. From Transtension to Transpression along the Southern Caribbean Plate Boundary off Cuba: implications for the Recent motion of the Caribbean plate, *Tectonophysics,* **186**, 329-350.

Calais, E., and Mercier de Lépinay, B., 1990. A natural model of active transpressional tectonics: The *en échelon* structures of the Oriente deep along the northern Caribbean transcurrent plate boundary (Southern Cuban margin), *Rev. Inst. Fr. Pét.* **45**, 147-160.

Campillo, M., Planet J. L., and Bouchon M., 1985, Frequency-dependent attenuation in the crust beneath central France from Lg waves: data analysis and numerical modelling, *Bull. Seism. Soc. Am.* **75**, 1395-1411.

Case, J.E., W.D. MacDonald and P.J. Fox (1990). Caribbean crustal provinces; Seismic and gravity evidence, *in The Geology of North America, The Caribbean Region*, Vol. H, pp. 15-36, ed. Dengo, G. & Case, J.E., Geological Society of America, Boulder, Colorado.

Cotilla, M. (1998). An overview on the seismicity of Cuba, *Journal of Seismology,* **2**, 323-335.

De Mets, C., P. E. Jansma, G. S. Mattioli, T. Dixon, F. Farina, R. Bilham, E. Calais, and P. Mann (2000). GPS geodetic constraints on Caribbean - North American Plate motion, *Geophys. Res. Lett.* **27**, 437 – 440.

Edgar, N.T., Ewing J.I., and Hennion, J., 1971. Seismic Refraction and Reflection in the Caribbean Sea, *Am. Assoc. Petr. Geol. Bull.* 55, 833-870.

Enman, S.V., T. P. Belousov, M. E. Marquez, J. S. Rueda, and G. D. Jorge, (1997). Recent Crustal Movements and Morphostructural Pattern of Southeastern Cuba: Santiago de Cuba Geodynamic Research Site, *Izvestiya, Physics of the Solid Earth*, **1**, 55-69.

Ewing J., J. Antoine and M. Ewing (1960). Geophysical measurements in the western Caribbean Sea and in the Gulf of Mexico, *J. Geophys. Res.*, **65**, 4087-4126.

Gundavaram S., 1996. *CGI programming on the World Wide Web*, O'Reilly & Associates, Inc.

Hall, M., 2002, *More Servlets and JavaServer Pages*, Java[TM] 2 Platform, Enterprise Edition Series, Sun Microsystems Press.

Hutton, L. K. and Boore, D. M., 1987, The Ml scale in Southern California, *Bull. Seism. Soc. Am.* **77**, 2074-2094.

Iturralde, M. (1977). *The tectonic movements of the development plataformic stage of Cuba*, File Report 20, Inst. of Geology and Paleontology, Acad. of Sciences of Cuba, 20 pp.

Kanamori, H., 1977, The energy release in great earthquakes, *J. Geophys. Res.* **82**, 1,981-1,987.

Kissling, E. 1988. Geotomography with local earthquake data, *Rev. Geophys.* **26**, 659-698.

Kissling, E., Ellsworth, W. L., Eberhart Phillips, D. and Kradolfer, U. 1994. Initial reference models in local earthquake tomography, *J. Geophys. Res.* **99**, 19635-19646.

Kissling, E., Kradolfer, U. and Maurer, H. 1995. VELEST user's guide – Short introduction, Institute of geophysics and Swiss seismological service, ETH Zürich, 25pp.

Kvamme, L. B. and Havskov, J., 1989, Q in southern Norway, *Bull. Seism. Soc. Am.* **79**, 1575-1588.

Langston, C.A., 1979, Structure under Mount Rainier, Washington, inferred from teleseismic body waves, *J. Geophys. Res.* **84**, 4749-4762.

Lienert, B. R. & Havskov, J., 1995. A computer program for locating earthquakes both locally and globally, *Seism. Res. Lett.*, **66**, 26-36.

Moreno B., 2002. The new Cuban Seismograph Network, *Seism. Res. Lett.,* **73**, 505-518.

Monson-Haefel, R., 2002, *Enterprise JavaBeans^{TM}, Second Edition*, O'Reilly & Associates, Inc.

Mukhar, K., Lauinger T., Carnell J., and eight others, 2001, *Beginning Java Databases*, Wrox Press

Otero, R., Prol, J.L., Tenreyro, R. and Arriaza, G.L., 1998, Caracteristicas de la corteza terrestre de Cuba y su plataforma marina (Characteristics of the Earth's crust in Cuba and its marine platform), *Mineria y Geologia* **15**, 31-35.

Perrot, J., E. Calais, and B. Mercier de Lépinay (1997). Tectonic and Kinematic Regime along the Northern Caribbean Plate Boundary: new insights from Broad-band Modelling of the May 25, 1992, Ms=6.9 Cabo Cruz, Cuba, earthquake, *Pure Appli. Geophys*. **147**. 475-487.

Powell, T. A., 2000, *HTML: The complete reference, Third Edition*, Osborne McGraw-Hill

Rautian, T. G. and Khalturin, V. I., 1978, The use of the coda for determination of the earthquake source spectrum, *Bull. Seism. Soc. Am.* **68**, 923-948.

Shcherbakova, B.E., Bovenko, V.G., and Hernández, H., 1977, 1978, Stroyeniye zemnoy kory Zapadnoy Kuby (Crustal structure in West Cuba), *Sovetskaya Geologya* **8**, 138-143; translation in *International Geology Review* **20**, 1125-1130.

Weber J. L. 1998. *Special Edition Using Java 1.2, Fourth Edition*. QUE$^{®}$ United States of America.

White C., Quin, L., and Burman, L., 2001, *Mastering XML^{TM}, Premium Edition*, Sybex.

Zoback, M. L. (1992). First and Second-Order Lithospheric Stress Patterns. *J. Geophys. Res.*, **97**, 11703-11728.

ATENUATION AND MAGNITUDE SCALES FOR EASTERN CUBA

Bladimir Moreno Toiran

Institute of Solid Earth Physics, University of Bergen, Allegt. 41, 5007 Bergen, Norway

Centro Nacional de Investigaciones Sismólogicas, Calle 17, No. 61 e/ 4 y 6 Vista Alegre, Santiago de Cuba, Cuba

ABSTRACT[1]

Attenuation parameters to calculate moment magnitudes have been estimated and new local and coda magnitude scales are proposed. Coda Q indicates a frequency-dependent quality factor of Qc = 76f$^{0.80}$. Based on spectral ratio between two stations, Q for direct S waves was found near equivalent to Qc with the relationship Qs = 71f$^{0.79}$ An average near-surface attenuation factor kappa of 0.03 was obtained from 20 displacement spectra recorded at distances shorter than 20 km. Peak Amplitudes from 602 simulated Wood-Anderson waveforms recorded on horizontal components were used to determine the following local magnitude scale

$$Ml = \log_{10}(A) + 0.89\log_{10}(\Delta) + 0.0031\Delta - 1.804$$

The coda magnitude scale determined from 243 coda-length measurements is represented as

$$Mc = 1.89\log_{10}(t) + 0.0017\Delta - 0.97$$

Both the frequency-dependent quality factor Q and the attenuation function obtained in the local magnitude scale suggest high attenuation in eastern Cuba. The station corrections for the local magnitudes values suggest strong attenuation-ray-path dependency, which can be associated with tectonic features in the area.

Key words: Cuba, Local Magnitude, Coda magnitude, Quality factor, Kappa.

1. INTRODUCTION

Since the Cuban Seismograph network began operation in 1979 with more than 3 stations, different magnitude scales have been used in earthquake analysis (Alvarez and Bune, 1977; Alvarez et al., 1999; Alvarez et al., 2000). Most of the scales were imported from other countries, where the attenuation characteristics might be different in comparison to Cuba. The first local magnitude scale equivalent to Richter's local magnitude scale (Richter, 1935) was developed by Moreno (1998). The scale was implemented by using the maximum amplitudes of 286 photographic seismograms recorded on the vertical components of Russian SKM-3 instruments. The amplitudes, which generally had frequencies above 1 Hz, were assumed equivalent to Wood-Anderson amplitudes considering that the SKM-3 seismometers have a flat displacement response above 1 Hz (Moreno, 1998) and Wood-Anderson seismometers have a flat displacement response above 1.25 Hz (Richter, 1958). Therefore, the main difference was in the scaling factor.

---

[1] Statement of exclusive submission: This paper has not been submitted elsewhere in identical or similar form, nor will it be during the first three months after its submission to Journal of Seismology

The deployment of the new digital seismograph network in 1998 opened new opportunities to determine other types of magnitudes that were not feasible to report before. Spectral analysis for calculating moment magnitudes and synthetic Wood-Anderson seismograms for determining local magnitudes now can be performed. The aim of this study is to establish for Eastern Cuba the magnitude scales normally reported in international seismological bulletins. In this sense, a moment magnitude is established and a new coda-length and local magnitude scales are proposed. Since moment magnitude needs an attenuation relationship, which did not exist for Cuba, the quality factor Q and the near-surface attenuation factor kappa were also determined.

2. TECTONICS AND SEISMICITY

The island of Cuba can be considered as a block (Iturralde, 1977; Cotilla, 1998), which is limited to the north by Nortecubana fault system (NCFS) and to the south by OFZ and Surcubana fault system (SCFS) (Figure 1). Along the southern Cuban margin lies the Oriente Fault Zone (OFZ), a fault system marking part of the boundary between the North American and Caribbean Plates, where strike-slip deformation dominates (Rosencrantz and Mann, 1991). It extends over 900 km from the Cayman Spreading Center (CSC) to the central Dominican Republic (Figure 1). The CSC is an oceanic crust spreading center that has been active since the Middle Eocene and is currently spreading at a rate of about 15 mm/year (Rosencrantz et al., 1988). According to De Mets et al., (2000) the Caribbean Plate is moving eastward relative to the North American Plate (NAP) an average of 18-20 ± 3 mm/yr with 18 ± 2 mm/yr of boundary-parallel slip and 3 ± 3 mm/yr of boundary-normal convergence south of eastern Cuba. This eastward motion of the Caribbean plate produces left-lateral slip along

the Enriquillo (EFZ) and Walton Fault Zones (WFZ), and left-lateral strike-slip deformation along the OFZ (Figure 1).

The OFZ, EFZ and WFZ mark the north and south boundaries of the Gonave Microplate (GM). Along the releasing and restraining bends of the OFZ there are two local structures affecting the tectonic regime in this area: (1) the Cabo Cruz Basin (CCB) and (2) the Santiago Deformed Belt (SDB). More than 90% of the seismic activity along the southern Cuban is generated in these structures. The CCB is a narrow E-W trending depression (8-15 km wide by 80 km long), bordered on the north and south by two segments of the OFZ and divided by normal faults into a series of oblique horsts and grabens (Calais & Mercier de Lépinay. 1991). The discontinuous trace of the OFZ includes left-stepping offsets that generate local tensional strain and causes pull-apart subsidence (Cotilla, 1998; Perrot et al., 1997). The SDB is a narrow submarine mountain range extending over 300 km along the OFZ in the eastern half of the southern Cuban margin. Its en echelon folds and thrust faults show clear evidence of transpressional deformation (Calais & Mercier de Lépinay. 1990).

The earthquake activity in Cuba is concentrated along the OFZ (Figure 1) but is not restricted to interplate seismicity, as small and moderate intraplate events are occurring throughout the country. The intraplate seismicity seems to be localized along the pre-existing zones of crustal weakness (Cotilla, 1998).

3. SEISMOGRAPH NETWORK AND DATA

The new Cuban seismograph network (CSN) consists of 7 broadband stations and 4 telemetered short-period stations (Figure 2 and Table 1). The broadband stations are equipped

with Chinese 3-component FSB-3 seismometers recording at a frequency band of 0.05 to 40 Hz. The short-period stations are equipped with Russian 3-component CM3 seismometers. All the stations are sampling at 100 Hz with a dynamic range of 96 db (Moreno, 2002).

Data preparation and most of the computation was done with the SEISAN software (Havskov and Otemöller, 2001). To estimate the quality factor Q and the near-surface attenuation factor kappa, waveforms recorded during the first two years of the CSN were used (Figure 1). During the data selection, all the traces were checked by visual inspection. The earthquakes used to determine the new coda and local magnitude scales were also selected from this dataset (Figure 2). The data selection was based on two principles: (1) uniform distribution of earthquake locations across the area and (2) wide range of earthquakes magnitudes. Unfortunately, the distribution of seismic activity in Cuba makes difficult to follow the first criteria. The earthquakes are concentrated along the releasing and restraining bends of the major Oriente transform fault (Moreno, 2002). A wide range of magnitudes also was difficult to obtain given the sparse occurrence of moderate and strong earthquakes. Only 3 events with magnitudes bigger than 4 and 1 event with magnitude bigger than 5 (5.6 Mw) were found in two years of seismic activity (Figure 2). The geographical distribution of the seismic stations limited the selection of earthquakes with magnitude lower than 1.5. The previous magnitudes found in the earthquake catalogue were determined with the local magnitude scale developed by Moreno (1998). A total of 68 earthquakes were re-analysed by checking arrival times and amplitude values of the observed phases.

4. THE MOMENT MAGNITUDE

The moment magnitude can be determined from spectral analysis assuming that the displacement source spectrum of the earthquakes follow the Brune's source model (Brune, 1970). According to Kanamori (1977) the moment magnitude is defined as

$$M_w = \frac{\log(M_0)}{1.5} - 6.06 \qquad (4.1)$$

with $M_0 = 4\pi\rho v^3 \Omega_0 G(r,h)C$, where v is the seismic wave velocity (P or S) at the source, $G(r,h)$ is geometrical spreading, r is epicentral distance, h is focal depth, Ω_0 is the flat spectral level on the displacement source spectrum and C is a factor to correct for the free surface effect and radiation pattern.

The displacement source spectrum can be represented as

$$S(f) = \frac{\Omega_0}{1 + (\frac{f}{f_0})^2} \qquad (4.2)$$

where fo is known as the corner frequency. The spectrum is flat for f<fo and decays as f^2 for f>fo.

The observed source spectrum at the receiver is affected by the seismic wave attenuation along the ray path. This attenuation can be described as

$$A(f,t) = A_0 e^{-\pi f \kappa} e^{-\frac{\pi f t}{Q(f)}} \qquad (4.3)$$

6

where A_0 is the initial amplitude, k (kappa) is a constant to correct the attenuation for the near surface layers (1-3 km) and Q(f) is a function to correct the attenuation for the rest of the ray path. For local crustal studies, Q has often been considered to be constant along the ray path but it has been shown that near surface layers generally have a much lower Q than the rest of the path and tend to filter out high frequency energy (Abercrombie 1995, 1997). The function Q, also called the quality factor Q, is frequency dependent (in general for f > 1Hz) in the form

$$Q(f) = Q_0 f^{\alpha} \quad (4.4)$$

Therefore, the multiplication of (4.2) by (4.3) gives the complete shape of the observed spectrum as

$$A(f,t) = A_0 \frac{\Omega_0}{1+(\frac{f}{f_0})^2} e^{-\pi f \kappa} e^{-\frac{\pi f t}{Q(f)}} \quad (4.5)$$

We must then estimate the parameters k, Qo and α to model the displacement source spectrum.

4.1. Estimation of the quality factor Q

The quality factor Q was estimated following two distinct procedures: (1) Coda Q and (2) spectral ratio between two stations. The first method assumes that coda waves are S to S backscattered waves (Aki, 1981), which is consistent with the observation of equivalence between coda Q and Q of direct shear waves (Aki, 1980). The second method is based on the principle that if the seismic waves are recorded at two different stations with similar site

conditions then the difference in amplitude, at a given frequency, is due to attenuation and geometrical spreading. Below is shown a brief description of both methods.

Coda Q method

According to Aki and Chouet (1975), coda waves decrease in amplitude due to attenuation and geometrical spreading as

$$A(f,t) = t^{-\beta} A_0 e^{-\pi f \kappa} e^{-\frac{\pi f t}{Q(f)}} \qquad (4.6)$$

where β represents the geometrical spreading (1 for body waves and 0.5 for surface waves) and t is the elapsed time measured from origin. Usually it is assumed that coda waves are body waves. Taking the logarithm, (4.6) can be written as

$$\ln(A(f,t)) + \beta \ln t = (\ln(A_0) - \pi f \kappa) - \frac{\pi f t}{Q(f)} \qquad (4.7)$$

The Q value is determined by linear regression of ln(A(f,t))+βln(t) as a function of t at a constant frequency. The amplitude A(f,t) is obtained by bandpass- filtering the signal with a narrow passband around f and fitting a time decay envelope to the filtered signal (Rautian and Khalturin, 1978). The linear least-squares analysis of (4.7) is applied to one particular bandpass-filtered recording. To obtain an averaged Q from a number of events, all data can be inverted simultaneously for one particular frequency. However, in order to eliminate bad fit for each individual case we follow Kvamme (1985), who has shown that obtaining one Q value for each decay curve and averaging the Q^{-1} value gives the same result.

Spectral ratio method

The amplitudes of a single event recorded at two stations (after removal of the instrument response) can be written as

$$A_1(f,t_1) = t_1^{-\beta} A_0 e^{-\pi f \kappa} e^{-\frac{\pi f t_1}{Q(f)}} \quad \text{and} \quad A_2(f,t_2) = t_2^{-\beta} A_0 e^{-\pi f \kappa} e^{-\frac{\pi f t_2}{Q(f)}} \quad (4.8)$$

Therefore, the spectral ratio at a given frequency between the stations is defined as

$$\frac{A_2(f,t_2)}{A_1(f,t_1)} = (\frac{t_2}{t_1})^{-\beta} e^{\frac{\pi f (t_2-t_1)}{Q(f)}} \quad (4.9)$$

Q(f) is the only unknown in (4.9) and can be determined as

$$Q(f) = \frac{-\pi f (t_2 - t_1)}{\ln(A_2(f,t_2)/A_1(f,t_1)) + \beta \ln(t_2/t_1)} \quad (4.10)$$

In this method there are two features that may affect the results, which are the local site effect at the station and the source radiation. To decrease the local site effect, use of vertical components are recommended and stations with good signal-to-noise ratio must be selected. The effect of the source radiation can be removed by requiring that the stations and the source are on one line (same azimuth with respect each other). More details about the method can be found in Campillo et al. (1985) and Kvamme and Havskov (1989).

Coda Q estimation

The Q values were determined by bandpass-filtering the signal with center frequencies 2, 4, 8, 12 and 16 Hz, with respective band-widths of 1, 2, 4, 4 and 4 Hz. The filter used was an eight-pole recursive Butterworth filter with zero phase shift. Given the limited frequency band of the telemetered short-period stations, only the broadband stations were used. The bandpass filters were applied mainly to a coda-window length of 20 sec starting at 2 times the S travel time as recommended by Rautian and Khalturin (1978) (Figure 3) but others window-length and lapse-time were also tested. Signal-to-noise ratios were automatically checked in all frequency bands by calculating the ratio between the RMS amplitude of the last 5 sec of the coda signal and the noise before 5 sec of the P phase. It has been pointed out that data with a signal-to-noise ratio lower than 5 could affect the calculated Q values (Havskov et al., 1989). In this study, results with signal-to-noise ratio lower than 20 and correlation coefficient, obtained by fitting a time decay envelope of equation (4.7), lower than 0.6 were rejected. These selection criteria were based on a compromise between rejecting too much data and obtaining a high standard deviation in individual Q values.

It has been shown the variation of coda Q as a function of the lapse time and the window length (Lee et al., 1986; Kvamme and Havskov, 1989). The sampling volume for back-scattered coda waves at lapse time t is an ellipsoid with source and station at the focal points and semi-major axis equal to $v_s t/2$, where v_s is the S-wave velocity (Scherbaum and Kisslinger, 1985; Havskov et al., 1989). Therefore, increasing lapse time has been interpreted as increasing Q with depth (Ibañez et al., 1990). In order to investigate this issue the Q values were calculated for two different groups of data and for the entire dataset with different lapse times and window lengths (Table 2).

The data was categorized according to focal depths as shallow ($\leq$ 24 km) or deep ($>$ 24 km). The range of depth selected was based on the average of the focal-depth error, which is about 12 km and the deepest earthquake (49 km) of the dataset. The results obtained for the two groups do not show significant differences considering that they overlap within 1 standard deviation (Table 2). The average lapse time for the deep earthquakes is smaller because the concentration of relatively deep seismicity in the Santiago deformed belt (SDB) (Moreno, 2002), which have shorter average hypocentral distances in comparison with CCB and MOA zones (Figure 2), provide smaller average lapse time for this group. Therefore the gentle increase of Q obtained cannot be associated with depth because in fact the group of shallow earthquakes are sampling deeper structures. The result of Q for the group of deep earthquakes is biased for greater number of earthquakes recorded by RCC as compared to others stations. CIES station is very close to RCC but it has recorded few earthquakes due to unstable operation. Since the group of deep earthquakes is only 20% of the data, the result obtained from shallow earthquake reflects the averaged Q values for the entire region. Unfortunately there is not a good control in depth to group the earthquakes by narrower range of focal depths.

The average quality factor Q using all the data was determined applying different window length and lapse time. The Q values seem to increase when using a longer window-length. However, when using larger lapse time the results are quite similar and do not show any tendency to increase. Both the minimum and maximum sampled volumes defined by the lapse times used include the crust and part of the mantle, suggesting that the attenuation does not change significantly at least from 50 to 100 km depth. Here, we do not have enough data with short lapse time to see changes of Q within a crust of thickness 15-30 km (Otero et al., 1998).

Most of the solutions shown in Table 2, excepting the results obtained with a 25 and 30 sec of window-length, fall within 1 standard deviation. Based on the standard deviation, using 20 sec of window-length seems to be suitable to obtain a more reliable solution. Considering the number of station-event-frequency combinations used as well as the standard deviation, the solution obtained when using lapse time of 2 times the S travel time and a window-length of 20 sec is chosen as a final solution.

Spectral ratio between two stations

Regarding the requirements mentioned before, it was only possible to use one pair of stations, MOA and MAS. For this purpose were used the group of earthquakes close to the Moa station (at North-West of Moa station) which are just below (following the CNF) of the cluster of earthquakes located in the apparent interception of the NCFS and CNF (Figure 1). The selected waveforms were required to have a signal-to-noise ratio of 10. The time window was chosen to include S waves within a length of 3 sec. This time-window length represents a compromise between trying to include only direct S waves and not using a too narrow frequency-band. Figure 4 shows the results of the Q values using the coda Q (Figure 4A) and the average spectral differences of 8 displacements spectral (Figure 4B). The results overlap within 1 standard deviation, which indicate that the quality factor obtained from coda Q analysis is quite representative for the region and equivalent to the Q of direct S waves.

4.2. Near-surface attenuation

The principle to determine the constant k (kappa), which is associated with near-surface attenuation, is based on the assumption that the straight line fitting the logarithm of (4.5) for

frequencies f < fo has slope of $\pi(k+t/Q)$, if Q is frequency independent (Havskov and Otemöller, 2001). Here, we consider (4.5) to represent the spectral content of a signal with a constant travel time t. If t/Q is small, the slope will be directly proportional to k. Therefore, to reliably determine k without knowing Q, short hypocentral distances should be used. This restriction implies the use of small earthquakes to avoid saturation problems. The corner frequency fo depends on the stress drop and seismic moment (Lee and Stewart, 1981). In general the smaller the earthquake, the higher the corner frequency. Thus, the use of small earthquakes permits an increase in the length of the fitting straight line and therefore constrains the slope, but on the other hand, a high signal-to-noise ratio might not be present. The distribution of the seismic activity in Cuba (Moreno, 2002) makes difficult to develop this kind of study. There are two stations (CIES and RCC) recording earthquakes at relatively short hypocentral distances of about 40 km, but small earthquakes in this area were characterized by poor signal to noise ratio.

A good opportunity to estimate k was given by a swarm, which occurred very close (less than 20 km) to the MOA station in July 1999 (Moreno, 2002). The location accuracy of the swarm was improved with the installation of additional field stations in this area. Several small earthquakes were visually checked for a reasonable signal-to-noise ratio. Over 95 kappa (k) values were determined and those with correlation coefficient of the straight line fitting the logarithm of (4.5) larger than 0.75 were selected. The displacement spectra of S waves were calculated within a time window of 2 sec. Figure 5 shows the results of k obtained from 20 earthquakes having magnitudes between 0.8 and 1.2. The averaged k=0.03 is consistent with results obtained for rock sites, which is normally between 0.02 and 0.04 (Anderson and Hough, 1984). Site conditions at seismic stations in Cuba do not have significant differences. Most of the stations in eastern Cuba are located in exposed pre mid-Eocene basic to ultra-

basic igneous and volcanic rocks (Pardo, 1975; Draper and Barros, 1994). Therefore, it is assumed that the obtained value of k could be applied to all of the seismic stations in this region.

In summary, to calculate moment magnitude the following constants are used: Q_0=76, α=0.8 and k=0.03.

5. THE NEW LOCAL MAGNITUDE SCALE

Following Hutton and Boore (1987), the local magnitude scale can be written as

$$Ml = \log_{10}(A) + \alpha\Delta + \beta\log_{10}\Delta + K + Cs \qquad (5.1)$$

where A is the maximum amplitude in millimeters of the Wood-Anderson instrument, Δ is the hypocentral distance, α and β are the attenuation and geometrical spreading, respectively, and K is a constant which allows to fit the magnitude scale to an established scale. The Cs terms are the station correction factors. The absolute value of the scale is defined so that an amplitude of one millimeter on the seismogram at a distance of 100 km gives a magnitude of 3.

The attenuation coefficients, earthquake magnitudes and station corrections are determined from regression analysis represented by the following equation

$$-\log_{10}(A_{ij}) = \alpha\Delta_{ij} + \beta\log_{10}(\Delta_{ij}) - Ml_j + Cs_i \qquad (5.2)$$

where i goes from 1 to the number of stations (N) and j goes from 1 to the number of earthquakes (M). The system is subjected to two constraints: (1) trace amplitude of one millimeter at 100 km distance gives magnitude 3 and (2) the sum of the station corrections must be zero. The constraints are represented as

$$-\log_{10}(\frac{1000000}{2050}) = \alpha 100 + \beta \log_{10}(100) - 3 \qquad (5.3)$$

$$0 = Cs_1 + Cs_2 + Cs_3 + ... + Cs_N \qquad (5.4)$$

Since ground displacements normally are given in nanometers, the one millimeter amplitude on the Wood-Anderson trace in (5.3) was converted to nanometers. Note that 2050 is the magnification of the Wood-Anderson instrument (Hutton and Boore, 1987). There is some uncertainty in the magnification to be used for the Wood-Anderson instruments. Hutton and Boore (1987) pointed out that the effective magnification of operating Wood-Anderson instruments seems to be much lower than 2800, which is the value that it has been normally used (Richter, 1958).

The first constraint (5.3) and the equation (5.2) are combined as

$$-\log_{10}(A_{ij}) - 3 + \log_{10}(488) = \alpha(\Delta_{ij} - 100) + \beta \log_{10}(\frac{\Delta_{ij}}{100}) - Ml_j + Cs_i \qquad (5.5)$$

which represents an over-determined inverse problem with N + M + 2 unknowns. The inverse problem can be solved through the least squares method subjected to the constraint 5.4 (Menke, 1989).

15

To determine the attenuation function a total of 602 waveforms were selected. The waveforms consist of horizontal components, where both components of the station were used as individual data. For each event at least 6 readings were required. The waveforms were simulated to Wood-Anderson traces by applying an 8 pole band-pass filter in the frequency band from 1.25 Hz to 20 Hz after instrument correction (Havskov and Otemöller, 2001). Table 3 shows the distribution of magnitudes versus hypocentral distances for the selected waveforms. In general there is an acceptable coverage in both magnitude and distance for performing an inversion process.

The results of the inversion process gave 0.89 ($\pm$0.21) for the geometrical spreading (β) and 0.0031 ($\pm$0.0009) for the attenuation (α). The station corrections Cs with the corresponding standard deviations are shown in Table 4. Differences in stations corrections are thought to arise from differences in site geology. However, when earthquakes are not widely distributed across the area, differences in attenuation along the path could affect the station correction (Hutton and Boore, 1987). Due to the fact that the seismicity in Cuba is clustered in few seismogenic sources (Moreno, 2002) the attenuation along the path must be considered as a possible factor affecting the station corrections (see discussion). The scaling factor K is determined by anchoring the obtained magnitude scale to the original Richter scale at a given distance. Hutton and Boore (1987) suggested that local magnitude must be defined such that an event of magnitude 3 corresponds to 10 mm of motion on a Wood-Anderson (WA) instrument at a hypocentral distance of 17 km. This definition is consistent with Richter's (1935) original definition and allows more flexibility when the attenuation within the first 100 km has a large geographic variation. Following this new definition, the Cuban scale was anchored at a distance of 17 km. The new Cuban local magnitude scale is defined as

$$Ml = \log_{10}(A) + 0.89\log_{10}(\Delta) + 0.0031\Delta - 1.804 \qquad (5.6)$$

with A the trace amplitude on the simulated WA record, K=-1.804 and Δ the distance in km.

6. THE NEW CODA MAGNITUDE SCALE

A coda magnitude scale has never been developed in Cuba. According to Lee et al. (1972) the coda magnitude scale can be represented as

$$Mc = a\log_{10}(t) + b\Delta + c \qquad (6.1)$$

where t is the coda length in seconds, Δ is the hypocentral distance in km and a, b and c are constants to be determined. The coefficients are obtained from regression analysis by replacing the left term in (6.1) by a known magnitude. In this case the moment magnitudes (Mw) of the earthquakes plotted in Figure 2 were used.

The least square solution of the system formed by 243 equations gave values of a=1.89 ($\pm$0.30), b=0.0017 ($\pm$0.0010) and c=0.97 ($\pm$0.27). Therefore the coda magnitude scale is calculated as

$$Mc = 1.89\log_{10}(t) + 0.0017\Delta - 0.97 \qquad (6.2)$$

This scale can be compared to the scale obtained by Lee et al. (1972) for central California

$$Mc = 2.0\log_{10}(t) + 0.0035\Delta - 0.87 \qquad (6.3)$$

and the scale obtained by Real and Teng (1973) for southern California (Mc < 3.9)

$$Mc = 1.89 \log_{10}(t) + 0.0009\Delta - 1.01 \qquad (6.4)$$

Independent of the tectonic setting, the scale of Lee et al. (1972) seems to over correct for distance when compared to scales developed for other regions (Chaplin et al., 1980; Havskov and Macias, 1983). The larger distance-correction factor obtained in this study in comparison to (6.4) suggests that coda waves have higher attenuation in eastern Cuba and this may be due to a thinner oceanic crust in eastern Cuba as compared to a continental crust in California.

Note that the station corrections were not determined for the coda magnitude scale. The station corrections in this case are quite subjective because the coda length also depends on the signal-to-noise ratio, which has random variation. Therefore, it is difficult to associate station corrections with geological site condition since local noise sources also might influence the station corrections.

7. DISCUSSION AND CONCLUSIONS

Attenuation of body waves in Cuba seems to be stronger in comparison with other regions (Figure. 6). The quality factor Q and the local magnitude attenuation curve for eastern Cuba indicates higher attenuation when compared to southern Norway and southern California. Southern Norway with the lowest attenuation reflects a continental region, which is part of the Baltic Shield area. It is an old shield area with low seismic activity (Kvamme and Havskov, 1989). Southern California has also a continental crust but in contrast to southern Norway it

has a younger lithosphere subjected to intensive deformation (Humphreys, 1990). Part of eastern Cuba and Jamaica, on the other hand, are within an oceanic crust (Case et al., 1990), and this suggest higher attenuation in comparison to southern California. The attenuation in eastern Cuba seems to be a little lower than Jamaica. They are located in different tectonic plates, North America and Caribbean plates, with different tectonic pattern. It has been pointed out (Draper and Barros, 1994) that Cuba contains Precambrian rocks and extensive outcrops of continental margin, sedimentary rocks of Jurassic to Cretaceous age, which are not present in the other islands of the Greater Antilles.

The new Cuban attenuation curve for Ml (lower graph in Figure 6) is almost identical in the first 140 km to the one obtained by Hutton and Boore (1987) for the southern California, but with some increases for larger distances. The apparent lower attenuation shown in the previous magnitude scale developed by Moreno (1998) may be accounted for by some systematic error in the amplitude values measured on visual records. At short distances (less than 150 km) there is not significant change in the magnitude values when using any of the attenuation curves plotted in Figure 6. At a distance of 300 km the magnitude is underestimated, when applying the previous Moreno (1998) local magnitude scale, by 0.3 units with relation to the new local magnitude scale.

Figure 7 shows a relationship between the moment magnitudes with the new coda and local magnitudes obtained in this study. Considering Mw as the most reliable magnitude scale (Lay and Wallace, 1995), the Ml-Mc relationship in Figure 7 suggests that the local magnitude scale underestimates the magnitude of small earthquakes (less than 3.0) and overestimates the magnitude of moderate and strong earthquakes. The difference could be -0.3 units for Mw=1.0 and +0.3 units for Mw=6. However, these relationships are biased by the non-

uniform distribution of the magnitudes, since more than 50% of the earthquakes have magnitudes between 2 and 3 and few have magnitudes above 4. Note that the dashed line representing a one-to-one correlation shows narrow scatter along the entire magnitude range. A possible magnitude-dependence in the shape of the attenuation curves of local magnitudes has been previously suggested (Luco, 1982), but the study developed by Hutton and Boore (1987) denied this assumption. Unfortunately, in this study the magnitude resolution is not sufficient to assess this problem. The Mw-Mc relationships also shows narrow scatter, although for the largest earthquake (Mw=5.6) there is a significant difference of 0.4 units. Real and Teng (1973) observed a gradual change in the slope of the relationship between Ml and log(t) for magnitudes above 3.8 and, therefore, a quadratic term in log(t) was included. The disagreement observed in this study may suggest that the proposed scale might not be suitable for earthquakes with magnitude above 5, but unfortunately there is not enough data to develop a coda-length scale for this range of magnitudes.

Another aspect to be discussed is the station corrections for the local magnitude scale. To see how the attenuation varies along the ray path, the stations corrections of three stations from average residual of equation (5.6) were determined for two different zones, the CCB and MOA zones (Figure 2 and Figure 8). Figure 8 shows a difference of 0.65 units between RCC and LMG for the earthquakes located in the CCB zone. However, the difference goes down to 0.17 for the earthquakes located in the MOA zone. Source radiation has a little effect because there is not significant difference in backazimuths between these stations. The difference in the station-hypocenter distance between both zones is also not significant to make the distance-correction coefficient responsible for such a change. The observed decrease of about 0.48 units in the station correction obtained for the MOA zone is mainly attributed to a different attenuation along the path. The ray-paths of earthquakes recorded by RCC, which

are generated in the CCB zone, follow an E-W oriented plate boundary zone (Figure 2) where lateral seismic wave velocity variations have been observed (Ewing et al., 1960). This complex crustal structure causes highly scattered seismic waves along the plate boundary. Furthermore, since it is not practical to have azimuth dependence in the station corrections for all stations and not enough data is available to calculate them, the station corrections obtained in this study are not recommended to be used in the local magnitude determination. Because the low number of earthquakes with magnitude greater than 4 and 5 used in this study, the proposed magnitude scales could be not suitable for earthquakes with magnitudes greater than 5.

The conclusions of this study can be summarized as follows:

1. Both the quality factor Q and the attenuation relationship for the local magnitude scale obtained in this study suggest high attenuation for eastern Cuba.

2. The station-corrections of magnitude values suggest that the attenuation seems to have strong ray-path dependence caused by the complex crustal structure along the boundary of the Caribbean and North American plates.

3. For the first time a moment magnitude and a more reliable coda and local magnitudes can be reported in the Cuban catalogue.

ACKNOWLEDGMENTS

REFERENCES

Abercrombie, R.E., 1995, Earthquake source scaling relationships from −1 to 5 Ml using seismograms recorded at 2.5-km depth, J. Geophy. Res., **100**, 24015-24036.

Abercrombie, R.E., 1997, Near-surface attenuation and site effects from comparison of surface and deep borehole recordings, *Bull. Seism. Soc. Am.* **87**, 731-744.

Alvarez, L., Mijailova, R.S., Vorobiova, E.O., Chuy, T.J.,Zhakirdzhanova, G.N., Perez, E.R., Rodionova, L.M., Alvarez, H.,Mirzoev, K.M., 2000, Terremotos de Cuba y áreas aledañas. *in Sismicidad de Cuba y estructura de la corteza en el Caribe*. Editorial Academia. ISBN 959-02-0242-X, pp. 7-35.

Alvarez, L. Chuy, T., Garcia, J., Moreno, B., Alvarez, H., Blanco, M., Expósito, O., Gonzales, O., Fernandez, A.I., 1999, An earthquake catalogue of Cuba and neighboring areas, ICTP Internal Report IC/IR/99/1, Miramare, Trieste, 60 pp.

Alvarez, L. and Bune, V.I., 1977, Estimación de la peligrosidad sísmica para la región suroriental de Cuba (en ruso).Izvestiya Akademii Nauk SSSR, Fizika Zemli, No. 10, pp. 54-67.

Anderson, J. G. and Hough, S. E., 1984, A model for the shape of the fourier amplitude spectrum of acceleration at high frequencies, *Bull. Seism. Soc. Am.* **74**, 1969-1993.

Aki, K., 1980, Attenuation of shear waves in the lithosphere for frequencies from 0.05 to 25 Hz, *Phys. Earth Planet. Interiors* **74**, 615-631.

Aki, K., 1981, Attenuation and scattering of short-period seismic waves in the lithosphere, *in Identification of Seismic Sources - Earthquakes or Underground Explosions*, ed. Husebye, E. S. and Mykkeltveit, S., D. Reidel Publishing Co., Dordrecht, The Netherlands.

Aki, K. and Chouet B., 1975, Origin of coda waves: source, attenuation and scattering effects, *J. Geophys. Res.*, **80**, 3322-3342.

Brune, J. N., 1970, Tectonic stress and spectra of seismic shear waves, *J. Geophys. Res.* **75**, 4,997-5,009.

Campillo, M., Planet J. L., and Bouchon M., 1985, Frequency-dependent attenuation in the crust beneath central France from Lg waves: data analysis and numerical modelling, *Bull. Seism. Soc. Am.* **75**, 1395-1411.

Case, J.E., MacDonald, W.D., and Fox, P.J., 1990, Caribbean crustal provinces; Seismic and gravity evidence, *in The Geology of North America, The Caribbean Region*, Vol. H, pp. 15-36, ed. Dengo, G. & Case, J.E., Geological Society of America, Boulder, Colorado.

Calais, E., and B. Mercier de Lépinay, 1990, A natural model of active transpressional tectonics: The *en échelon* structures of the Oriente deep along the northern Caribbean transcurrent plate boundary (Southern Cuban margin), *Rev. Inst. Fr. Pét.* **45**, 147-160.

Calais, E., and B. Mercier de Lépinay, 1991, From Transtension to Transpression along the Southern Caribbean Plate Boundary of Cuba: implications for the Recent motion of the Caribbean plate, *Tectonophysics,* **186**, 329-350.

Chaplin, M. P., Tayler, S. R., and Toksoz, M. N, 1980, A coda-length magnitude scale for New England, *Earthquake Notes*, **51**, 15-22.

Cotilla, M., 1998, An overview on the seismicity of Cuba, *Journal of Seismology,* **2**, 323-335.

De Mets, C., P. E. Jansma, G. S. Mattioli, T. Dixon, F. Farina, R. Bilham, E. Calais, and P. Mann, 2000, GPS geodetic constraints on Caribbean - North American Plate motion, *Geophys. Res. Lett*. **27**, 437 – 440.

Draper, G. and Barros, J.A., 1994, Cuba (chapter 4), *in Caribbean Geology: An Introduction*, pp. 65-85, U.W.I. Publishers' Association, Kingston.

Ewing, J., Antoine, J. and Ewing M., 1960, Geophysical measurements in the western Caribbean Sea and in the Gulf of Mexico, *J. Geophys. Res.*, **65**, 4087-4126.

Havskov, J., and Macias, M., 1983, A coda-length magnitude scale for some Mexican stations, Geofisica Internacional, **22**, 205-213.

Havskov, J., Malone, S., McClurg, D. and Crosson R., 1989, Coda Q for the state of Washington, *Bull. Seism. Soc. Am.* **79**, 1024-1038.

Havskov J. and L. Otemöller (editors), 2001, *SEISAN: The earthquake analysis software*, Version 7.2, Institute of Solid Earth Physics, University of Bergen, Norway, 255 pp.

Humphreys, E. D., 1990, A kinematic model for the late Cenozoic development of southern California crust and upper mantle, *J. Geophys. Res.* **95**, 19,747-19,762.

Hutton, L. K. and Boore, D. M., 1987, The Ml scale in Southern California, *Bull. Seism. Soc. Am.* **77**, 2074-2094.

Ibañez, et al., 1990, Depth dependent seismic attenuation in the Granada zone (Southern Spain), Bull. Seism. Soc. Am. **80**, 1460-1472.

Iturralde, M. (1977). *The tectonic movements of the development plataformic stage of Cuba*, File Report 20, Inst. of Geology and Paleontology, Acad. of Sciences of Cuba, 20 pp.

Kanamori, H., 1977, The energy release in great earthquakes, *J. Geophys. Res.* **82**, 1,981-1,987.

Kvamme, L.B., 1985, Attenuation of seismic energy from local events in Norwegian areas, *M. Sc. Thesis*, University of Bergen, Norway

Kvamme, L. B. and Havskov, J., 1989, Q in southern Norway, *Bull. Seism. Soc. Am.* **79**, 1575-1588.

Lay, T. and Wallace, T.C., 1995, *Modern Global Seismology*, Academic Press, New York.

Lee, W. H. K., Bennet, R. E. and Meaguer, L., 1972, A method for estimating magnitude of local earthquakes from signal duration, U.S.G.S. Open file report.

Lee, W. H. K. and Stewart, S. W., 1981, Principles and applications of microearthquake networks, Academic press., New York.

Lee, W. H. K., Aki, K., Chouet B., Johnson, P., Marks, S., Newberry, J. T., Ryall, A. S., Stewart, S. W., and Tottingham, D. M., 1986, A preliminary study of coda-Q in California and Nevada, *Bull. Seism. Soc. Am.* **76**, 1133-1142.

Luco, J. R., 1982, A note on near-source estimates of local magnitude, *Bull. Seism. Soc. Am.* **72**, 941-958.

Menke W., 1989, Geophysical data analysis: Discrete inverse theory, Academic Press, Inc. San Diego, California.

Moreno, 1998, Local magnitude scale for eastern Cuba and softwares for macroseismic database and paleoseismology, *M. Ss. Thesis*, University of Bergen, Norway, 123 pp.

Moreno B., 2002, The new Cuban Seismograph Network, *Seism. Res. Lett.,* **73**, 505-518.

Otero, R., Prol, J.L., Tenreyro, R., Arriaza, G.L., 1998, Caracteristicas de la corteza terrestre de Cuba y su plataforma marina (Characteristics of the Earth's crust in Cuba and its marine platform), *Mineria y Geologia* **15**, 31-35.

Pardo, G., 1975, Geology of Cuba (chapter 13), *in The Ocean Basins and Margins,* Vol. 3, pp. 553-615, ed. A.E.M., Nairn and F.G., Stehli, Plenum Publishing, New York.

Perrot, J., E. Calais, and B. Mercier de Lépinay (1997). Tectonic and Kinematic Regime along the Northern Caribbean Plate Boundary: new insights from Broad-band Modelling of the May 25, 1992, Ms=6.9 Cabo Cruz, Cuba, earthquake, *Pure Appli. Geophys*. **147**. 475-487.

Raoof, M., Herrmann, R. B., and Malagnini, L., 1999, Attenuation and Excitation of Three-component Ground Motion in Southern California, *Bull. Seism. Soc. Am.* **89**, 888-902.
Rautian, T. G. and Khalturin, V. I., 1978, The use of the coda for determination of the earthquake source spectrum, *Bull. Seism. Soc. Am.* **68**, 923-948.

Real, C. R., and Teng, T., 1973, Local Richter magnitude and total signal duration in Southern California, *Bull. Seism. Soc. Am.* **63**, 1809-1827.

Richter, C. F., 1935. An instrumental earthquake magnitude scale, *Bull. Seism. Soc. Am.* **25**, 1-32.

Richter, C. F., 1958, *Elementary Seismology*, W. H. Freeman and Co., San Francisco, 578 pp.

Rosencrantz, E. and P. Mann (1991). Sea MARC II mapping of transform faults in the Cayman Trough, Caribbean Sea, *Geology* **19**, 690-693.

Rosencrantz, E., M. I. Ross, and J. G. Sclater (1988). Age and spreading history of the Cayman Trough as determined from depth, heat flow, and magnetic anomalies, *J. Geophys. Res.* **93**, 2,141-2,157.

Scherbaum, F., and Kisslinger C., 1985, Coda Q in the Adak seismic zone, *Bull. Seism. Soc. Am.* **75**, 615-620.

FIGURES CAPTIONS AND TABLES

Figure 1. Kinematic framework along southern Cuban margin. OF- Oriente Fault; WFZ – Walton Fault Zone; EFZ – Enriquillo Fault Zone; CNF – Cauto Nipe fault; NCFS – Nortecubana fault system; SFZ- Swan Fracture Zone; CSC - Cayman Spreading Centre; GM- Gonave Microplate; CCB- Cabo Cruz Basin; SDB- Santiago Deformed Belt. The mapped OF including the CCB and SDB is taken from the interpretation made by Calais and Mercier de Lépinay (1990, 1991) during the SEACARIB II oceanographic cruise. Dashed lines represent assumed traces of faults. Open circles shows 569 earthquakes recorded by 3 or more stations during March 1998 to July 2000.

Figure 2. Seismic stations (triangles) and earthquakes (circles) used to determine the local and coda magnitude scales. OF – Oriente Fault, CCB – Cabo Cruz Basin, SDB – Santiago Deformed Belt. Moa zone is defined to label the group of earthquakes located at North of Moa seismic station.

Figure 3. Example of an unfiltered and bandpass-filtered trace used in the Coda Q determination.

Figure 4. Result of the Q values with the corresponding standard deviations (dashed line). A - Coda Q, B - Average of 8 displacement spectral ratio.

Figure 5. Results of the factor kappa (k) obtained from 20 earthquakes having magnitudes between 0.8 and 1.2. A - Averaged displacement spectrum and standard deviation (dashed line), B – Individual k values.

Figure 6. Attenuation relationship for eastern Cuba and other regions. Upper graph - Frequency-dependent quality factor Q, (A) Southern Norway (Kvamme and Havskov, 1989), (B) Southern California (Raoof et al., 1999) (C) Eastern Cuba (This study), (D) Jamaica (Personal communication by Margaret Grandison). Lower graph – Attenuation curves for the local magnitude scale.

Figure 7. Correlation of local and coda magnitudes with moment magnitudes.

Figure 8. Station corrections of local magnitude of three stations calculated for two different zones in eastern Cuba and the corresponding standard deviations.

Table 1. Seismic stations of the CSN.

Station	Instrument Type	Latitude North (°)	Longitude West (°)	Elevation (meters)	P-wave Correction (sec)	S-wave Correction (sec)
CCC	Broad B.	21.1937	77.4172	90	1.22	3.37
RCC	Broad B.	19.9953	75.6965	100	0.00	-0.15
LMG	Broad B.	20.0673	77.0047	200	-0.02	0.08
MOA	Broad B.	20.6583	74.9568	140	-0.11	----
MAS	Broad B.	20.1760	74.2310	350	0.83	----
MCG	Broad B.	22.3333	80.0000	100	----	----
SOR	Broad B.	22.7830	83.0180	206	----	----
CIES	Short P.	20.0020	75.7710	40	-0.05	-0.10
YARC	Short P.	20.2000	76.2200	100	-0.15	-0.10
PINC	Short P.	20.4870	75.7910	647	0.00	0.96
SABC	Short P.	20.3800	75.1900	100	-0.11	0.18

Table 2. Results of Coda Q for three groups of earthquakes categorized by focal depth and for the entire dataset. N is the number of station-event-frequency combinations used. Numbers in brackets are the standard deviations.

Groups of earthquakes	Lapse Time (sec)	Window Length (sec)	N	Freq. 2 Hz	Freq. 4 Hz	Freq. 8 Hz	Freq. 12 Hz	Freq. 16 Hz	Q_o	α
Shallow < 24km	50	20	181	132	227	391	538	675	76	0.79
(Std. Deviation)	(±28)			(±11)	(±20)	(±35)	(±48)	(±60)	(±7)	(±0.04)
Deep > 24 km	37	20	38	139	254	464	662	850	76	0.87
	(±17)			(±21)	(±39)	(±72)	(±102)	(±132)	(±12)	(±0.07)
All	48	20	219	132	231	403	558	703	76	0.80
	(±27)			(±12)	(±21)	(±37)	(±51)	(±64)	(±7)	(±0.04)
All	45	25	261	177	304	524	720	903	102	0.78
	(±26)			(±18)	(±31)	(±53)	(±73)	(±92)	(±11)	(±0.05)
All	47	30	276	200	336	566	767	952	119	0.75
	(±27)			(±15)	(±26)	(±44)	(±60)	(±75)	(±9)	(±0.04)
All (constant lapse time)	30	20	81	149	263	466	650	824	84	0.82
				(±22)	(±40)	(±71)	(±99)	(±126)	(±13)	(±0.06)
All (constant lapse time)	40	20	77	142	252	447	625	793	80	0.83
				(±10)	(±19)	(±34)	(±47)	(±60)	(±6)	(±0.03)
All (constant lapse time)	50	20	63	141	249	440	613	776	80	0.82
				(±4)	(±8)	(±15)	(±21)	(±27)	(±3)	(±0.02)

Table 3. Distribution of amplitude values used in the local magnitude scale for different ranges of magnitudes and distances. The ranges are 0.5 units for magnitudes and 50 km for distances.

Magnitude/ Distance (km)	1.75	2.25	2.75	3.25	3.75	4.25	4.75	5.25
25	13	17	20	0	2	7	0	0
75	25	42	55	6	8	9	0	4
125	19	34	37	10	18	7	6	2
175	4	31	40	12	19	2	4	6
225	0	10	19	8	1	4	0	0
275	0	2	19	30	10	0	4	4
325	0	2	2	10	0	0	0	0
375	0	2	0	8	0	0	0	0
425	0	0	0	4	0	0	0	0

Table 4. Station corrections for the local magnitude scale obtained in this study.

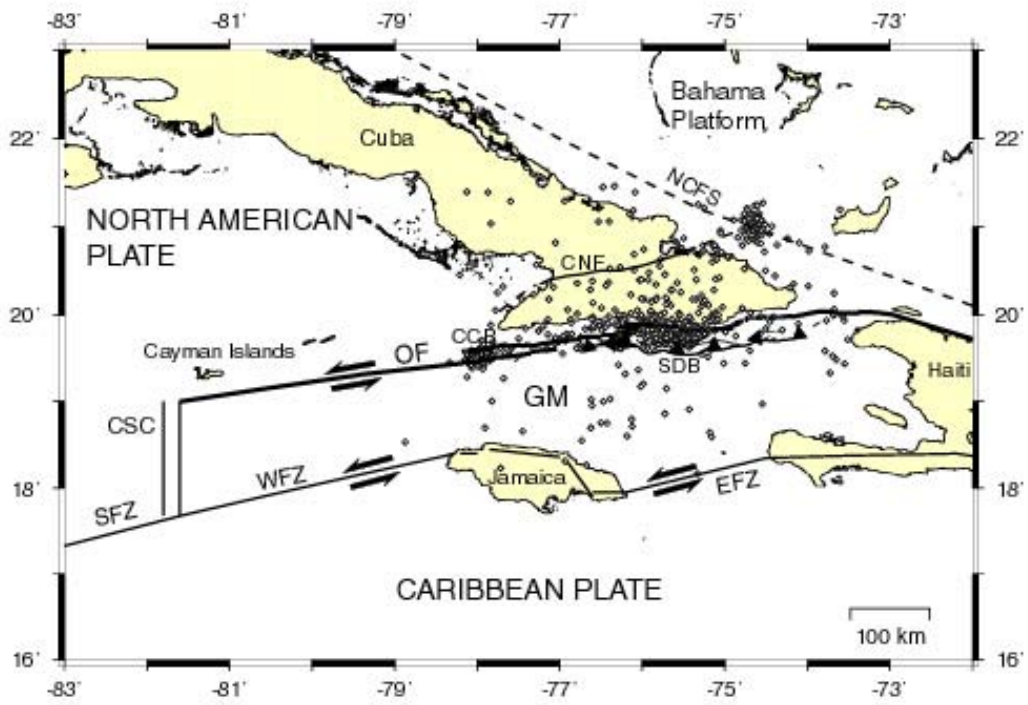| Station	LMG	CCC	RCC	MAS	MOA	YARC	PINC	SABC	CIES
Ml Correction	-0.36	0.21	0.27	0.30	-0.08	0.15	-0.18	-0.10	-0.21
Stand. Dev.	0.14	0.12	0.12	0.14	0.22	0.12	0.12	0.14	0.12

FIGURA 1

FIGURA 2

FIGURA 3

A) Coda Q

$Qo = 76 (\pm 7)$
$\alpha = 0.80 (\pm 0.04)$

B) Spectral ratio MOA/MAS

$Qo = 71 (\pm 10)$
$\alpha = 0.79 (\pm 0.08)$
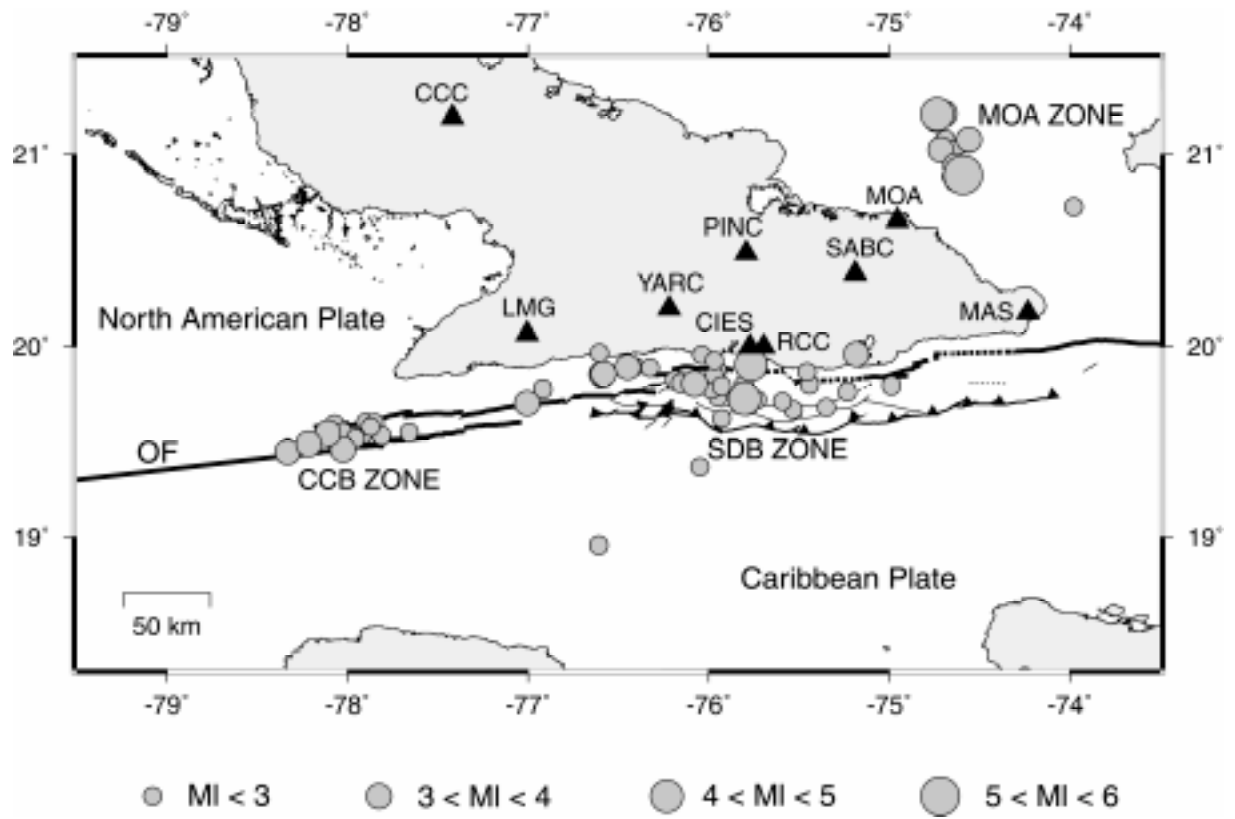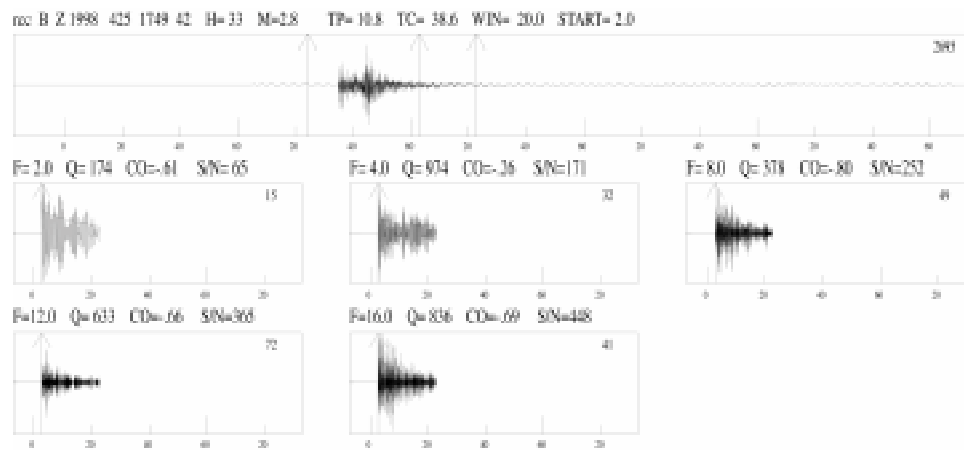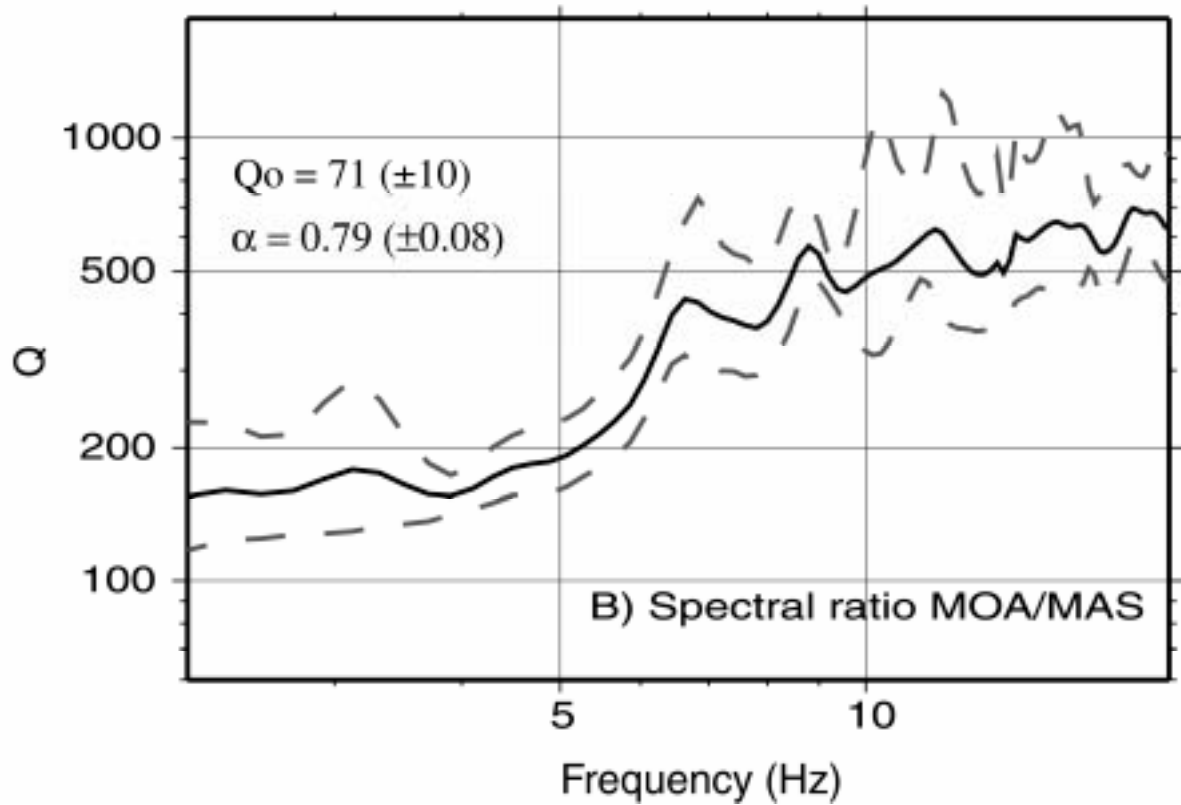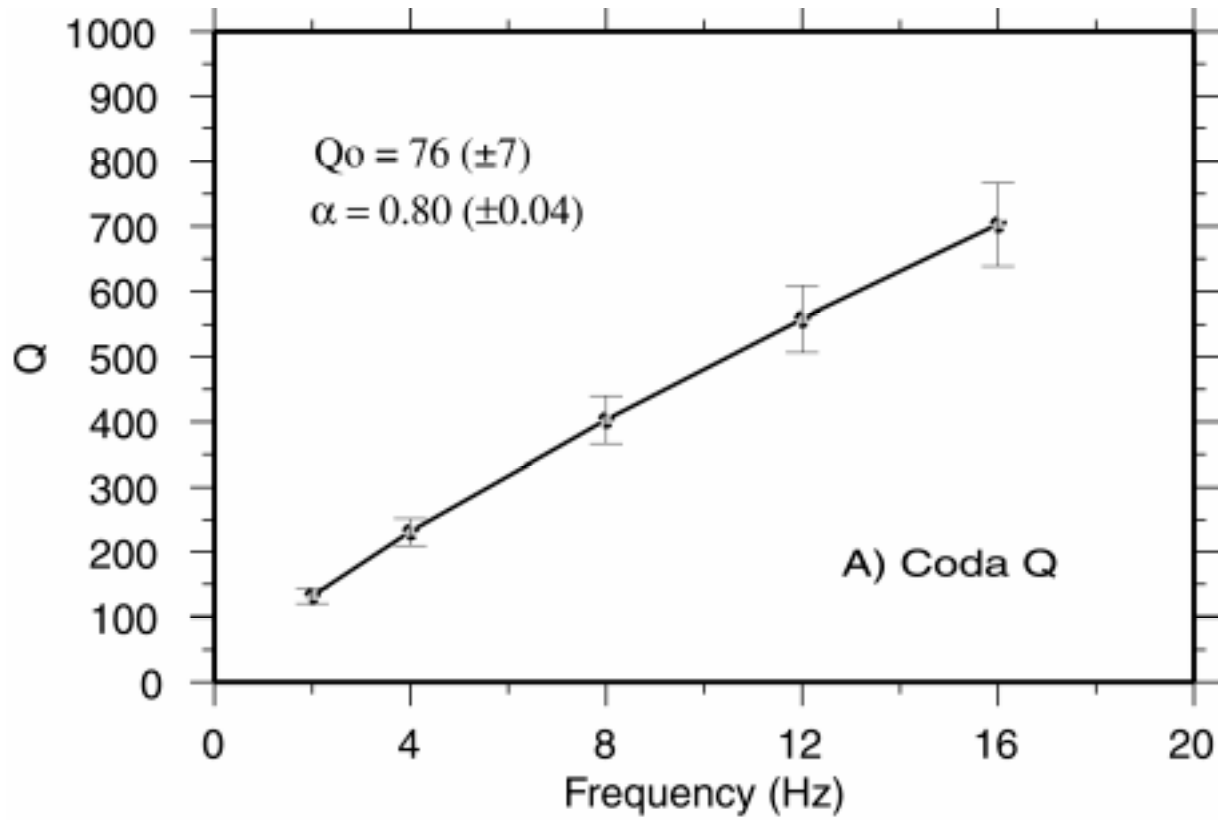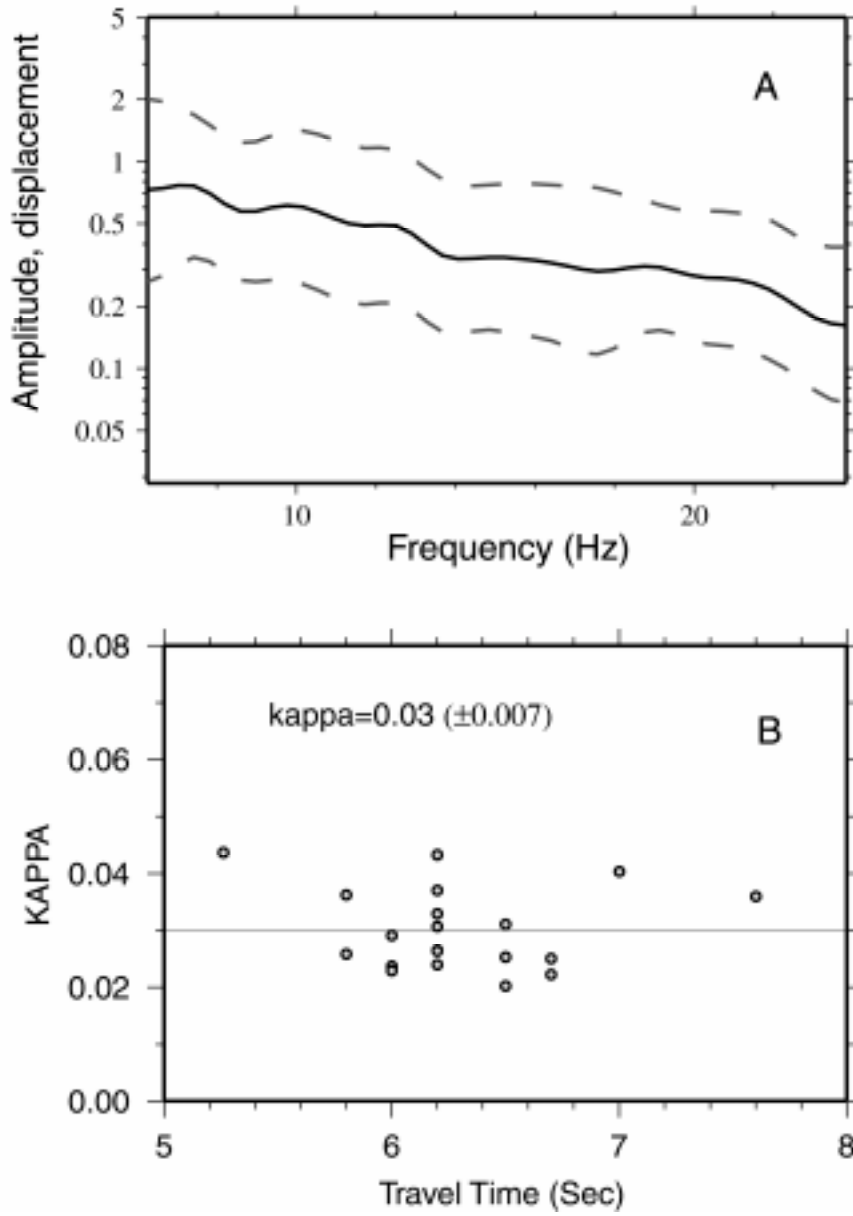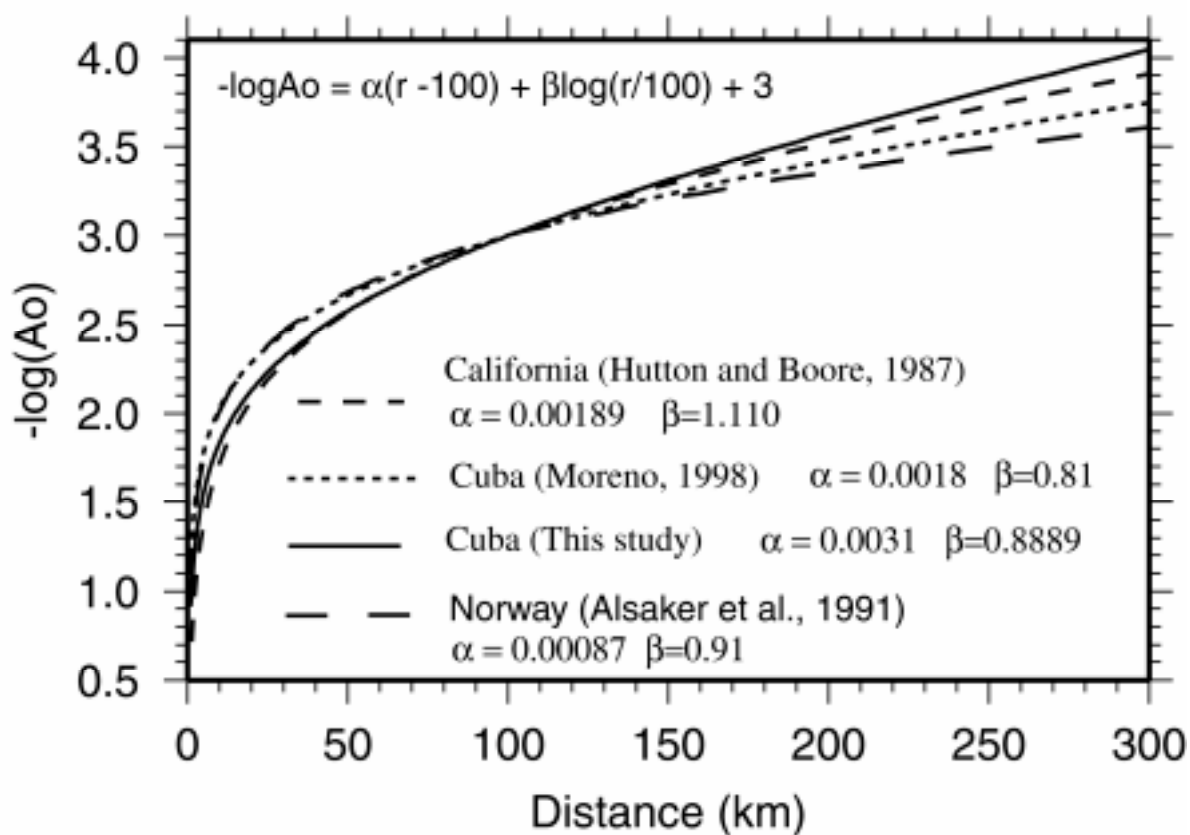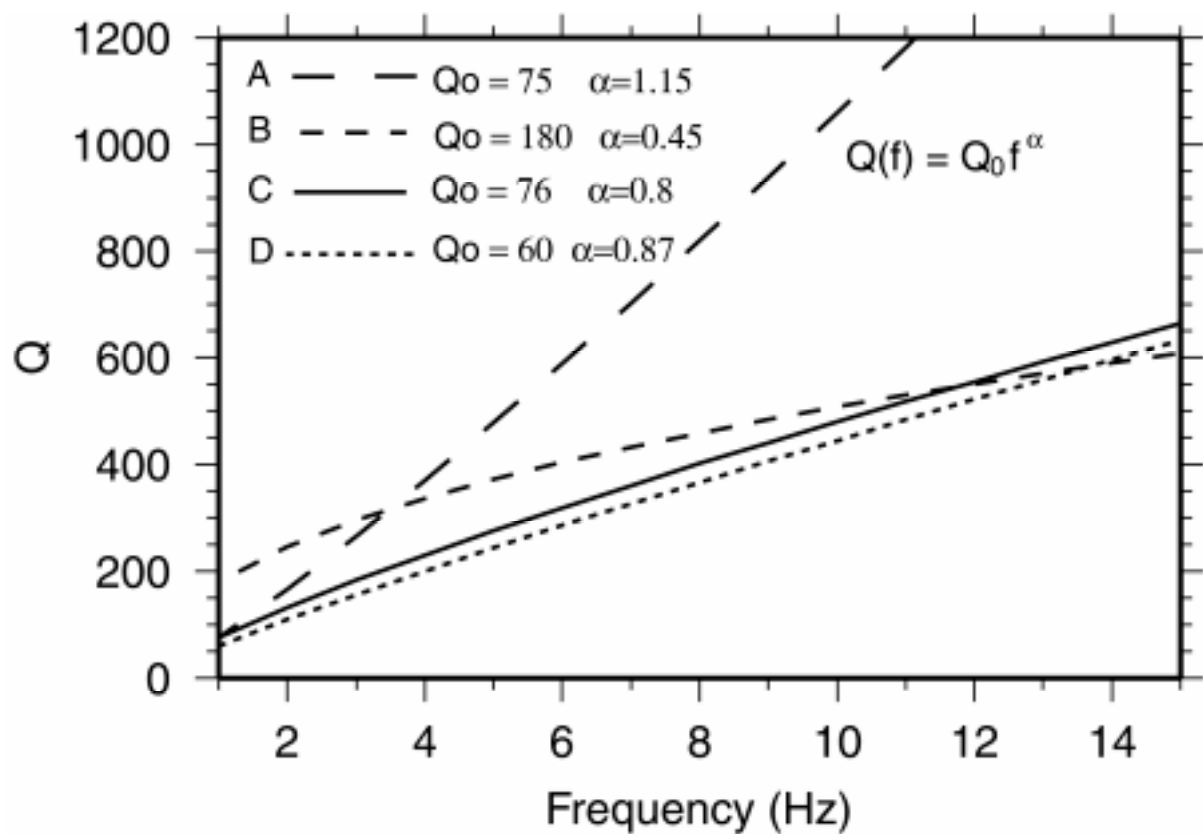
FIGURA 4
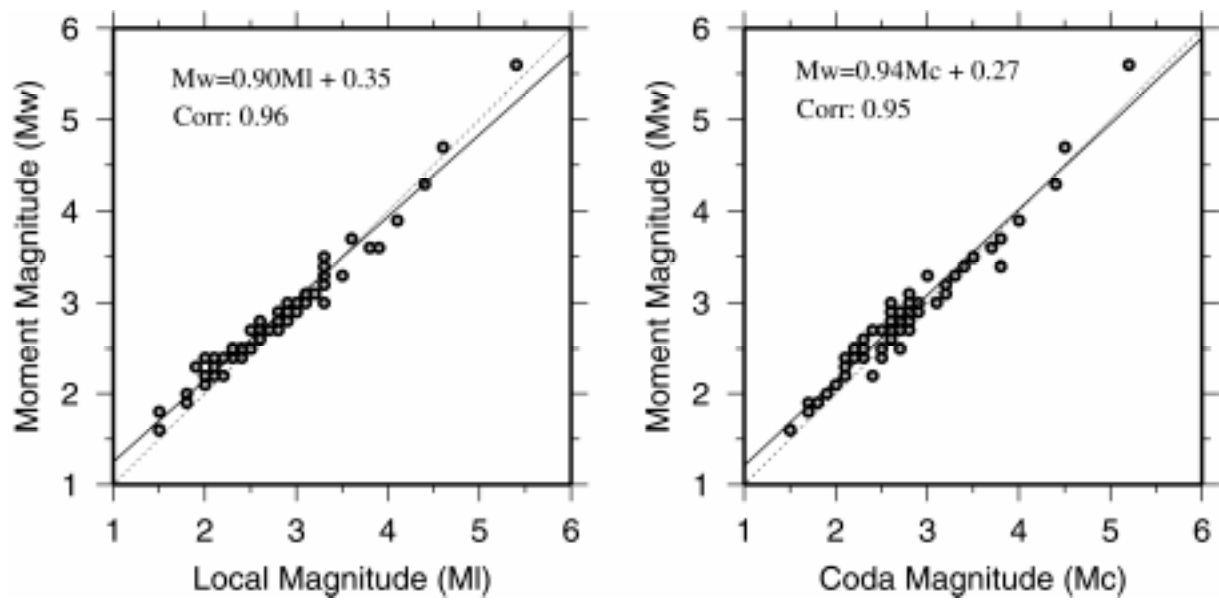
Average spectra with sd for MOA_B_Z

FIGURA 5

FIGURA 6

FIGURA 7
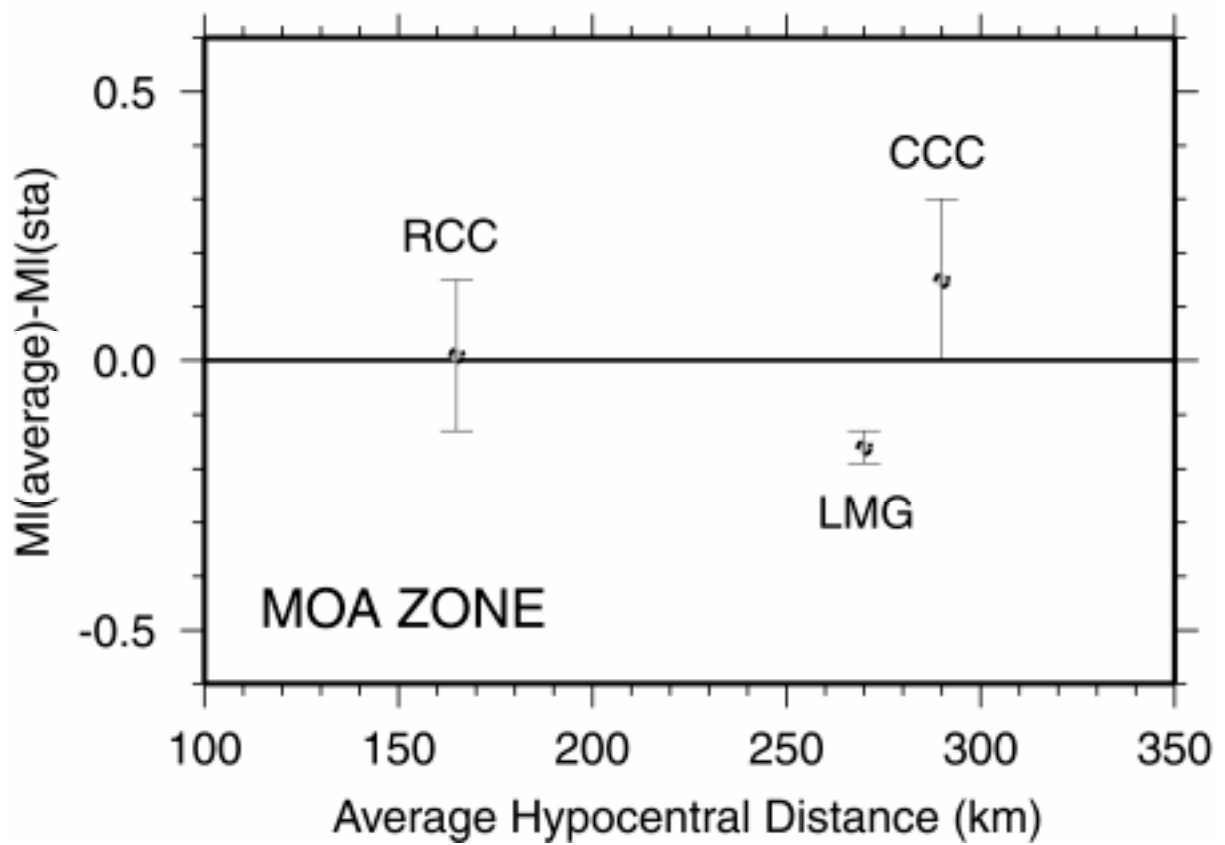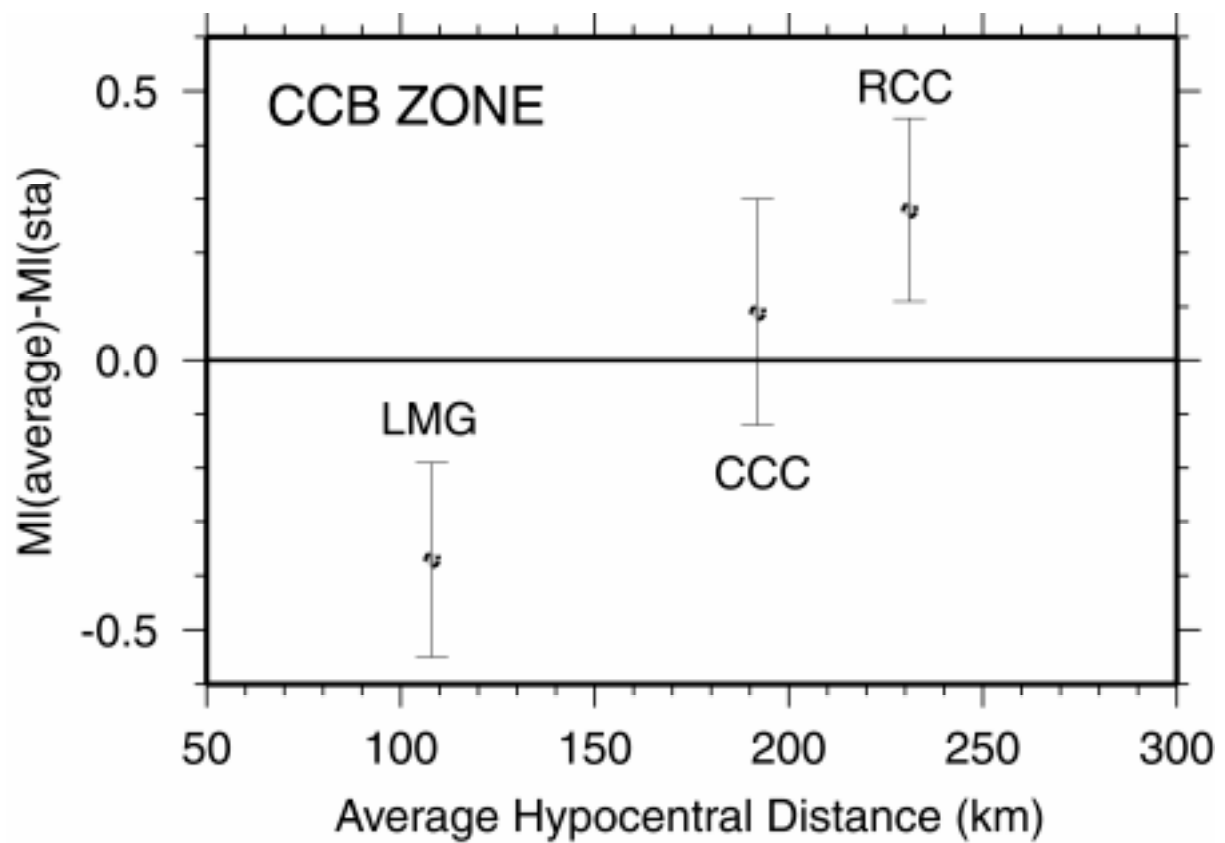
FIGURA 8

THE NEW CUBAN SEISMOGRAPH NETWORK.

Bladimir Moreno Toiran

Institute of Solid Earth Physics, University of Bergen, Allegt. 41, 5007 Bergen, Norway

Centro Nacional de Investigaciones Sismólogicas, Calle 17, No. 61 e/ 4 y 6 Vista Alegre, Santiago de Cuba, Cuba

INTRODUCTION

Evidence of instrumental seismic data can be found in Cuba as early as the beginning of the twentieth century. The first Cuban seismological station was installed in 1907 by the Jesuits of Belén Observatory in Luyanó, Ciudad Havana and remained working until the 1920s. The station was equipped with two seismometers of Bosch-Omori type recording on smoked paper (Cotilla, 1998). Some moderate earthquakes were recorded during that period of time but unfortunately the seismograms from those instruments were lost. The second station Soroa (SOR), the first of the current seismograph network (Figure 2), began to operate in 1964. It was located in west Cuba for monitoring the seismic activity of the Pinar fault (Figure 1), responsible for the 1880 San Cristóbal earthquake (Table 1). One year later in 1965, station Río Carpintero (RCC) began operation in the eastern Cuba (Figure 2), the most seismically active part of the country. Activity in eastern Cuba is generated mostly by a major transform fault, the Oriente Fault Zone (OFZ) (Figure 1). To monitor the OFZ activity and improve the coverage of the area, three more stations were installed in the eastern Cuba in 1979, Pinares (PIN), Las Mercedes (LMG) and Maisí (MAS) and three years later Cascorro (CCC) (Figure 2). Most of the stations were instrumented with short-period three-component electromagnetic seismometers SKM-3 (of Russian manufacture) recording on photographic paper. The

seismograph network consisted of 18 stations in 1989, including a local telemetered network of 8 stations in the surroundings of Santiago de Cuba. The locations of these stations can be found in Cotilla, 1998. The local telemetered network was equipped with one vertical component short-period seismometer with visual recording. The economic limitations of the country during the 1990s caused serious damage to the seismograph network. Only 3 or 4 stations were working regularly from 1994 to 1997 and many earthquakes were poorly located. The situation changed in 1998 when the old technology of photographic and visual recording was replaced by digital recording. Broadband seismometers were installed along the Island and a digital telemetered network, composed of short-period three-component seismometers, began operation in eastern Cuba (Figure 2). The new network opened new opportunities for studies that were not feasible before 1998. The aim of this paper is to discuss the network and present some preliminary results of the new Cuban seismograph network during the first two years of operation (1998 and 1999). The seismicity and kinematics of the area based on the new local data are discussed and a quantitative analysis of the location accuracy is also presented.

TECTONICS

The island of Cuba can be considered as a block (Iturralde, 1977), a tectonic unit separating the quiescent Bahama platform from the seismically active Cayman trough. Its formation is associated with the interaction of the westward-moving South and North American Plates and the break up of their margins (Enman et al., 1997). According to Cotilla (1998) the Cuban block is limited to the north by Nortecubana fault system (NCFS) and to the south by OFZ and Surcubana fault system (SCFS) (Figure 1). Along the southern Cuban margin lies the OFZ, a fault system marking part of the boundary between the North American and Caribbean

Plates, where strike-slip deformation dominates (Rosencrantz and Mann, 1991). It extends over 900 km from the Cayman Spreading Center (CSC) to the central Dominican Republic (Figure 1). The CSC is an oceanic crust spreading center that has been active since the Middle Eocene and is currently spreading at a rate of about 15 mm/year (Rosencrantz et al., 1988). The spreading ridge is about 110 km long and consists of a V-shaped axial valley that separates two areas of normal faulting (Cotilla, 1998). According to DeMets et al., (2000) the Caribbean Plate is moving eastward relative to the North American Plate (NAP) an average of 18-20 ± 3 mm/yr with 18 ± 2 mm/yr of boundary-parallel slip and 3 ± 3 mm/yr of boundary-normal convergence south of eastern Cuba. This eastward motion of the Caribbean plate produces left-lateral slip along the Enriquillo (EFZ) and Walton Fault Zones (WFZ), and left-lateral strike-slip deformation along the OFZ (Figure 1).

The OFZ, EFZ and WFZ mark the north and south boundaries of the Gonave Microplate (GM). Mullins et al. (1992) pointed out that the northeastern corner of the Caribbean plate (the area of the present-day GM) has become impeded in a strike-slip restraining bend adjacent to the southeast extension of the Bahama carbonate platform. The GM is essentially being 'left behind' and being accreted to the NAP as its eastward progress is impeded by the Bahama platform (Mullins et al., 1992; Dolan and Wald, 1994; Mann et al., 1995). Along the releasing and restraining bends of the OFZ there are two local structures affecting the tectonic regime in this area: (1) the Cabo Cruz Basin (CCB) and (2) the Santiago Deformed Belt (SDB). More than 90% of the seismic activity along the southern Cuban is generated in these structures. The CCB is a narrow E-W trending depression (8-15 km wide by 80 km long), bordered on the north and south by two segments of the OFZ and divided by normal faults into a series of oblique horsts and grabens (Calais & Mercier de Lépinay. 1991). The discontinuous trace of the OFZ includes left-stepping offsets that generate local tensional

strain and causes pull-apart subsidence (Cotilla, 1998; Perrot et al., 1997). The SDB is a narrow submarine mountain range extending over 300 km along the OFZ in the eastern half of the southern Cuban margin. Its en echelon folds and thrust faults show clear evidence of transpressional deformation (Calais & Mercier de Lépinay. 1990).

HISTORICAL SEISMICITY

Historical records of strong earthquakes in Cuba go back to the sixteen century (Table 1 and Figure 1). Most events have been generated along OFZ, particularly in the vicinity of Santiago de Cuba, the largest and most important city after Havana. There have been 19 strong and moderate earthquakes (Ms >= 5.7) since 1578 reported in Santiago de Cuba (Alvarez et al., 1973). Table 1 and Figure 1 show only the earthquakes with magnitude (Ms) bigger than 6, reported in Santiago de Cuba, and magnitude bigger than 5 for the rest of the country. The strongest earthquakes in the Cuban historical records (Ms=7.5 and Ms=7.3) occurred in 1766 and 1852 in the vicinity of Santiago de Cuba. In both cases several churches collapsed, most of the buildings in the city were damaged and several people died (about of 120 people died in the 1766 earthquake) (Alvarez et al., 1973).

Fairly detailed information is available on the destructive consequences of the 1932 Santiago de Cuba earthquake (Ms=6.7), the largest felt event in the city since 1852. The earthquake destroyed several houses and caused significant damages to hospitals, factories, and schools. The strongest earthquake in Cuba since 1932 took place in 1992 with a magnitude of Ms=6.9 and epicenter in the CCB (Figure 1). This event, the largest ever instrumentally recorded in that region, offered a unique opportunity to better understand the tectonic and kinematic regime along the OFZ (Perrot et al., 1997).

THE NEW SEISMOGRAPH NETWORK

The new Cuban Seismograph Network (CSN) consists of 7 broadband stations along the island and 4 telemetered short-period stations concentrated in the eastern part of Cuba (Table 2 and Figure 2). The broadband stations are equipped with FBS-3A seismometers (of Chinese manufacture), which record over a 0.05 Hz to 40 Hz frequency band. The telemetered network consists of CM3 seismometers (of Russian manufacture) with a one-second natural period. All of the stations have three components and operate at a dynamic range of 96 db. The waveforms are digitized at 100 samples per second with a 16-bit GPS time-stamp digitizer EDAS-3 (of Chinese manufacture). Broadband stations are connected by telephone line with the Central Recording Station (CRS) located in Santiago de Cuba and the data are downloaded daily. The data from the short-period stations are also digitized in the field and transmitted in the VHF frequency band continuously, using digital telemetry at 4800 bps, to the CRS. The seismic data recorded by the CSN is available through the SeisWeb software (Moreno et al., 2002) at http://www.ifjf.uib.no/seismo/seisweb/seisweb.html.

Typical noise spectra of the CSN stations indicate that they fall within acceptable noise limits as defined by the Peterson Curves (Peterson, 1993). Two typical noise spectra of the CSN stations, one short period (PINC) and one broadband (RCC), are shown in Figure 3. Both noise spectra fall between the high and the low noise curves, which are used as a model for characterizing the noise level of the station. In general, the CSN stations are located in sites with good signal-to-noise ratios.

The first station (RCC) began operation at end of February 1998, followed by CCC one month later. The CSN began to work with 3 or more stations in May 1998. Table 3 shows the installation date of each station as well as the number of local and teleseismic events recorded until December 1999. The distribution of the number of earthquakes recorded by three or more stations including the old and the new CSN is shown in Figure 4. The high number in 1992 is due to the May 25th Cabo Cruz earthquake (Ms=6.9) and its aftershocks. The reduction of the number of earthquakes from 1994 to 1997 is accounted for by the decline in network operations during that time.

The detection threshold for the CSN is shown in Figure 5. The isolines define the approximate area where at least three stations can record an earthquake of a given magnitude. The map was created as follows: (1) the maximum recording distance for each magnitude limit was determined from the catalogue (Table 4); (2) circles were drawn with radius equal to the maximum epicentral distances and centers at the station locations; (3) the detection threshold was defined by the area of intersection of three circles. This simple method assumes that the seismic wave attenuation is the same in all directions and that the sensitivity of the stations is the same. Geophysical investigations (Ewing et al., 1960; Bush and Shcherbakova, 1986) have shown lateral variation of the seismic wave velocities in this area, which suggest that the attenuation may depend on epicentral azimuth, but there is no significant difference in the station sensitivities. Figure 4 therefore represents only an approximation of the detection threshold under ideal conditions.

SEISMICITY

The earthquake activity in Cuba is concentrated along the OFZ (Figure 6) but is not restricted to interplate seismicity, as small and moderate intraplate events are occurring throughout the country. The intraplate seismicity seems to be localized along the pre-existing zones of crustal weakness (Cotilla, 1998). Given the fact that most of those intraplate events are very small, and are often not well-recorded given the station geometry, their locations are in many cases constrained by only one or two seismic stations applying 3-component location method. Therefore there is not a good correlation of their locations with individual faults. Seismic activity along the OFZ recorded by the old Cuban seismograph network (upper map in Figure 6) involves large errors in the hypocenter determination because the only stations to the south, the Jamaican seismic stations (description and locations can be found in Wiggins-Grandison, 2001), were never used. Therefore, the preliminary seismicity and kinematic analysis in this study will be based on the new data alone.

Lower map in Figure 6 shows the seismic activity from March 1998 to December 1999. The solid-grey line at $-79°$ of longitude separates two regions. In eastern Cuba, earthquakes located with three or more stations are shown. In many cases (106 events) more than 3 Jamaican seismic stations were used, which improved the location error along the OFZ. On the left side in western Cuba, earthquake locations are poorly resolved, with locations determined from analysis of 3-component data from fewer stations. The P-wave velocity model (Moreno et al., 2001) used in the hypocenter determination is shown in Table 5.

There are four clusters of seismic events label as A,B,C and D in the lower map of Figure 6. Cluster A is correlated with CCB (Figure 7), a pull-apart zone characterized with shallow seismicity (depths less than 20 km). This zone is well defined by earthquake activity and was responsible for the 6.9 Ms Cabo Cruz earthquake on May 25th, 1992. Cluster B corresponds to the SDB, a narrow submarine mountain range undergoing compressive deformation. Both, shallow and relatively deep earthquakes (depth greater than 30 km) are observed in this area. Note that in Figure 7, only earthquakes with travel time residual (RMS) less than 1 second and focal depth error less than 20 km are shown. The error in depth is still large. However, several earthquakes were located with the Cuban and Jamaican seismic stations and some of them (15 events) have focal depth below 30 km with small errors (less than 7 km). Shallow seismicity in the SDB might be generated by the thrust and reverse faults mapped by Calais and Mercier de Lépinay (1990,1991). On the other hand, it is unlikely to have earthquakes with focal depth below 30 km in oceanic crust, where the thickness of the crust barely reaches 20 km (Ewing et al., 1960; Edgar et al., 1971; Case et al., 1990). Another process, perhaps crustal thickening or oblique subduction could be taking place (see kinematics).

Cluster C includes aftershocks of Mw=5.6 earthquake on December 28th 1998 (Figure 7), the largest seismic event ever recorded in this area. About 116 events were registered during the month after the main shock. The main shock seems to have been generated by the NCFS, which is undergoing compressive deformation probably as result of the contact zone between the Bahama platform and the Cuban block. The hypocentral errors in this area are large because it is outside of the CSN but our solution, including both focal depth (15 km) and epicenter, is very close to the NEIC solution. The focal depths of the aftershocks plotted in Figure 7 are obviously overestimated (see location accuracy). The depth of the mainshock suggests that they must be shallow as well.

The last cluster (D) corresponds to an earthquake swarm during July 1999 (Figure 8). From more than 1000 seismic events, only 22 were recorded by three or more stations and none had magnitude above Ml=3.6. The swarm could have been triggered by stress transfer following the December 28th (Mw=5.6) earthquake. The fault correlated with this swarm is not clearly identifiable. The swarm could be associated with the trace of Cauto Nipe fault (CNF) mapped in Figure 7, but also with NW-SE oriented faults, which have been identified from geomorphological data. The CNF is an important seismogenic structure in eastern Cuba, probably responsible for the Bayamo (1551,1624) and Manzanillo (1926) earthquakes (Table 1 and Figure 1). Cotilla (1998) suggested that the CNF is cut at its southern and northern borders by the OFZ and NCFS, but the seismicity only weakly supports this assumption.

The Gutenberg-Richter relationship for 1.5 years of seismic activity recorded by the CSN is shown in Figure 9. The relationship is determined from earthquakes in eastern Cuba (the right side of the solid-grey line in lower map of Figure 6). The estimated *b*-value of 0.95 is close to the earth's global average (*b*=1). In the limited period of time the 1999 swarm can affect the b value. But it was essentially removed because only 22 earthquakes are included: those recorded by three or more stations. The statistics from 1.5 years of earthquake activity suggest that one earthquake of magnitude 6 is expected every 10 years and one earthquake of magnitude 7 is expected every 100 years, which is in agreement with the statistics derived from the historical records. The detection threshold derived from the magnitude-frequency relationship seems to be 2.5 for the whole area, which is consistent with the detection threshold of the CSN shown in Figure 5.

KINEMATICS

Figure 10 shows a number of earthquake focal mechanisms determined using P-wave first - motion polarities from the Cuban and Jamaican seismic stations (Table 6). The nodal planes have been resolved to within ±15° using the SEISAN software (Havskov & Ottemöller 1999), which follows the algorithm developed by Snoke et al. (1984). The solutions are divided into three groups: (1) those associated with CCB; (2) those associated with SDB; and (3) events associated with NCFS. The rose diagram on the upper-left corner shows the maximum horizontal compressive stress (σ_h) for the first group (P1, 5, 2, 4, 10, 9, 3, 18). The event labelled as P1 is the 1992 Cabo Cruz earthquake (Perrot et al., 1997). The σ_h values are determined from the T (tension) and P (compression) axes, according to the method of Zoback (1992). Two clear dominant σ_h orientations are found for the CCB events. The axis with azimuth N10°-20°E correlates with the normal NE-SW faults mapped in the basin, such as faults associated with events 10, 9 and 3. This σ_h orientation is consistent with the expected W-E horizontal extension in this pull-apart zone. The second axis, oriented N40°-50°E, corresponds to W-E segments of the OFZ, which generated events 4 and 18. This stress orientation is in agreement to a regional σ_h (Zoback, 1992) driving left-lateral strike slip along the OFZ.

The σ_h orientations for the second group (1, 16, 15, 9, 0, 6, 7, 19, 17, 8, C1, C2, C3, C4) are shown by the rose diagram on the lower right corner of Figure 10. The events labelled as C1, C2, C3, C4 are taken from the Harvard CMT catalog. The stress orientation for this group shows rather complex σ_h patterns and variable fault plane solutions. This is not unexpected considering the non-uniform orientation of the thrust faults in SDB. The area is dominated by reverse faulting with a few strike-slip faults that can be correlated with W-E segments of the

OFZ. Some earthquakes show compressive deformation at relatively deep focal depths (below 30 km). Those earthquakes are located in oceanic crust, where the Moho is at about 18-21 km (Case et al., 1990). It is evident that the shallow thrust faults of SDB cannot generate earthquakes at such depths. Their solutions support what has been suggested in previous studies, that the Caribbean plate is underthrusting beneath the Cuban block (Enman et al., 1997), probably causing crustal thickening in SDB area.

In the area between CCB and SDB, which is dominated by strike-slip faulting, there is another important feature (Figure 10). The earthquakes 4 and 18, which belong to the first group, have a minor normal component. However, once we move eastward the earthquakes 1 and 6 begin to exhibit a minor reverse component. This pattern shows evidence of the transition from transtension to transpression along the OFZ. The third group has no rose diagram, but the stress orientations (N20°-40°E) are consistent with the regional σ_h, which may cause thrust faulting in NW-SE oriented structures. The focal mechanisms correspond to the main shock (event number 11) and two aftershocks of the last moderate earthquake (Mw=5.6) on December 28th, 1998. The fault plane solutions correlate with the NCFS, a NW-SE structure, which defines the external northern limit of the Cuban block. The solution is also consistent with the one reported in Harvard CMT catalog.

LOCATION ACCURACY

Several factors affect the location accuracy of earthquakes. First, there is an error due to the precision in the readings of the person who analyzes the data. This error was reduced significantly with the introduction of digital seismograms. The velocity model, including station corrections, is the most critical remaining source of uncertainty. Small changes in the

velocity model can result in a 20 km change in hypocentral location. Another critical factor is the geometrical arrangement of the seismic stations. For events in Cuba, the Jamaican seismic stations have to be used, given the fact that the seismicity is concentrated outside the CSN.

Figure 11 shows the epicentral errors (calculated with the HYPOCENTER program; Lienert and Havskov, 1995) for the same set of events shown in Figure 7. The four boxes in Figure 11 enclose the most important seismogenic zones in Cuba. It is evident that the hypocentral error varies between these boxes. The smaller errors (about ±5 km) are found in the Oriente fault segment (OFS) and SDB, where the azimuthal gap is less than 180° when Jamaican stations are used. The bigger ellipses with major axes of about 20 km in the CCB and SDB are the events for which Jamaican seismic stations were not used.

There is another factor that could affect the location accuracy, particularly the focal depth. The inversion process for the hypocenter determination is basically a search for models fitting the observations using a gradient-based inversion algorithm to find optimal solutions. The absolute minimum will be found only if the starting model is close to the optimal solution. To see how the initial focal depth could affect the hypocentral solution, typical RMS-DEPTH curves for the four seismogenic zones were determined (Figure 12). In all cases with the starting focal depth at 0 km the global minimum was reached. Hypocenters are more poorly constrained in the Moa Zone. The minimum solution involves focal depths with large errors due to the big azimuthal gap.

CONCLUSION

The new Cuban seismograph network combined with the Jamaican seismograph network offers a unique opportunity to develop new insights on the tectonic and kinematic regime along the northern Caribbean plate boundary. For the first time local seismic data can be used as a reliable constraint for the seismotectonic interpretations in the area. Preliminary results after two years of operation suggest that:

1. The more active structures along the OFZ are the CCB and the SDB. The CCB is characterized by shallow seismicity with normal faulting (small strike-slip component) and the SDB experiences shallow and relatively deep seismicity dominated by thrust faulting.

2. Compressive deformation at relatively deep depths in SDB area supports a previous suggestion (Enman et al., 1997) that the Gonave Microplate is underthrusting the Cuban block.

3. The NCFS, which marks the northern limit of the Cuban block, is undergoing compressive deformation, probably as a result of the contact between the Bahama platform and the Cuban block.

4. The earthquake focal mechanisms along the CCB and the SDB show evidence that transtension and transpression are occurring at the same time and with short distances along a major transcurrent fault segment (OFZ).

5. The detection threshold of the CSN seems to be 2.5 for eastern Cuba. The hypocenters along OFZ are well constrained when both CSN and Jamaican seismograph network are used.

ACKNOWLEDGEMENTS

REFERENCES

Alvarez, J., P. Blanco, S. V. Medvedev, L. Menende, and V.V. Shteynberg (1973). The seismic conditions of Santiago de Cuba. *Bull. (Izv.) Acad. Sci. USSR, Earth Phys.* **5**, 320-324.

Bush, V. A., and I. N. Shcherbakova (1986). New Data on the Deep Tectonics of Cuba. *Geotectonics*, **20**, 192-203.

Calais, E., and B. Mercier de Lépinay (1990). A natural model of active transpressional tectonics: The *en échelon* structures of the Oriente deep along the northern Caribbean transcurrent plate boundary (Southern Cuban margin), *Rev. Inst. Fr. Pét*. **45**, 147-160.

Calais, E., and B. Mercier de Lépinay (1991). From Transtension to Transpression along the Southern Caribbean Plate Boundary of Cuba: implications for the Recent motion of the Caribbean plate, *Tectonophysics,* **186**, 329-350.

Case, J.E., W.D. MacDonald and P.J. Fox (1990). Caribbean crustal provinces; Seismic and gravity evidence, *in The Geology of North America, The Caribbean Region*, Vol. H, pp. 15-36, ed. Dengo, G. & Case, J.E., Geological Society of America, Boulder, Colorado.

Cotilla, M. (1998). An overview on the seismicity of Cuba, *Journal of Seismology,* **2**, 323-335.

De Mets, C., P. E. Jansma, G. S. Mattioli, T. Dixon, F. Farina, R. Bilham, E. Calais, and P. Mann (2000). GPS geodetic constraints on Caribbean - North American Plate motion, *Geophys. Res. Lett*. **27**, 437 – 440.

Dolan, J.F. and D.J. Wald, (1994). Consequences of time-transgressive, oblique underthrusting of the southeastern Bahamas: Localization of large thrust earthquakes and controls on large-scale forearc subsidence events. *Geol. Soc. Am., Abstr. Programs*, 26, A-251.

Draper, G. and J. A. Barros (1994). Cuba (chapter 4), *in Caribbean Geology: An Introduction*, pp. 65-85, U.W.I Publishers' Association, Kingston.

Edgar, N. T., J. I. Ewing, and J. Hennion (1971). Seismic Refraction and Reflection in the Caribbean Sea, *Am. Assoc. Petr. Geol. Bull.* 55, 833-870.

Enman, S.V., T. P. Belousov, M. E. Marquez, J. S. Rueda, and G. D. Jorge, (1997). Recent Crustal Movements and Morphostructural Pattern of Southeastern Cuba: Santiago de Cuba Geodynamic Research Site, *Izvestiya, Physics of the Solid Earth*, **1**, 55-69.

Ewing J., J. Antoine and M. Ewing (1960). Geophysical measurements in the western Caribbean Sea and in the Gulf of Mexico, *J. Geophys. Res.*, **65**, 4087-4126.

Havskov J., and L Otemöller (1999). SEISAN: The earthquake analysis software, Version 7.0, Institute of Solid Earth Physics, University of Bergen, Norway, 226pp.

Iturralde, M. (1977). *The tectonic movements of the development plataformic stage of Cuba*, File Report 20, Inst. of Geology and Paleontology, Acad. of Sciences of Cuba, 20 pp.

Lienert, B. R. and J. Havskov (1995). A computer program for locating earthquakes both locally and globally, *Seism. Res. Lett.*, **66**, 26-36.

Mann, P., F. W. Taylor, R. Lawrence Edwards, and Teh-Lung Ku (1995). Actively evolving microplate formation by oblique collision and sideways motion along strike-slip faults: An example from the northeastern Caribbean plate margin, *Tectonophysics*, **246**, 1-69.

Moreno B., M. Grandison, and K. Atakan (2002). Crustal velocity model along the southern Cuban margin: Implications for the tectonic regime in an active plate boundary, *Geophys. J. Int.* (in review).

Moreno B., L. Otemöller, J. Havskov, and K. A. Olsen (2002). SeisWeb: A client-server-architecture-based interactive processing tool for earthquake analysis, *Seism. Res. Lett.*, **73**, 84-89.

Mullins, H.T. and nine others (1992). Carbonate platforms along the southeast Bahamas-Hispaniola collision zone. *Mar. Geol.*, **105**, 169-209.

Perrot, J., E. Calais, and B. Mercier de Lépinay (1997). Tectonic and Kinematic Regime along the Northern Caribbean Plate Boundary: new insights from Broad-band Modelling of the May 25, 1992, Ms=6.9 Cabo Cruz, Cuba, earthquake, *Pure Appli. Geophys*. **147**. 475-487.

Peterson, J. (1993). *Observation and Modeling of Seismic Background Noise*, U.S. Geol. Surv. Open-File Report 93-322, 95 pp.

Rosencrantz, E. and P. Mann (1991). Sea MARC II mapping of transform faults in the Cayman Trough, Caribbean Sea, *Geology* **19**, 690-693.

Rosencrantz, E., M. I. Ross, and J. G. Sclater (1988). Age and spreading history of the Cayman Trough as determined from depth, heat flow, and magnetic anomalies, *J. Geophys. Res.* **93**, 2,141-2,157.

Snoke, J. A., J. W. Munsey, A. G. Teague and G. A. Bollinger, 1984. A program for focal mechanism determination by combined use of polarity and SV-P amplitude ratio data. *Earth quake notes*, **55**, 1-15.

Wiggins-Grandison, M. (2001). Preliminary Results from the New Jamaican Seismograph Network, *Seism. Res. Lett.* **72**, 525-537.

Zoback, M. L. (1992). First and Second-Order Lithospheric Stress Patterns. *J. Geophys. Res.*, **97**, 11703-11728.

FIGURES CAPTIONS AND TABLES

Figure 1. Kinematic framework along the southern Cuban margin. OFZ- Oriente Fault Zone; WFZ – Walton Fault Zone; EFZ – Enriquillo Fault Zone, SFZ- Swan Fracture Zone; CSC - Cayman Spreading Centre; CCB – Cabo Cruz Basin; SDB – Santiago Deformed Belt; CNF – Cauto Nipe Fault; PF – Pinar Fault; NCFS – Nortecubana Fault System; SCFS – Surcubana Fault System. The mapped OFZ trace, including CCB and SDB is taken from Calais and Mercier de Lépinay (1990, 1991). The PF and CNF traces are taken from Draper and Barros (1994).

Figure 2. New Cuban Seismograph Network

Figure 3. Typical noise spectra of a short period (PINC) and a broadband (RCC) seismic stations of the CSN. Dashed lines according to Peterson (1993).

Figure 4. Distribution of the number of earthquakes recorded with three or more stations, 1979 to 1999.

Figure 5. Detection threshold map of the CSN.

Figure 6. Upper map shows earthquakes with Ml > 3 recorded by the old CSN from 1979 to 1997. The lower map shows earthquakes recorded by the new CSN from March 1998 to December 1999. The area on the right side of the solid-grey line (eastern Cuba) shows earthquakes located with three or more stations. On the left side (western Cuba) the earthquakes are poorly resolved with less than three stations by using three components. Clusters of earthquakes explained in the main text.

Figure 7. Epicentral map of earthquakes with residual travel time (RMS) less than 1 sec and focal-depth error less than 20 km. Structural features as Figure 1.

Figure 8. Distribution of the number of earthquakes recorded by the new CSN from March 1998 to December 1999.

Figure 9. Gutenberg-Richter relationship of the seismic activity from Jun 1998 to December 1999.

Figure 10. Earthquake focal mechanisms along the most active seismogenic sources in Cuba including data from Jamaican Seismograph Network.

Figure 11. Epicentral errors for the earthquakes plotted in Figure 7. Boxes are enclosing the most active seismogenic zones in Cuba. CCB – Cabo Cruz Basin; SDB – Santiago Deformed Belt; OFS – Oriente fault segment.

Figure 12. Typical RMS-DEPTH curves for the enclosed area shown in Figure 11.

Table 1. Historic Cuban Earthquakes. Macroseismic determination is represented in parenthesis. Only earthquakes Ms>6 (Santiago de Cuba) and Ms>5 (rest of the country) are shown.

Year	Month	Day	Lat. N	Lon. W	Intensity (MSK)	Ms	Locality
1551			(20.40)	(76.60)	8	(5.8)	Bayamo
1578	AUG		(19.90)	(76.00)	8	(6.7)	Santiago de Cuba
1624	OCT		(20.40)	(76.60)	7	(5.2)	Bayamo
1678	FEB	11	(19.90)	(76.00)	8	(6.7)	Santiago de Cuba
1766	JUN	12	(19.90)	(76.10)	9	(7.5)	Santiago de Cuba
1842	JUL	07	(19.90)	(76.00)	7	(6.0)	Santiago de Cuba
1852	AUG	20	(19.75)	(75.32)	9	(7.3)	Guaninicum (S. de Cuba)
1852	NOV	26	(19.60)	(76.25)	8	(7.0)	Santiago de Cuba
1880	JAN	23	(22.70)	(83.00)	8	(6.0)	San Cristóbal (P. del Río)
1906	JUN	22	(19.65)	(76.25)	7	(6.2)	Santiago de Cuba
1914	FEB	28	(21.30)	(76.20)	7	(6.2)	Gibara (Holguin)
1914	DEC	25	(19.60)	(76.30)	7	(6.2)	Santiago de Cuba
1926	AUG	3	(20.30)	(77.00)	7	(5.5)	Manzanillo
1932	FEB	3	(19.75)	(75.58)	8	6.7	Santiago de Cuba
1939	AUG	15	(22.50)	(79.25)	7	5.6	Remedios (Las Villas)
1947	AUG	7	(19.75)	(75.70)	7	(6.3)	Santiago de Cuba
1976	FEB	19	19.88	76.87	8	5.7	Pilon (Granma)
1982	DEC	16	22.60	81.25	6	5.0	Torriente (Matanzas)
1990	AUG	26	19.59	77.87	6	5.1	Cabo Cruz (Granma)
1992	MAY	25	19.61	77.87	7	6.9	Cabo Cruz
1998	DEC	28	21.03	74.64	6	5.6	Moa (Holguin)

Table 2. Seismic stations of the CSN.

Station	Instrument Type	Latitude North (°)	Longitude West (°)	Elevation (meters)	P-wave Correction (sec)	S-wave Correction (sec)
CCC	Broad B.	21.1937	77.4172	90	1.22	3.37
RCC	Broad B.	19.9953	75.6965	100	0.0	-0.15
LMG	Broad B.	20.0673	77.0047	200	-0.02	0.08
MOA	Broad B.	20.6583	74.9568	140	-0.11	----
MAS	Broad B.	20.1760	74.2310	350	0.83	----
MCG	Broad B.	22.3333	80.0000	100	----	----
SOR	Broad B.	22.7830	83.0180	206	----	----
CIES	Short P.	20.0020	75.7710	40	-0.05	-0.10
YARC	Short P.	20.2000	76.2200	100	-0.15	-0.10
PINC	Short P.	20.4870	75.7910	647	0.00	0.96
SABC	Short P.	20.3800	75.1900	100	-0.11	0.18

Table 3. Statistics of the seismic stations behaviour.

Station	Installation Date	No. events (Local and Regional)	No. events. only recorded at this station (Local and Regional)	No. events (Distant)	No. events only recorded at this station (Distant)
RCC	02/98	839	1440	86	6
CCC	03/98	322	168	128	41
LMG	05/98	480	418	38	1
YARC	05/98	183	4	24	0
PINC	05/98	388	1	21	0
SABC	05/98	252	0	22	0
SOR	08/98	17	23	31	2
CIES	10/98	276	0	15	0
MAS	11/98	273	170	11	0
MOA	01/99	422	1033	16	0
MCG	07/99	6	3	12	0

Table 4. Maximum distance at which one earthquake of the listed magnitude was recorded.

Magnitude (Ml)	Distance (km)
1.0	85
1.5	132
2.0	230
2.5	361
3.0	498

Table 5. P-wave velocity model used in the hypocenter determination.

Layer #	Velocity (km/sec)	Depth (km)	Thickness (km)
1	4.9	0	3
2	5.4	3	2
3	6.0	5	2
4	6.9	7	13
5	7.6	20	6
6	7.8	26	8
Half space	8.0	34	-------

Table 6. Earthquake focal mechanism solutions for the earthquakes shown in Figure 10. P-trn, P-plg, T-trn and T-plg are the trend and the plunge of the P (compression) and T(tension) axes, respectively. σh (maximum horizontal compressive stress) directions and Reg. (faulting regime) according to Zoback (1992). Po/bp: number of polarities and bad polarities. h-err: focal depth error.

| No.	Date	Time	Lat. (N)	Lon. (W)	h	Mag. (Mw)	P trn	P plg	T trn	T plg	σh	Reg.	Po./ bp	h-err.
0	25/04/98	1751	19.68	75.14	34	3.2	67	9	173	59	67	TF	7/0	10
1	17/05/98	1954	19.89	76.45	15	3.9	41	6	134	28	41	SS	10/0	8
2	20/05/98	1531	19.64	77.81	19	3.6	223	52	98	24	354	NF	8/0	9
3	02/06/98	1034	19.54	77.91	13	3.4	213	44	104	19	194	NS	9/0	8
4	18/06/98	1454	19.78	76.91	13	2.7	230	27	137	6	227	SS	8/0	8
5	30/06/98	0756	19.60	77.85	15	2.9	207	29	113	8	203	SS	8/0	9
6	23/07/98	2319	19.85	76.58	17	3.2	42	10	136	25	42	SS	9/0	4
7	08/09/98	1837	19.82	76.19	18	3.3	120	2	29	35	120	SS	8/0	5
8	01/11/98	0408	19.66	75.38	44	3.0	167	4	70	60	167	TF	8/0	7
9	23/11/98	0523	19.55	78.02	10	3.0	205	44	96	19	186	NS	8/0	12
10	27/11/98	0131	19.54	78.10	18	3.4	217	51	100	20	190	NS	10/0	14
11	28/12/98	0723	21.03	74.64	15	5.6	40	15	220	75	40	TF	16/1	12
12	30/12/98	0613	21.05	74.61	13	3.6	25	15	205	75	25	TF	13/2	20
13	05/01/99	0146	19.76	75.46	32	3.2	305	14	68	65	305	TF	9/0	8
14	05/01/99	1550	21.03	74.73	17	4.7	20	15	200	75	20	TF	15/2	15
15	19/01/99	1503	19.90	75.77	32	3.4	86	2	354	30	86	SS	8/0	2
16	04/02/99	0933	19.76	75.92	17	3.2	352	24	136	61	352	TF	10/0	5
17	13/02/99	2042	19.66	75.57	30	3.2	308	9	62	68	308	TF	11/1	6
18	29/03/99	0859	19.70	77.00	8	3.3	227	25	133	8	223	SS	12/0	7
19	16/12/99	0322	19.78	75.84	16	4.4	346	5	102	79	346	TF	13/1	10
P1	25/05/92	1655	19.61	77.87	19	6.9	221	23	120	25	----	U	----	--
C1	01/09/85	0101	19.77	75.31	10	5.0	324	7	104	80	324	TF	----	--
C2	12/02/89	1426	19.74	74.36	25	5.2	230	23	97	58	230	TF	----	--
C3	05/22/90	2035	19.79	76.07	15	5.3	241	17	131	47	241	TS	----	--
C4	09/04/90	0803	19.81	75.69	15	5.2	265	35	123	49	----	U	----	--
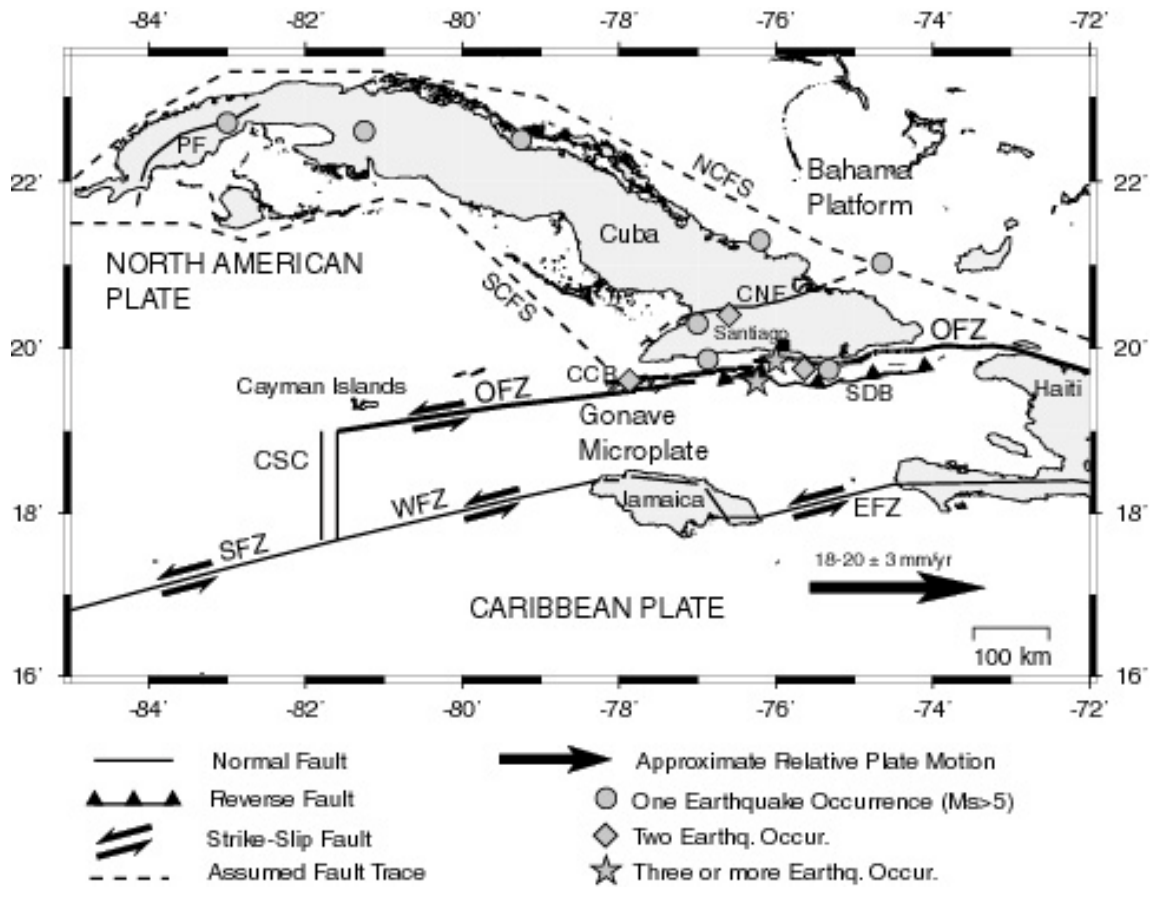
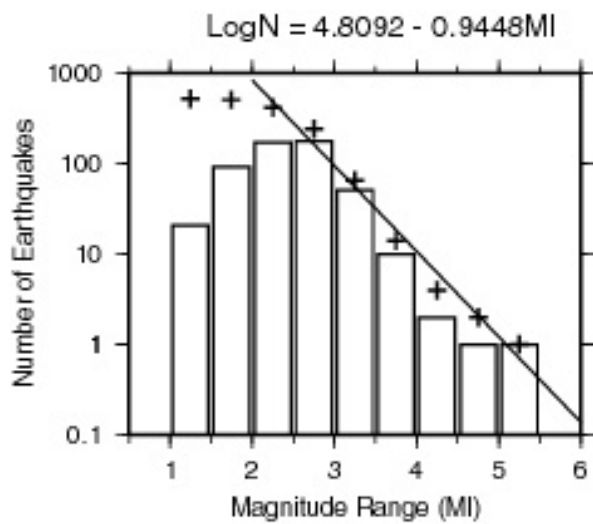FIGURA 1
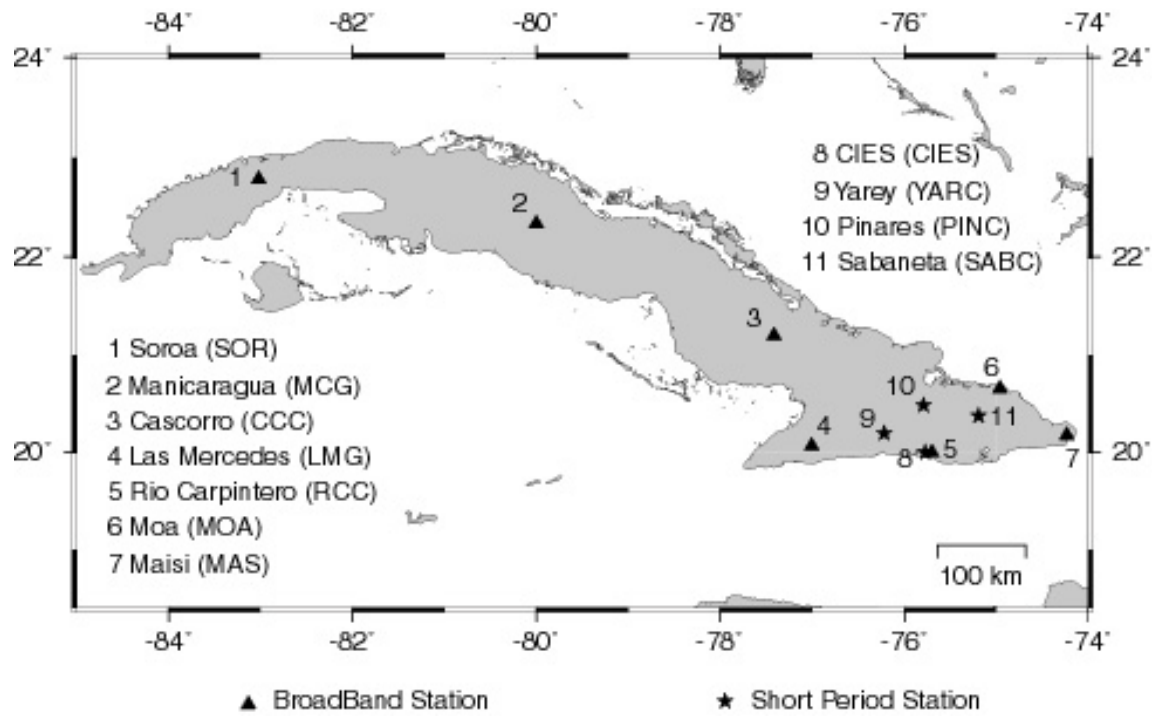
FIGURA 2
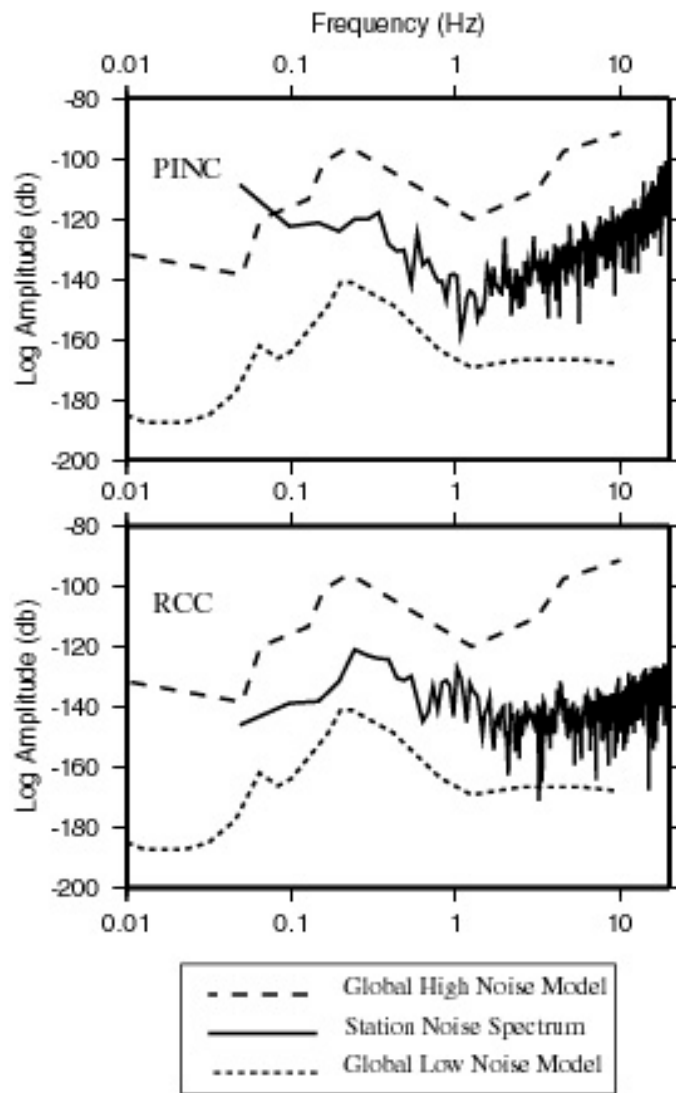
FIGURA 3
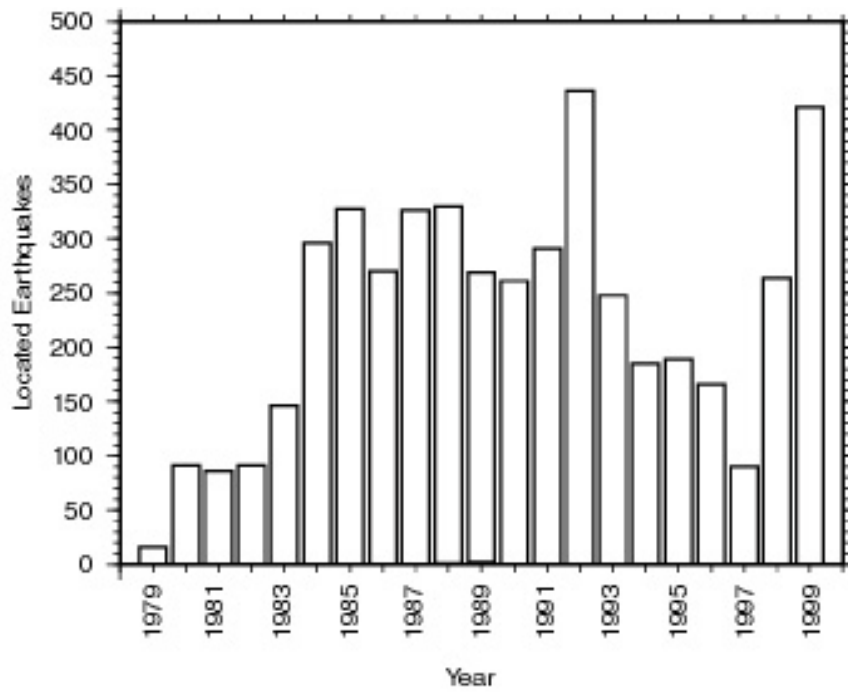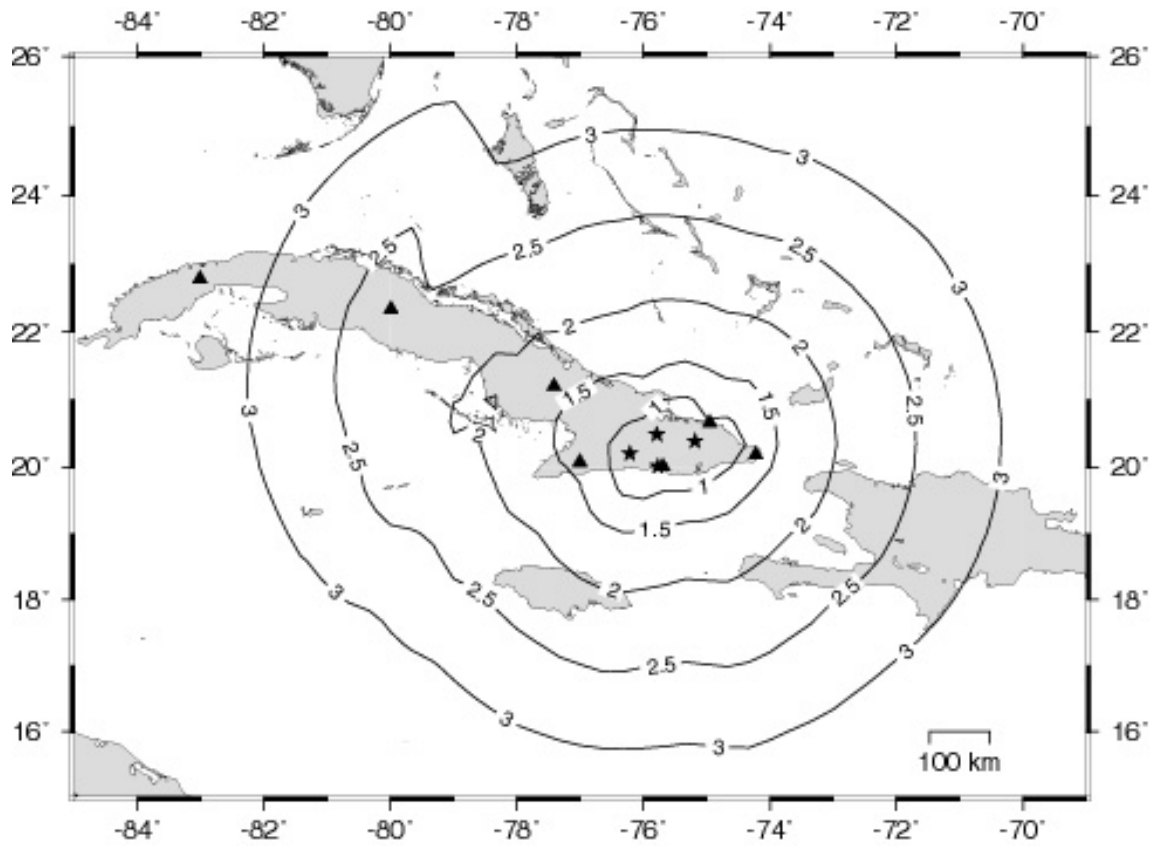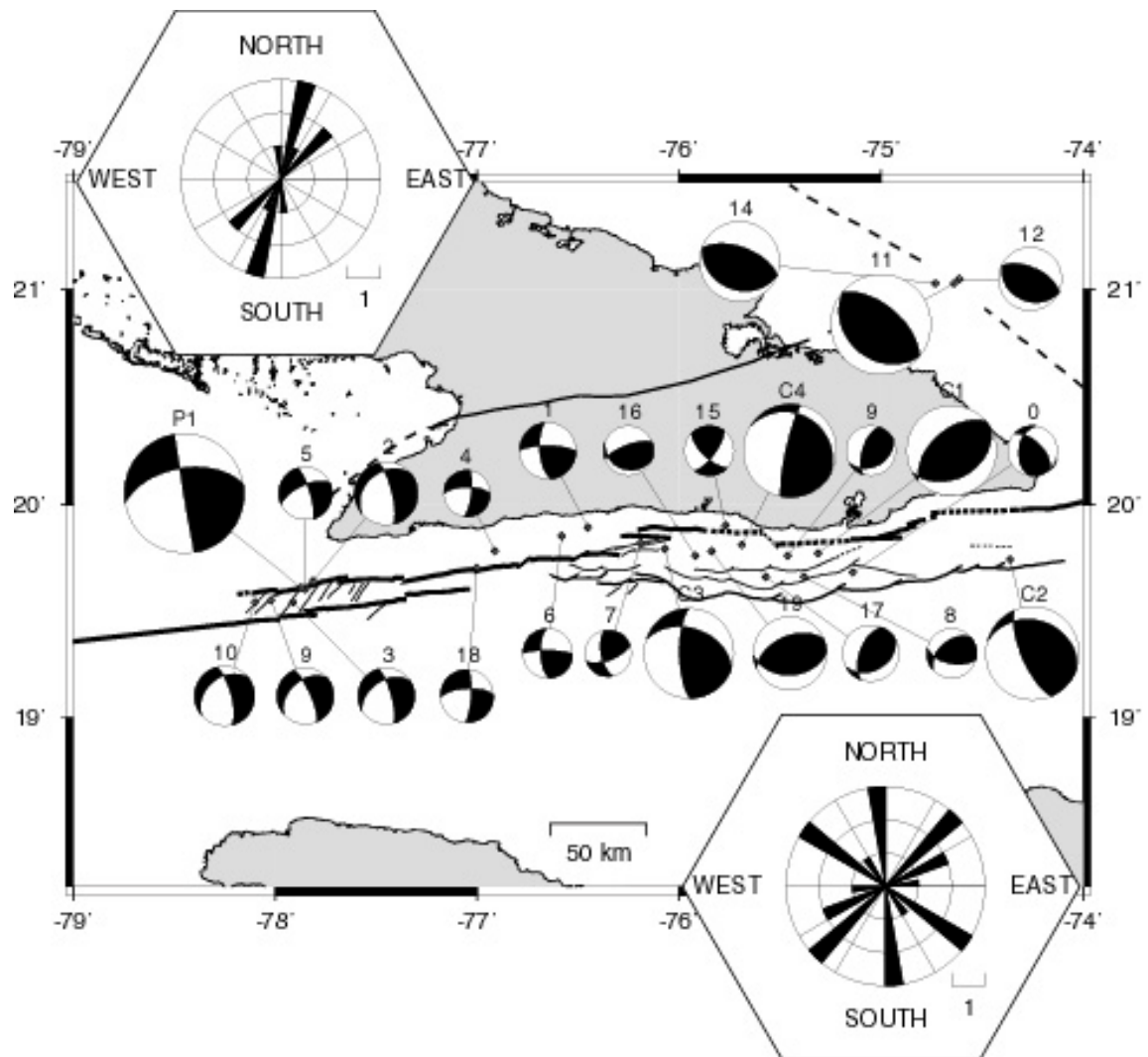
FIGURA 4
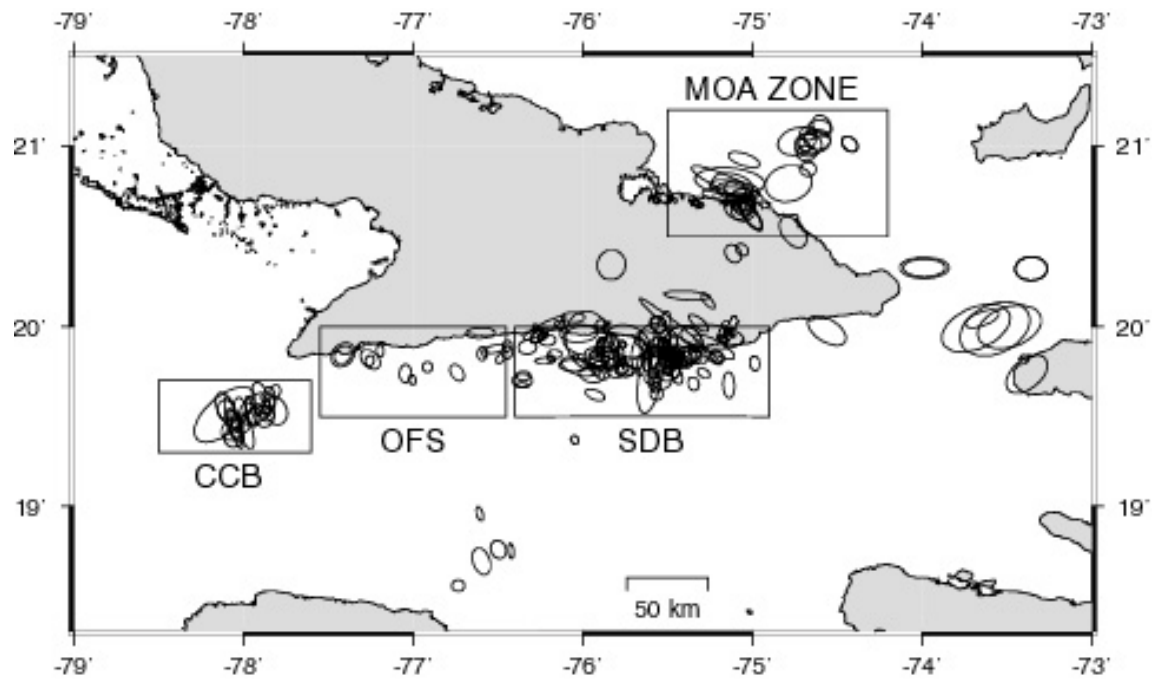
FIGURA 5
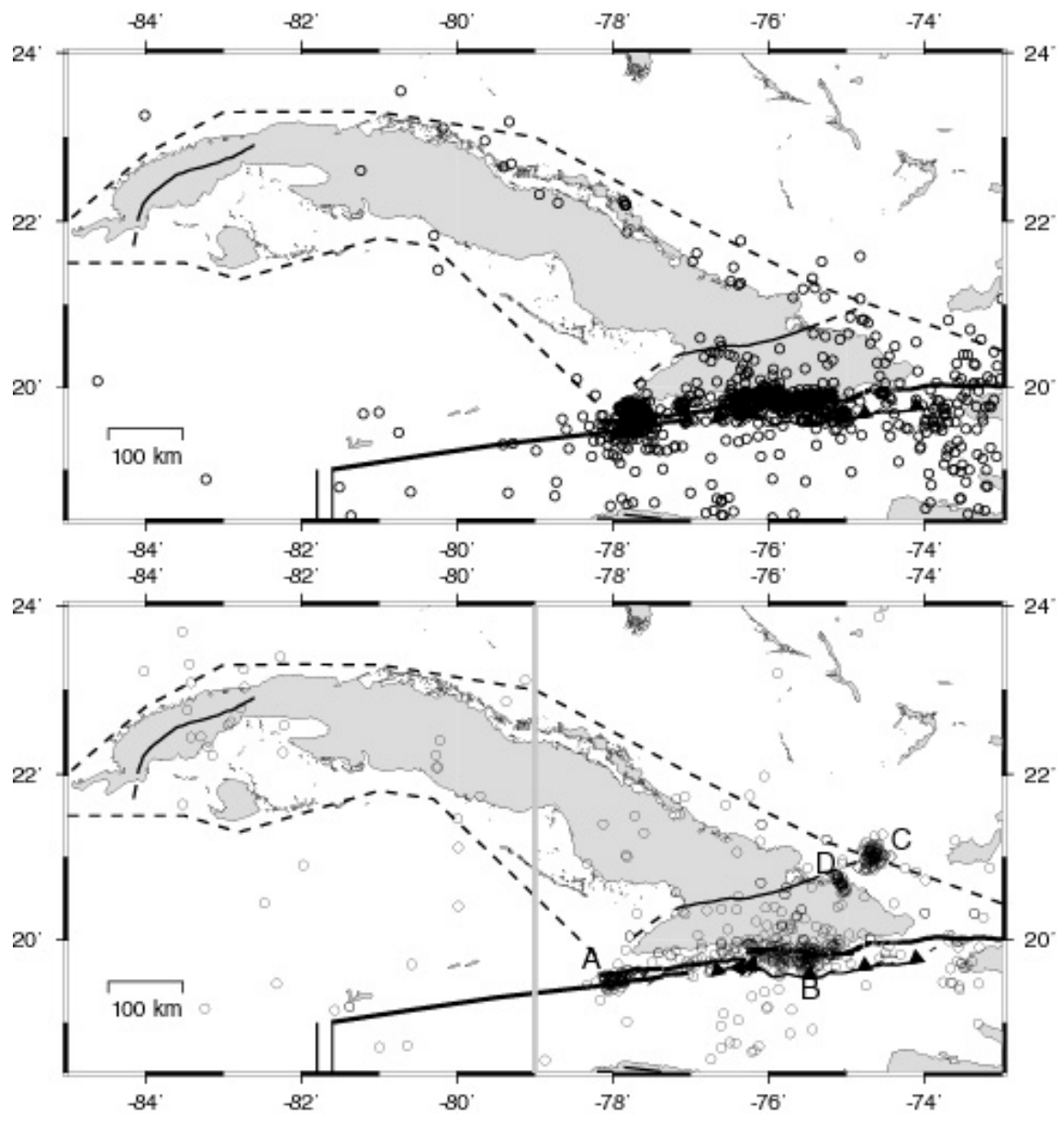
FIGURA 6
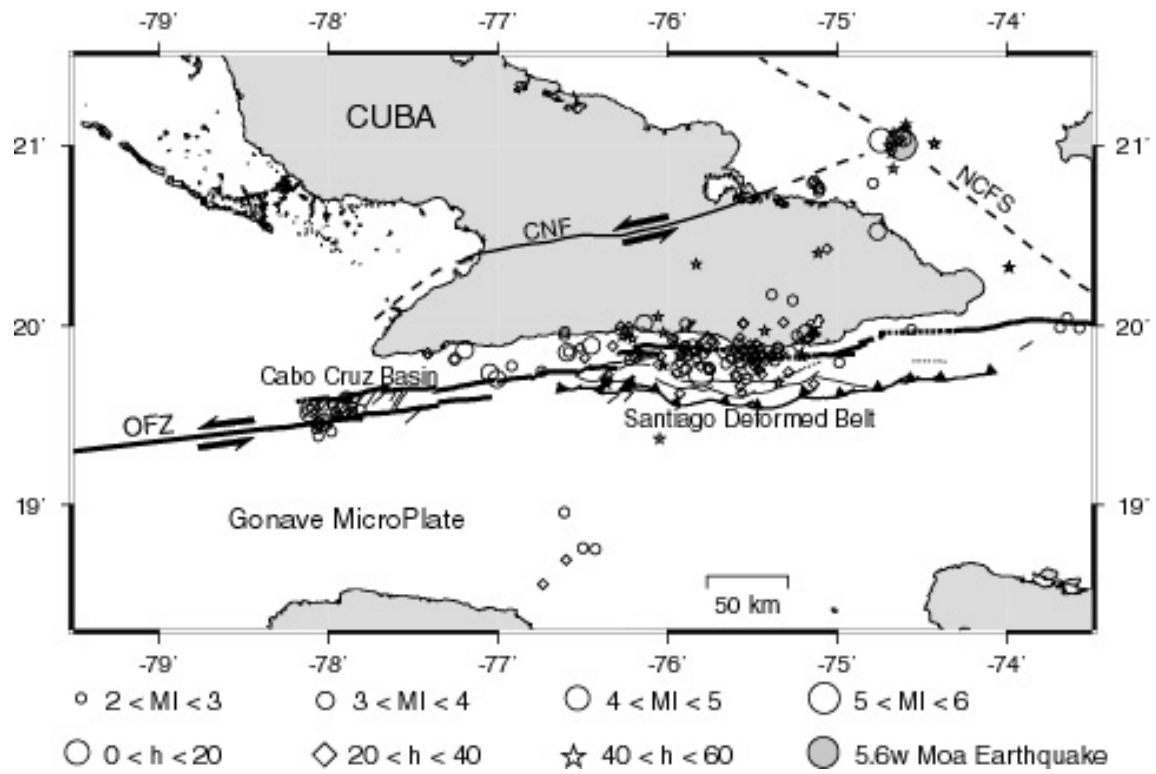
FIGURA 7
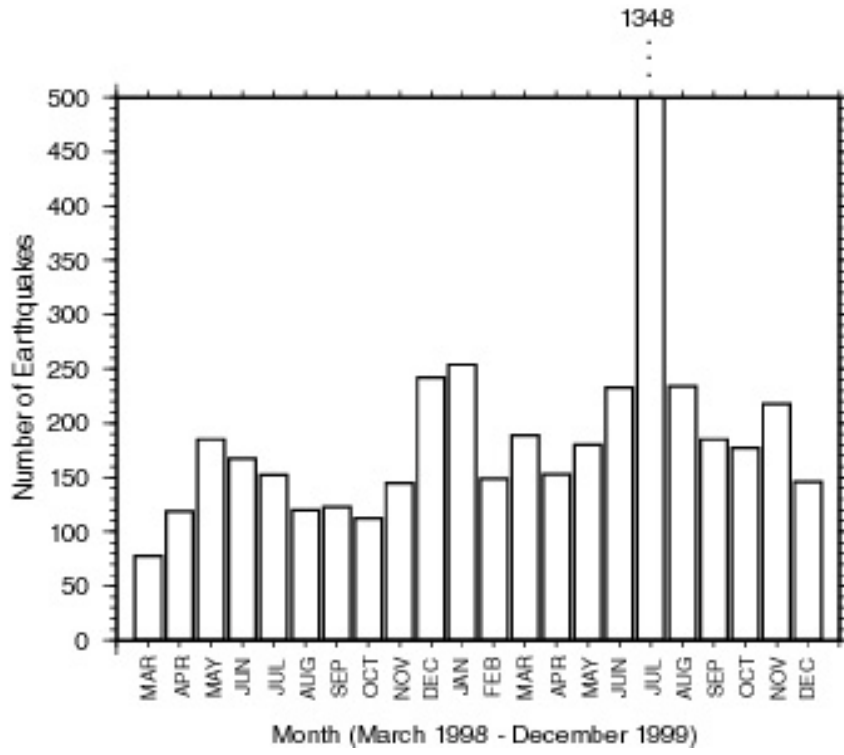
FIGURA 8

FIGURA 9

FIGURA 10

FIGURA 11
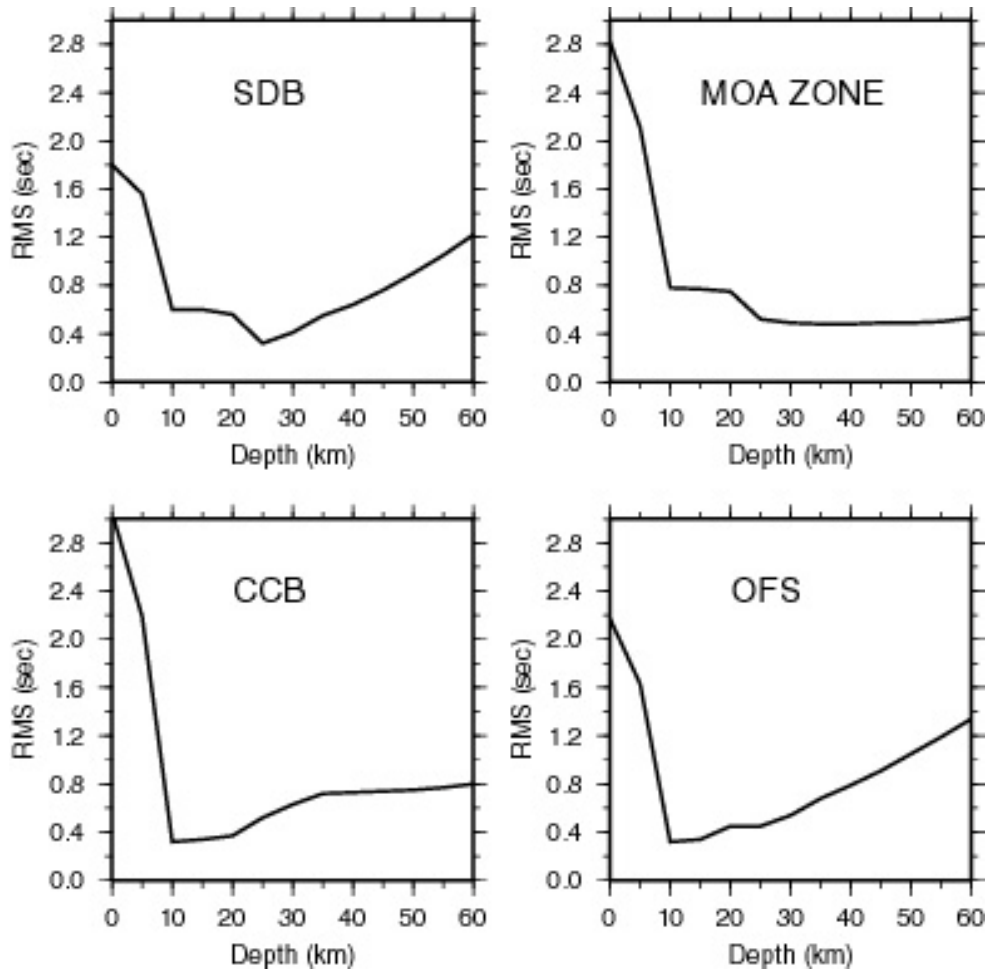
FIGURA 12

SEISWEB: A CLIENT-SERVER ARCHITECTURE BASED INTERACTIVE PROCESSING TOOL FOR EARTHQUAKE ANALYSIS

B. Moreno[1,3], L. Ottemöller[1], J. Havskov[1] and K. A. Olsen[2]

(1) Institute of Solid Earth Physics, University of Bergen. Allegt. 41, 5007 Bergen, Norway.

(2) Department of Informatics, Molde College. N-6401 Molde, Norway

(3) Centro Nacional de Investigaciones Sismologicas, Calle 17 No. 61 e/ 4 y 6 Vista Alegre, Santiago de Cuba, Cuba

Introduction

With the advances in computer and information technology, client-server architecture based tools for accessing earthquake data through the Internet have become feasible. The SeisWeb tool was designed to investigate the feasibility of remote access to seismological databases through the Internet. The SeisWeb software was written in Java. It is platform independent and will work through a web browser or as stand-alone application. The tool was designed to be database-oriented and to facilitate the most common basic functions of seismological processing. We hope that its simple graphical interface and easy access might make seismology more accessible to the public, increasing both interest and understanding. In this note we discuss the client-server architecture, processing and transfer speed, the graphical interface and security.

With the ongoing expansion of the Internet, the World Wide Web (WWW) has become an enormous source of information for people all over the globe. From its start in 1993 with a few hundred servers, this development has been growing extremely quickly, with an estimated 200 million servers in 1999. It is expected that in the future, web-clients will be just as widespread as television. Seismologists use the Internet extensively for many purposes: data exchange, data transfer from the field to the central recording site, dissemination of information on recent earthquakes, and educational information. Several interactive tools for access to parametric and waveform data have been developed by various institutions. At present most of these tools are data retrieval tools, but the development of tools for processing seismological information across the web has begun.

Among the data retrieval tools, Wilber, AutoDRM (Kradolfer, 1993; 1996) and SeismiQuery (the references to all software mentioned are given under the URL references) are the most widely used. The concept is to download data and process it locally using already installed software. This is satisfactory for most professional users, but it is not a practical solution for the occasional user or for a non-specialist who lacks the appropriate software on their own computer. Currently, Seisgram2K, the Seismicity Viewer and the Digital Seismology Tutor, present the first generation of Java based interactive processing tools. In these tools the data is downloaded from the server to the client and the processing is done on the client side, which means that these tools combine the task of extracting the data with processing. These tools are not linked to a parametric database.

Up to now, the processing done to obtain earthquake information has not been transparent to the public. This could change with the development of a simple-to-use web-based processing

system. Such a system could be offered to non-specialists to display the seismograms, even to pick phases and amplitudes, and to determine location and magnitude.

The purpose of this report is to investigate the issues relevant to web-based processing, discuss the practical aspects and to develop prototype software (SeisWeb). In its simplest implementation, a SeisWeb user will be able to inspect data on a remote database and in a full implementation, perform interactive processing. Since our effort is also directed towards occasional users and non-experts, the plan is to first implement only the most general functions of an earthquake analysis system.

Design Concept

Client-server architecture

If we think of a professional or non-professional user who wants to access seismological data, the user is on the client side and working locally. The data, together with the processing software, is stored on the server side. Obviously, some physical connection with some communication protocol between the client and server must exist. The Internets' transfer protocol, TCP/IP, is the most widely used, and we assume that an Internet connection between client and server exists. For simplicity we use the term Internet to refer to all connections between client and server based on TCP/IP (including local area network connections).

There are various possible ways that data and processing can be handled between client and server. We propose a system in which the data is kept on the server side and the processing is also done on the server side. The client software only handles the communication with the

server and is used to display the data obtained from the server. An alternative solution would be to do the processing on the client side, in which case the data needs to be transferred to the client.

There are some advantages and disadvantages with both systems. The "server-side processing" approach maximizes the use of existing software and guarantees the same results as obtained when working on the server directly. At the same time it minimizes the size of the client-based application. Another advantage of the server side processing is that the complete data set does not need to be transferred, but only what is needed to display the results. This leads to the disadvantage of the server side processing, which is that many messages between client and server need to be sent. An optimisation of the amount of data transmitted between client and server is therefore required. We consider that the advantages of the server side processing out-weight the disadvantages, particularly considering future increase in communication speed.

Speed

The speed of the client-server based system reflects both processing time on the server and the transfer rate between client and server and strongly depends on the software implementation. The processing time on the server is the same as when working directly on the server, which means the speed should be sufficient, since powerful computers are normally found on the server side. However, the performance could decrease if a large number of users are working simultaneously.

The transfer rate between client and server represents the bottleneck. A low transfer rate may make the proposed system impractical. The system must therefore be designed to transfer as little information as possible between client and server and to make use of data compression where possible. The largest amount of data that needs to be transferred is waveform data, which easily may exceed several mega-bytes for one event. Due to the processing being done on the server, however, it is not necessary to transfer the full waveform data. Instead, it is sufficient to only transfer the data needed to present visual images of seismic traces. Especially when working with multi-trace data, a large reduction in data size is to be expected.

Graphical user interface

The design of the graphical user interface (GUI) is essential, especially if the software is also meant for use by non-specialists, where the success of the development effort will be measured by the users' acceptance. The GUI is required to be simple and clear enough to be self-explanatory. In any system development task, it is essential to study the users' needs. The requirement for simplicity and reduction of the amount of data to be transferred makes it necessary to only include the functions most needed by the user.

To assess user needs, a questionnaire was prepared and sent to professional seismologists. The questionnaire was designed to determine what seismologists use the Internet for and to obtain the users' ideas on what a web-based processing tool should look like. A total of 26 responses were used to define the main functions needed. These functions were implemented in our web-based processing tool design. Non-specialists were not involved in the questionnaire because of the difficulty in finding occasional users with experience in retrieving

seismological information through the Internet. We believe that the needs of seismologists will be satisfactory for the occasional user as well. Non-specialists played the main role in refining the GUI. This process was performed using the "Thinking Aloud" protocol technique (Lindgaard, 1994). The method permits us to understand how the user approaches the interface and what considerations the user keeps in mind when using the interface. The main aspects considered in this study are the spatial distribution and connectivity of the options and the label of buttons identifying the options.

Implementation of SeisWeb

Following the design concept given above we developed a new software called SeisWeb. The main objective of the software is to provide interactive access to both parametric and waveform data, and to provide functionality for basic processing of earthquake data. Access to both parametric and waveform data is event based. SeisWeb was implemented and tested with the Seisan software and database (Havskov and Ottemöller, 1999). SeisWeb, however, is independent of Seisan and can work with other processing and database systems.

The main functions supported are given in the following list:

- display parametric data such as earthquake location, origin time, source parameters and phase readings
- search the database
- extract parametric information
- locate earthquakes
- produce epicenter maps

- extract waveform data

- display seismic traces in single- or multi-trace mode

- basic processing of the seismograms (filtering, instrument correction, phase picking, amplitude reading)

- update database on the server side (login and password needed)

Platform independence

SeisWeb is written in the Java programming language and thus is platform independent (Weber, 1998). This means that SeisWeb can run on various operating systems allowing the user to connect to the database on the server through the client on the system of his/her choice. SeisWeb can either run as an applet through a web browser or as local application. Applets are automatically downloaded upon request from the server and run on the client side in memory. Since the processing is performed on the server side, the applet remains relatively small in size, allowing fast download. There is practically no difference in speed or functionality if the software is running as an applet or as an application.

Client-server implementation

The SeisWeb applet or application runs on the client side. On the server side, SeisWeb is interacting with applications located on a web server that handles the   client-server communication protocol and data processing . SeisWeb was tested with the Apache web server software (see URL reference). The transfer of requests and data between client and server is based on the Common Gateway Interface (CGI) (Gundavaram, 1996).

A number of commands for communication between SeisWeb and the server were defined. These commands are independent of the processing software and database structure on the server side. However, the processing software must be able to understand the requests from SeisWeb. A description of the SeisWeb commands running on the server side are available from http://www.ifjf.uib.no/seismo/seisweb/commands.html. In principle the processing software could be located on the web server itself and the request interface implemented in the local processing software. However, to allow for greater flexibility we developed a script that interfaces between the client's requests and the server- side processing software. This script would need to be replaced when implementing another processing and database system. As an example, to request parameter data in time interval February 1998 to April 1999, the following SeisWeb command is sent :

extract_par -base BERGE -time   19980201 19990430 -outfile earthquake_list.out

The script on the server side, which is a CGI application, executes the processing software "extract_par" and sends back to SeisWeb the content of the output file "earthquake_list.out". An overview is shown in Figure 1.

User interface

SeisWeb was equipped with a graphical user interface in Windows style. User interaction is achieved through pushdown buttons and dialogue boxes. The function labels are self-explanatory. Additional help is given through an online help function. The user starts by requesting event data from a list of available databases (Figure 2). The search can be limited using search criteria. SeisWeb then displays a listing of events as returned by the server

(Figure 3). The user can view and modify the parametric data associated with a particular event and locate the event. Epicenter maps can be generated for individual events or a number of selected events. This process on the server side is performed by a script that generates maps using GMT (Wessel and Smith, 1999) and standardized commands.

Based on the listing, individual events can be selected for trace plotting (Figure 4), interactive processing and downloading of the data. To increase the speed during the waveform data transfer, only the points needed to create a visual image of the trace are transferred. This reduces significantly the amount of data to be transmitted. The user can switch between single and multi trace mode and perform basic processing like filtering, converting traces to ground motion, and picking amplitudes and phases. Based on the processing, the parametric information is updated in memory within the applet. The user thus can perform a complete routine analysis based on waveforms and/or parametric data and then calculate the hypocentral location and magnitude.

SeisWeb distinguishes between two types of databases: (1) pre-defined databases, which are defined on the server through SeisWeb and (2) user-defined databases, which are owned by the user that has access to his account through the web server. The user-defined database needs to be specified (database, login, password) by the user interactively and is not pre-defined through SeisWeb. Using SeisWeb on a user-defined database, the user can modify his data and update the database.

Formats

Both parametric and waveform data formats are in ASCII to simplify communication between different computer platforms. The most common ASCII format used for data exchange is probably GSE (GSETT-3, 1997), which was selected for the transfer of waveform data between the client and the server. The GSE parametric format, although widely used for data exchange, is a little hard to read and was therefore not used in SeisWeb. Instead, the Nordic format (Havskov and Ottemöller, 2000), another widely used format, was selected. The GSE waveform format includes the definition of compressed formats. For use with SeisWeb, the CMP6 compression was selected. For data download, both GSE and Seisan format are supported.

Security implementation

System security has been implemented on various levels of access to the database. The levels of access are set up on the server side in advance. Access can be restricted to not allow for e.g. waveform data download or database modification on the server side. The modification of data on the server side is only possible in user-defined databases. In this case the user has to enter the database, login and password. SeisWeb checks that login and password are the same as defined on the server, using a modern encryption algorithm (Schneier, 1996; Rhee, 1994).

Discussion

The design concept behind SeisWeb as an interactive processing tool in earthquake seismology is novel in the sense that it is based on a client-server architecture where most of the processing is performed on the server side. In other applications (e.g., Seisgram2K) the processing is performed on the client side. The main advantage of our design concept is that the tool can work with various processing and database systems. To work with a remote database and processing system, the user does not have to know the database structure and the processing system. All that is needed is a computer with Internet connection and Web browser software. With the increase of tele-communication speed and the advances in computer technology this approach may become more common.

Another novel aspect of SeisWeb is that the parametric and waveform data are associated and both can be inspected interactively. It is obvious that the professional seismologist could benefit from a tool like SeisWeb, since it will allow him or her to inspect and process earthquake data interactively without downloading it. SeisWeb will also provide easy access to seismological databases and basic processing tools to non-seismologist. Giving direct access to the data may increase the non-seismologist's interest and understanding and could be beneficial to educational projects.

The most critical aspect of SeisWeb is the speed of Internet connections, since with low transfer rates its use becomes impractical. We assume that the server has the capacity to process the data at least as fast as the local machine would, so delays when compared to client-side based processing are caused by the communication between client and server. On

the slow end, SeisWeb was found to work reasonably fast with 28.8 K baud modem connection or 64 K baud ISDN connection.

Conclusion

We have developed an interactive processing tool for earthquake seismology based in client-server architecture. We found that with the current transfer rates and computer systems, client-server based processing across the Internet is already feasible. The design allows SeisWeb to work with various processing and database systems. Basic routine processing functions were implemented with an easy-to-use graphical user interface. Considering the large number of seismological databases that could be accessed through the Internet, there is a large potential to make these data available for interactive use to professional seismologists and to non-experts. SeisWeb is not only a working tool in earthquake analysis but also an educational training tool for better understanding of seismology.

How to get and test SeisWeb

SeisWeb can be tested and obtained from the Institute of Solid Earth Physics, University of Bergen, web server: http://www.ifjf.uib.no//seismo/seisweb/seisweb.html.

Acknowledgements

We would like to thank Kuvvet Atakan and Margaret Grandison for their fruitful comments and reviewing the manuscript. Susan Hough, John Ebel and Steve Malone made valuable suggestions for improving the overall presentation of the manuscript. We also wish to express our gratitude to all who filled in the questionnaire.

References

Group of Scientific Experts Third Technical Test, GSETT-3, 1997. Provisional GSE 2.1. Message Formats & Protocols. Operations Annex 3. May 1997.

Gundavaram S., 1996. CGI programming on the World Wide Web, O'Reilly & Associates, Inc.

Havskov, J. and Ottemöller, L. 1999. Electronic Seismologist: SEISAN earthquake analysis Software, *Seismological Research Letters,* **70, 532-534**.

Kradolfer, U. 1993. Automating the exchange of earthquake information, *Eos, Trans. American Geophysics Union*, 74, 441-448.

Kradolfer, U. 1996. AutoDRM: The first five years, *Seismological Research Letters*, 67, 30-33.

Lindgaard, G., 1994. Usability Testing and System Evaluation: A Guide for Designing Useful Computer Systems, Chapman and Hall, London, U.K.

Rhee M. Y. 1994. Cryptography and Secure Communications, McGraw-Hill Book Co. Singapore 1994.

Schneier, B. 1996. Applied Cryptography, Second Edition, Protocols, Algorithms, and Source Code in C. John Wiley & Sons, Inc.

Weber J. L. 1998. Special Edition Using Java 1.2, Fourth Edition. QUE$^®$ United States of America.

Wessel P. and Smith W.H.F., 1999. The Generic Mapping Tools Technical Reference and Cookbook, Version 3.2, 115pp, School of Ocean and Earth Science and Technology, University of Hawai'i

URL References

Apache Software Foundation: [http://www.apache.org]

AutoDRM: [http://seismo.ethz.ch/autodrm/]

Digital Seismology Tutor: [http://lbutler.geo.uni-potsdam.de/TutorII/]

Seisgram2K: [http://www-geoazur.unice.fr/PERSO/lomax/ seisgram/ SeisGram2K.html]

Seismicity Viewer: [http://www-

geoazur.unice.fr/PERSO/lomax/nlloc/soft2.10/seismicity.html]

SeismiQuery: [http://www.iris.washington.edu/SeismiQuery]

Seismo-surfing: [http://www.geophys.washington.edu/seismosurfing.html]

WILBER: [http://www.iris.washington.edu/cgi-bin/wilber1frame.pl]

FIGURE CAPTIONS

Figure 1. Overview of SeisWeb in client-server architecture

Figure 2. Selection of database to work with

Figure 3. Main window of SeisWeb
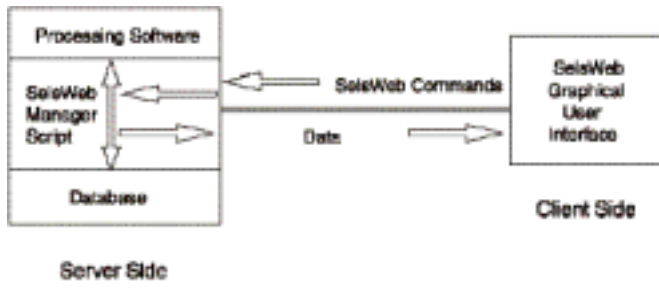
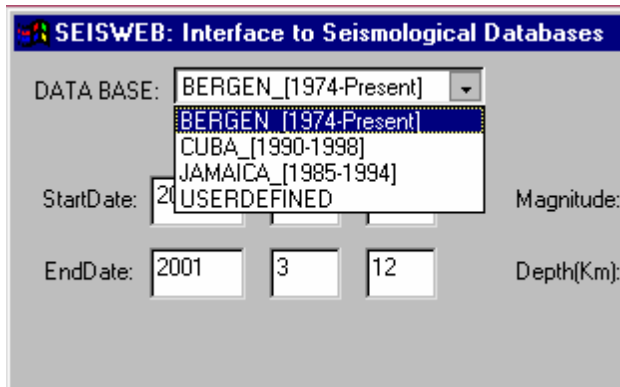Figure 4. Windows for plotting waveforms. (a) Multi-Traces mode, (b) Single-Trace mode
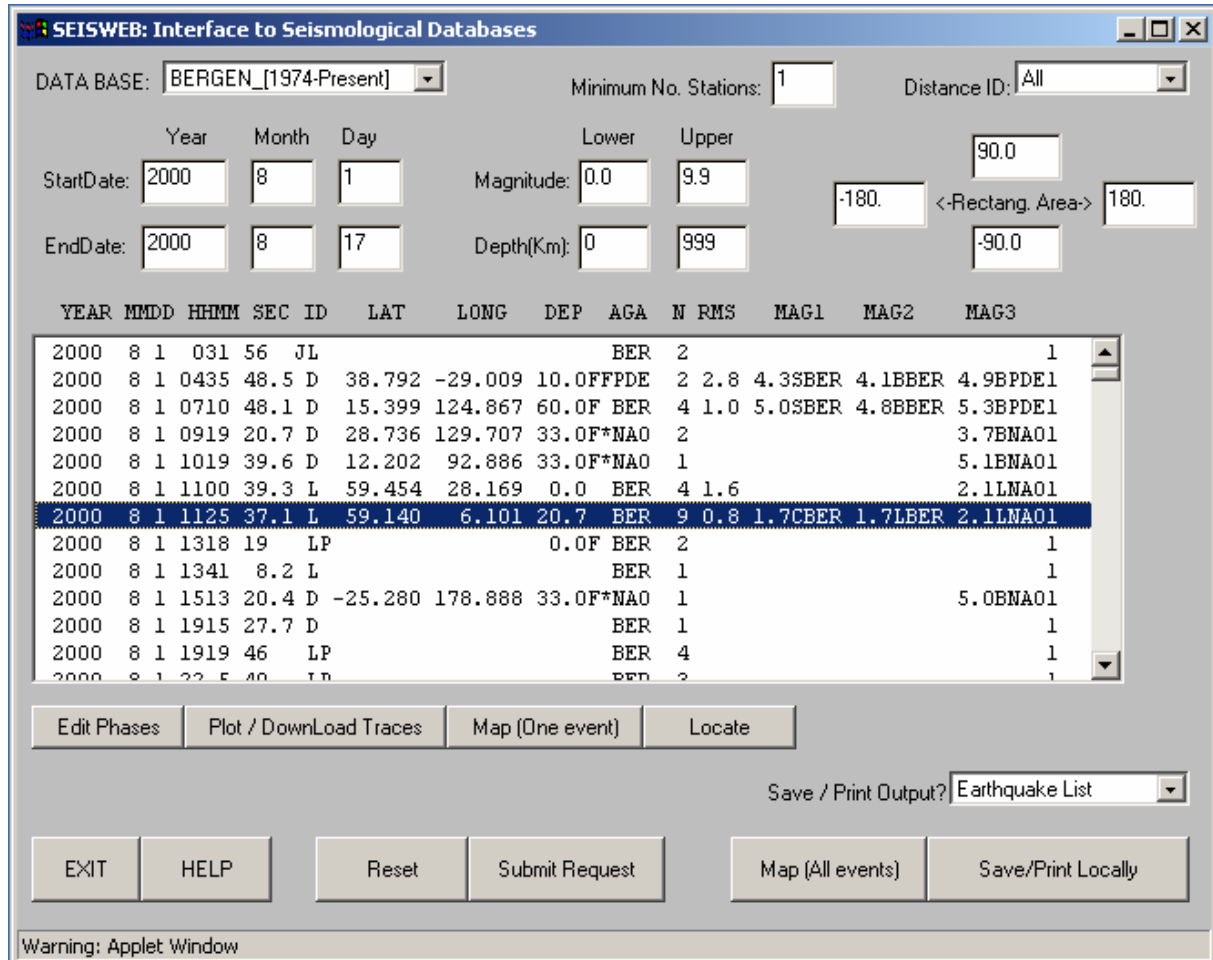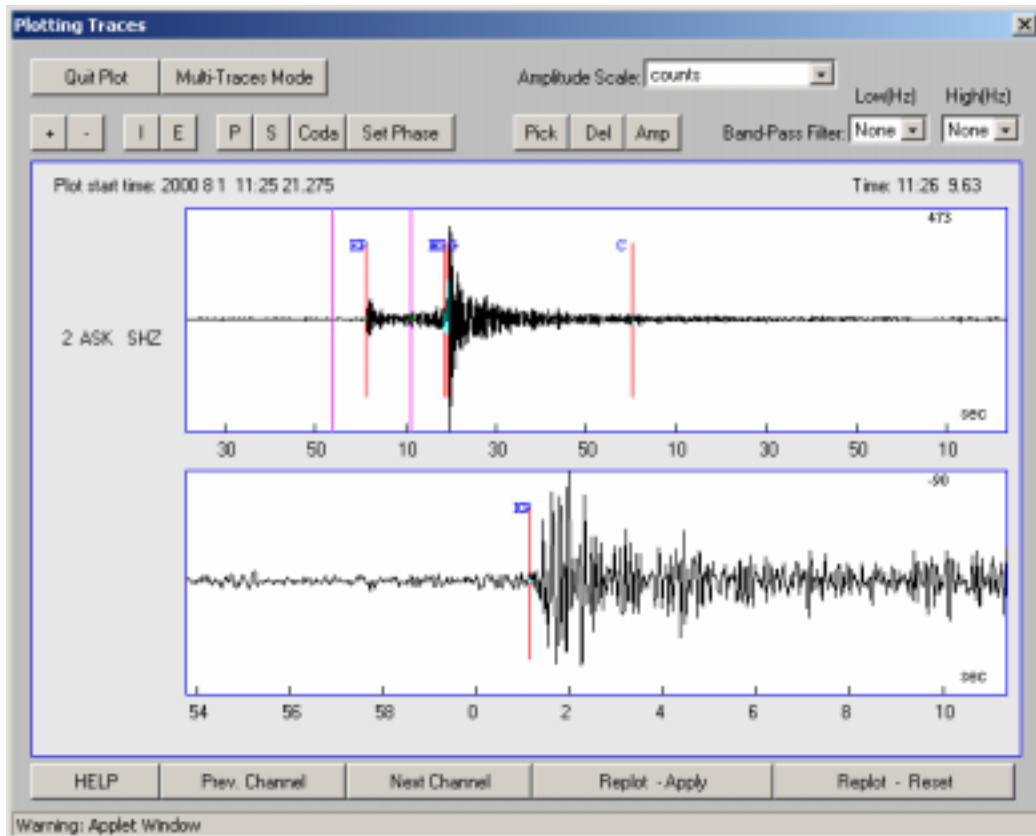
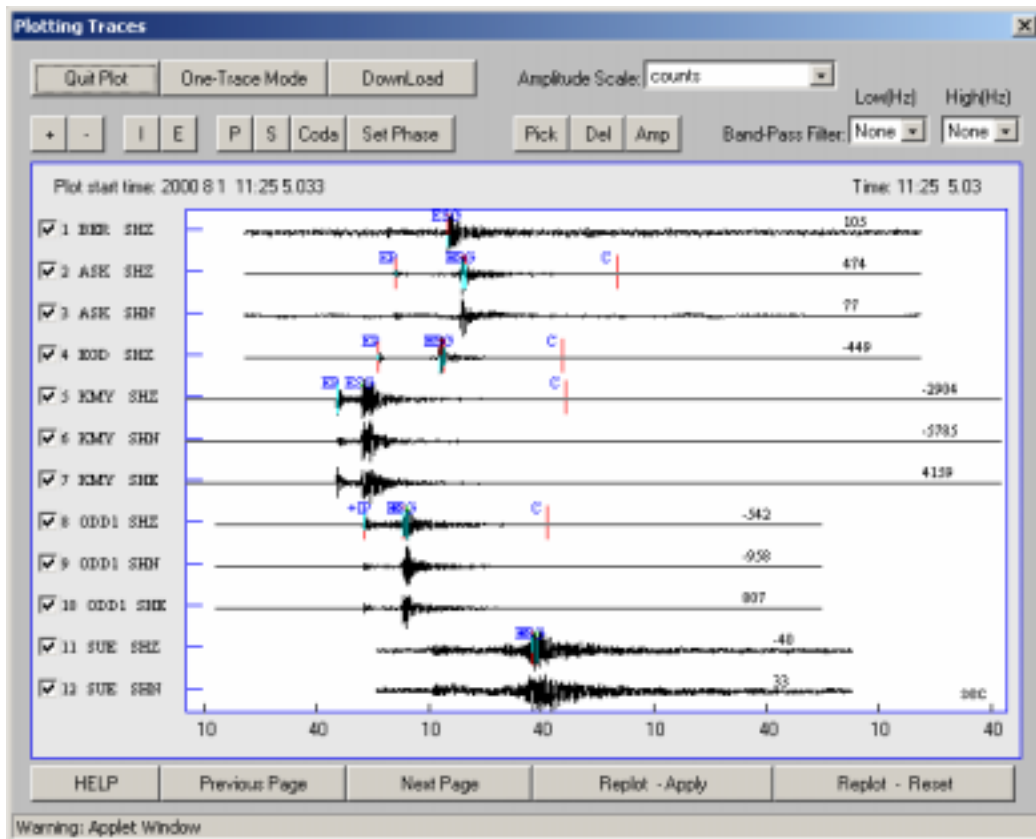FIGURA 1

FIGURA 2

FIGURA 3

FIGURA 4

Crustal velocity model along the southern Cuban margin: implications for the tectonic regime at an active plate boundary

Bladimir Moreno,[1,2] Margaret Grandison[1,3] and Kuvvet Atakan[1]

[1]*Institute of Solid Earth Physics, University of Bergen, Allégaten* 41, 5007 *Bergen, Norway. E-mail: bladimir@ifjf.uib.no*
[2]*Centro Nacional de Investigaciones Sismológicas, CENAIS,* Calle 17 No 61 e/4 y 6, *Vista Alegre, Santiago de Cuba, Cuba.*
E-mail: bladimir@sssn.ciges.inf.cu
[3]*Earthquake Unit, University of the West Indies, Mona Campus, Kingston* 7, *Jamaica*

SUMMARY

A new 1-D velocity model along the southern Cuban margin has been determined using local earthquake data, which are the result of the merged Cuban and Jamaican catalogues. Simultaneous inversion using joint-hypocentre determination was applied to solve the coupled hypocentre–velocity model problem. We obtained a seven-layer model with an average Moho interface at 20 km. The average velocity was found to be 7.6 km s^{-1} on the top of the crust–mantle transition zone and 6.9 km s^{-1} in the basaltic layer of the crust. The improvement in the earthquake locations allowed us for the first time to use local seismicity to characterize the activity on local faults and the stress regime in the area. For this purpose, 34 earthquake focal mechanisms were determined along the eastern segments of the Oriente Fault. These solutions are consistent with the known left-lateral strike-slip motion along this major structure as well as with the stress regime of two local structures: (1) the Cabo Cruz Basin and (2) the Santiago deformed belt. The first structure is dominated by normal faults with minor strike-slip components and the second by reverse faults. The shallow seismicity in the Cabo Cruz Basin is associated with fault planes trending N55°–58°E and dipping 38°–45° to the north. The Santiago deformed belt, on the other hand, exhibits diverse fault plane orientations. These local structures account for most of the earthquake activity along the southern Cuban margin. Deep seismicity observed in the Santiago deformed belt, supported by focal mechanisms, suggests underthrusting of the Gonave Microplate beneath the Cuban Block in this area. The principal stress orientations obtained from stress inversion of earthquake focal mechanisms suggest a thrust faulting regime along the Southern Cuban margin. We obtained a nearly horizontal σ_1 and nearly vertical σ_3, which indicates active compressional deformation along the major Oriente transcurrent fault in agreement with the dominant structural trend associated with the Santiago deformed belt.

Key words: crustal structure, Cuba, focal mechanisms, seismicity, stress, tectonic, velocity model.

1 INTRODUCTION

The Oriente Fault (OF) presents the highest seismic hazard in the southern Cuban margin. It defines a segment of the North American and the Caribbean Plate boundary along which strike-slip deformation dominates (Fig. 1). Much of this deformation is concentrated along the releasing and restraining bends of the OF such as the Cabo Cruz Basin (CCB) and the Santiago deformed belt (SDB). This zone, comprising part of the Bartlett–Cayman fault system, is responsible for more than 90 per cent of the seismicity and the largest earthquakes observed along the southern Cuban margin. According to historical data there have been 19 strong earthquakes during the last 400 years with intensity VII or higher on the MSK scale

(Alvarez *et al.* 1973). Earthquakes of magnitude 7 have occurred in this zone. The most recent strong earthquake recorded in this area took place on 1992 May 25th with a magnitude (M_s) of 6.9 and with a hypocentre located in the CCB (Perrot *et al.* 1997). We define the term 'Oriente Fault Zone' (OFZ) to include all structural features in the area between 79.5° and 73.5°W longitude and 19° and 20°N latitude, such as the CCB and SDB (Fig. 1).

Previous studies of crustal structure conducted for this area (Ewing *et al.* 1960; Edgar *et al.* 1971; Goreau 1983; Calais & Mercier de Lépinay 1990, 1991; Case *et al.* 1990; Donnelly 1994) were mostly based on seismic refraction, reflection and gravity measurements. These studies have shown a complex crustal structure with very irregular crustal thicknesses and seismic *P*-wave
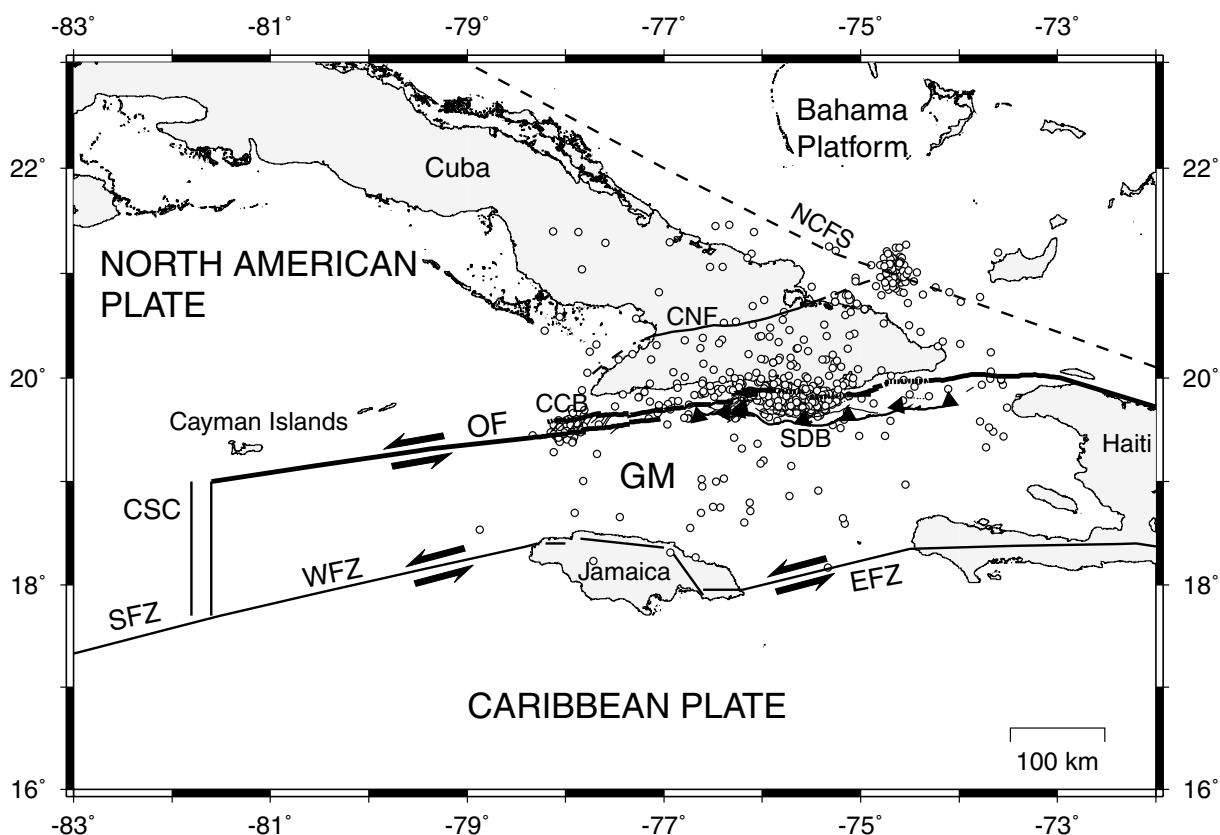
Figure 1. Kinematic framework along the southern Cuban margin. OF, Oriente fault; WFZ, Walton fault zone; EFZ, Enriquillo fault zone; CNF, Cauto Nipe fault; NCFS, Nortecubana fault system; SFZ, Swan fracture zone; CSC, Cayman spreading centre; GM, Gonave Microplate; CCB, Cabo Cruz Basin; SDB, Santiago deformed belt. The mapped OF including the CCB and SDB is taken from the interpretation made by Calais & Mercier de Lépinay (1990, 1991) during the SEACARIB II oceanographic cruise. Dashed lines represent assumed traces of faults. Open circles shows 569 earthquakes recorded by three or more stations during 1998 March–2000 July.

velocities. This inhomogeneity, together with the unfavourable geometrical arrangement of the Cuban Seismograph Network (CSN) (Fig. 2), makes it difficult to establish an average *P*-wave velocity model for the determination of the hypocentres. The Jamaican Seismic Network (JSN) (Fig. 2), the second local network recording data from this zone, is also located outside the OFZ. Owing to this uncertainty in earthquake locations, tectonic interpretation using local seismicity based on either of these networks alone has been difficult. In the present study, the earthquake data from the Cuban and the Jamaican seismic networks were merged to improve the location accuracy of earthquakes generated in the OFZ. The first objective of this work was to establish a reliable crustal velocity model. The obtained velocity model is then used for relocating the earthquakes with the aim of improved our understanding of the present tectonic regime in the area.

2 SOURCES OF DATA

The CSN is composes of six broad-band field stations along the island and five three-component telemetered short-period stations concentrated in the eastern part of Cuba. The JSN consists of 11 telemetered short-period stations, three of which have three components (Table 1 and Fig. 2). Both seismic networks are synchronized in time by the use of Global Positioning Systems (GPS). More information concerning the CSN and JSN can be found in Wiggins-Grandison (2001) and Moreno (2002).

A total of 99 earthquakes were collected from 1998 March to 2000 July (Fig. 2). Seven or more stations operating in both networks registered the seismic events, which had a local magnitude between 2.7 and 4.4. The criteria for selecting the data used in the inversion were for an earthquake to have 10 or more observed phases and an azimuthal gap of 180° and lower. This yielded only 60 earthquakes, so we included earthquakes with gaps up to 240°.

3 1-D VELOCITY MODEL

The part of the Caribbean Sea between Cuba and Jamaica has a complex crustal structure with lateral variations in seismic wave velocity and irregular thickness of oceanic crust. The crustal thickness varies between 5 and 20 km excluding water depth (Case *et al.* 1990). The Moho tends to be deeper along the south coast of Cuba and north coast of Jamaica. According to seismic refraction and reflection studies the *P*-wave velocity shows lateral variations from 7.8 to 8.2 km s^{-1} in the upper mantle and from 5.4 to 6.4 km s^{-1} in the basaltic layer of the crust (Ewing *et al.* 1960). Most of the Cuban seismic stations are located on a transitional crust, the interior part of the island arc with a range of crustal thicknesses from 17 to 30 km (Bush & Shcherbakova 1986). According to Bush & Shcherbakova (1986) the crust of Eastern Cuba can be divided into three layers: (1) a sedimentary volcanic layer with *P*-wave velocity from 4.0 to 4.8 km s^{-1}; (2) an upper layer of consolidated crust (5.8–6.4 km s^{-1}); and (3) a lower layer of consolidated crust
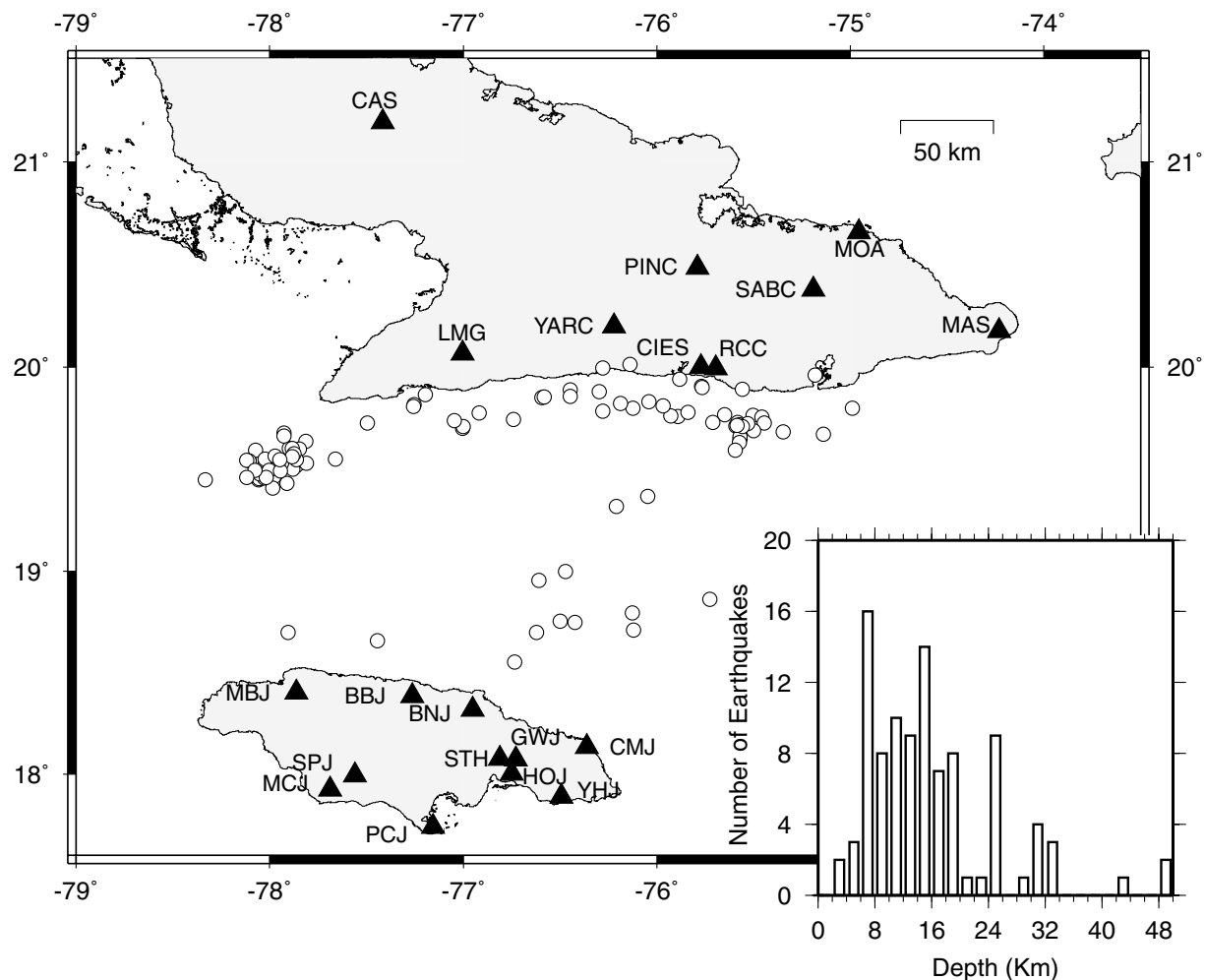
Figure 2. Seismic Networks of Cuba and Jamaica (black triangles) and epicentres of the earthquakes (open circles) used in the inversion process. The locations of the earthquakes were computed with the new velocity model obtained in this study. The inset shows the depth distribution of the earthquakes plotted in the map. The tick mark in the depth-axis assumes an interval of ±1 km.

(6.3–6.7 km s^{-1}). The Jamaican seismic stations are located on crust with an average thickness of 21 km. The basaltic crustal layer beneath the island is 12–15 km thick (Arden 1975).

3.1 Inversion process

The inversion process was achieved with the program VELEST (Kissling *et al.* 1995). The coupled hypocentre–velocity model problem was solved performing joint-hypocentre determination (JHD) using both *P* and *S* arrival times. The solution was obtained by a trial-and-error process with various initial velocity models and with different combinations of damping factors. For more details concerning the method see Kissling (1988) and Kissling *et al.* (1994).

No previous hypocentre–velocity structure inversion has been done for this area, therefore we used as the initial model for this inversion one of the available velocity models from the two networks involved (Fig. 3a). The Jamaican model was used to calculate the initial earthquake locations in the newly merged Cuban–Jamaican catalogue because more earthquakes had lower rms misfits when compared with the Cuban model (Fig. 5). The phase picks were reanalysed to reduce the number of badly picked phases. The number of observations per station of *P* and *S* waves is shown in Table 2.

The V_p/V_s ratio is an important parameter used by the inversion algorithm. To calculate this value we made a Wadati diagram using the SEISAN software (Havskov & Otemöller 1999) for the selected earthquakes and 1.74 was obtained with a standard deviation of 0.07. A reference station, which maintains its initial delay (normally set to zero) is also needed for the inversion process. Considering the spatial distribution of the earthquakes and the number of observations, we selected RCC as the control station (Fig. 2). This station has more than 85 per cent of the total readings and is located close to the major earthquake source.

The solution of the inverse problem depended strongly on the initial model and initial hypocentres. Since only 30 per cent of the selected earthquakes initially had an rms misfit below 0.5, we made several runs of VELEST using more earthquakes and a different initial model each time. After each run the velocity model obtained was used to relocate the entire catalogue and this served as the new input model for the next run. This procedure permitted us to increase the number of earthquakes having a low rms and then to use them as new initial hypocentres for the next run. Finally, we ended up with 89 earthquakes (90 per cent of the data) with an rms lower than or equal to 0.5 and a probable final model (Fig. 3a).

To test the variability of the convergence of the solution with respect to the input model, we ran VELEST with several input

Table 1. Seismic stations of Cuba and Jamaica used in this study with their delay time corrections.

Station	Instrument type and (no comp)	Latitude north (deg)	Longitude west (deg)	Elevation (m)	P-wave correction (s)	S-wave correction (s)
CCC	Broad B. (3)	21.1937	77.4172	90	1.22	3.37
RCC	Broad B. (3)	19.9953	75.6965	100	0.0	−0.15
LMG	Broad B. (3)	20.0673	77.0047	200	−0.02	0.08
CIES	Short P. (3)	20.0020	75.7710	40	−0.05	−0.10
YARC	Short P. (3)	20.2000	76.2200	100	−0.15	−0.10
PINC	Short P. (3)	20.4870	75.7910	647	0.00	0.96
SABC	Short P. (3)	20.3800	75.1900	100	−0.11	0.18
BBJ	Short P. (1)	18.3865	77.2623	766	−0.37	−1.14
BNJ	Short P. (1)	18.3210	76.9505	485	−0.43	−1.30
CMJ	Short P. (1)	18.1350	76.3613	333	−0.62	−1.02
GWJ	Short P. (1)	18.0742	76.7280	1170	−0.80	−1.35
HOJ	Short P. (1)	18.0050	76.7490	228	−0.41	−0.93
MBJ	Short P. (3)	18.4048	77.8630	513	−0.44	−1.07
MCJ	Short P. (3)	17.9253	77.6863	661	0.11	−0.19
PCJ	Short P. (1)	17.7412	77.1573	198	0.03	−0.45
SPJ	Short P. (1)	17.9960	77.5600	751	−0.40	−0.63
STH	Short P. (3)	18.0772	76.8097	504	−0.72	−1.19
YHJ	Short P. (1)	17.8920	76.4930	600	−0.29	−0.81
MOA	Broad B. (3)	20.6583	74.9568	140	−0.11	–
MAS	Broad B. (3)	20.1760	74.2310	350	0.83	–

models having different layer thickness and velocities (Fig. 3b). The input models do not have layer interfaces beyond 34 km owing to the shallow seismicity of the area and the known thickness of the crust. The set of solutions shows a similar geometry but indicates a large variability in the velocity range for the upper layers (Fig. 3c). The topmost layers did not converge very well owing to the small number of earthquakes with depths less than 7 km (inset of Fig. 2); most of the earthquakes are generated at more than 5 km below the seafloor. The rays arriving from bottom layers subvertically penetrate the topmost layers, therefore the ray lengths are shorter in the topmost layers and consequently, the traveltime segments carry less weight in the inversion process. The thinness and poor resolution of the topmost layers made the convergence of the inversion more difficult. Bottom layers show a tendency to converge within a very small velocity range. These results indicate that the inversion problem has a solution space with several local minima. How well the solution converges toward a local minimum depends on the initial model and the initial hypocentres.

The input models and their corresponding solutions indicate an average Moho depth of 20 km with velocities ranging between 7.5 and 7.7 km s^{-1}. The layer above the Moho up to 9 km depth exhibits a velocity range of 6.8–7.0 km s^{-1}. From the three probable solutions the one obtained using the input model with intermediate velocity had the lowest rms misfit. However, it is still not possible to claim that the absolute minimum of the solution space was found.

3.2 Selecting final model

The geometry of the final model was well defined by the inversion process. Selecting the velocity for each layer required an extra procedure. The range of velocities obtained from the simultaneous inversion for the near-surface layer was wide, so we used forward modelling to obtain a suitable solution. Several velocity models were tested using the HYPOCENTER program (Lienert & Havskov 1995) and the model with the overall lowest rms misfit was selected. According to the result of the inversion process and previous studies of seismic refraction, we defined a range of velocities for each

layer to be tested. The input models consisted of eight layers with fixed thickness and wide variations in velocity. Table 3 shows the range of velocities for each layer to be tested with a velocity step of 0.1 km s^{-1}.

More than 1462 models were tested with the same set of data used for the inversion process. The final calculation ended with only one minimum corresponding to the input model shown in Table 4. This model is similar to the probable final model obtained in the previously described inversion process, but with more near-surface layers (Fig. 3d).

3.3 Station corrections

The delay times for each station (station corrections) are determined with the hypocentres and velocity model during the inversion process. Since we selected the final model using forward modelling, the station corrections had to be calculated again. In order to obtain the station corrections for P and S waves, we ran VELEST in the JHD mode with the new final velocity model and the same set of data used previously. The velocity model was damped to keep it fixed during the inversion process. The P-wave correction for the reference station was kept constant at the initial value (zero) and for the S wave was free floating. The resulting values of the station corrections ranged from −0.80 to 1.22 s for P waves and from −1.35 to 3.37 s for S waves (Table 1 and Fig. 4). The station corrections are traveltime residuals with respect to the reference station and represent local anomalies in the velocity. In the case of Cuba, the station corrections are also affected by velocity anomalies along the ray path. The effect of the path is cancelled when the earthquakes are widely distributed in the area. However, the seismicity in Cuba is clustered in a few zones (Fig. 1). The local topography at Cuban seismic stations has little influence on the station corrections. The elevation above sea level and soil conditions are not significantly different. The biggest values in the station corrections are associated with differences in crustal thickness and seismic wave velocities throughout the area. The control station (RCC) is located where the Moho is 18–20 km deep, whereas some of the stations
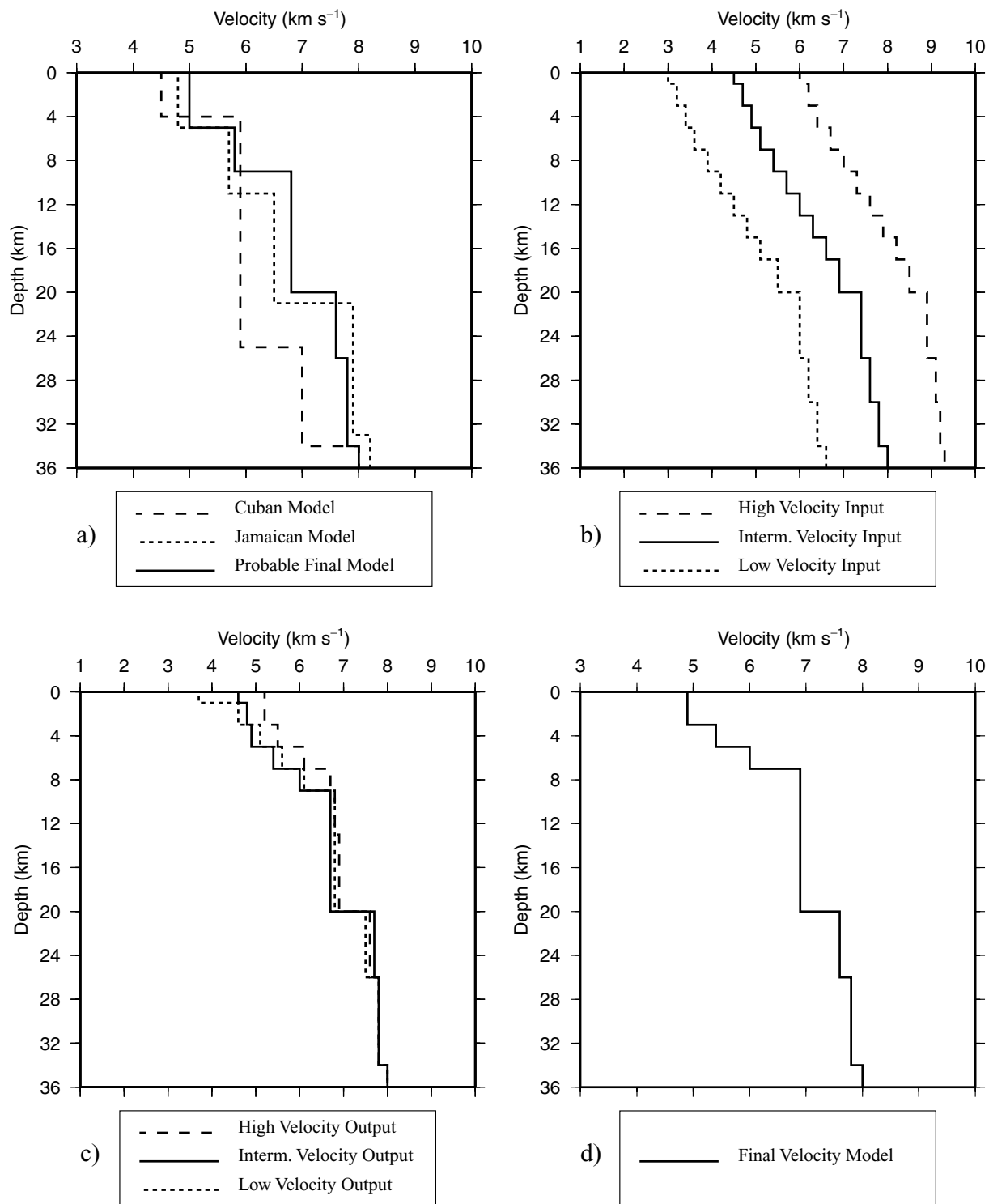
Figure 3. *P*-wave velocity models: (a) Cuban and Jamaican models and the probable final model derived from the inversion process; (b) input models used in the inversion process for testing the stability (convergence) of the solution proposed in (a); (c) output models of the inversion associated with the input models defined in (b); (d) final model obtained from forward modelling.

with high corrections values such as CAS are located where the Moho is 30 km deep (Bush & Shcherbakova 1986). The theoretical first arrival for this station should be a head-wave travelling along the Moho interface at 20 km depth, but in fact they have a longer ray path. The tendencies of negative values for the Jamaican stations are associated with first arrivals travelling southward at shallower Moho interfaces. The seismic rays coming from the major seismic sources are crossing a thin oceanic crust. Here, local topography and site conditions might also be affecting the station corrections.

Table 2. Number of observed phases for each station used in the inversion process.

Stations	No observ. of *P*	No observ. of *S*	Stations	No observ. of *P*	No observ. of *S*
STH	90	83	MCJ	20	14
RCC	85	65	PINC	23	8
GWJ	82	51	CMJ	19	11
LMG	77	68	CIES	15	10
BNJ	71	55	YHJ	11	11
CCC	62	41	SABC	10	7
BBJ	59	45	YARC	10	7
MBJ	52	50	MAS	8	–
PCJ	62	34	MOA	8	–
HOJ	36	29	SPJ	4	4

Table 3. Range of velocities to be tested in forward modelling using a step of 0.1 km s^{-1}.

Layer no	Velocity range (km s^{-1})	Depth (km)
1	4.3–4.9	0
2	4.9–5.4	3
3	5.4–6.0	5
4	6.0–6.9	7
5	6.9 (constant)	9
6	7.6 (constant)	20
7	7.8 (constant)	26
8	8.0 (constant)	34

Table 4. Final velocity model.

Layer no	Velocity (km s^{-1})	Depth (km)	Thickness (km)
1	4.9	0	3
2	5.4	3	2
3	6.0	5	2
4	6.9	7	13
5	7.6	20	6
6	7.8	26	8
Half-space	8.0	34	–

3.4 Relocation of the earthquakes

A total of 569 earthquakes recorded by three or more stations were collected during 2 years of monitoring (Fig. 1). The rms residuals in the hypocentre locations for the entire dataset computed with the obtained velocity model and the previous initial models are illustrated in Fig. 5. More than 55 per cent of the earthquakes have rms misfit lower than 0.5 s, which represents a significant improvement in the new earthquake locations when compared with the solutions obtained by using either the Cuban or Jamaican velocity models. The change in the earthquake locations using the new model with respect to the Cuban model is presented in Fig. 6. There are four boxes enclosing the zones with some tendencies in the orientation of the new location. Zone 'a' is associated with the seismicity of the CCB (Fig. 1). The new locations delineate this pull-apart zone very well. Zone 'b' moves the hypocentres southward in agreement with the location of the major Oriente strike-slip fault (Fig. 1). The new locations in zone 'c' move the hypocentres toward the SDB, and zone 'd' concentrates the aftershocks of the 1998 December 28th earthquake ($M_w = 5.6$) in the junction of the Cauto–Nipe fault (CNF) and the Nortecubana fault system (NCFS) (Fig. 1). The largest arrows are associated with the effect of changing an old solution with a very deep hypocentre to a new shallow solution. A summary of

the location errors for the previous Cuban and Jamaican models and the new velocity model is given in Table 5.

4 THE TECTONIC REGIME OF THE AREA

The relative motion between the North American and Caribbean plates governs the tectonic regime of the area at a regional scale (Fig. 1). The eastward motion of the Caribbean plate relative to the North American plate has been debated to be at a rate from 12 to 40 mm yr^{-1} (Sykes *et al.* 1982; De Mets *et al.* 1990; Deng & Sykes 1995; Dixon *et al.* 1998). Most recently, De Mets *et al.* (2000) estimate an average of 18–20 $\pm$ 3 mm yr^{-1} with 18 $\pm$ 2 mm yr^{-1} of boundary parallel slip and 3 $\pm$ 3 mm yr^{-1} of boundary normal convergence south of eastern Cuba. This eastward motion of the Caribbean plate produces left-lateral slip along the Enriquillo (EFZ) and Walton Fault Zones (WFZ), and left-lateral strike-slip deformation along the OF (Fig. 1). However, there are two important local structures affecting the tectonic regime in the area: (1) the CCB and (2) the SDB (Fig. 1). These structures account for more than 90 per cent of the seismicity along this part of the plate boundary. Despite the fact that this area includes the best known and studied segment of the OFZ (Calais & Mercier de Lépinay 1991), small and moderate earthquakes have never been used as additional data to support the interpretations made in terms of the present tectonic regime. Fig. 1 also shows the aftershocks of a 5.6M_w earthquake that occurred on 1998 December 28th at the junction of the CNF and NCFS. The focal mechanism (from the Harvard CMT catalogue) gives almost pure reverse faulting along a direction parallel to the strike of the NCFS. We do not attempt any characterization of the tectonic regime in this area because of the poor station coverage. In this study, our focus is toward those structures located along the OFZ (the CCB and SDB).

4.1 Earthquake focal mechanisms and seismicity of the CCB and SDB

In order to correlate earthquake activity with active faults we solved for 34 earthquake focal mechanisms along the OFZ (Figs 7 and 8). Normally, the reliability of a focal mechanism solution depends on the size of the earthquake and the method used for the solution (e.g. moment tensor, waveform modelling, first motion) but in our case all the earthquakes are small ($M < 4.5$) and the focal mechanisms were determined by using only *P*-wave first-motion polarities. The solutions were obtained using the SEISAN software (Havskov & Otemöller 1999), which uses the algorithm developed by
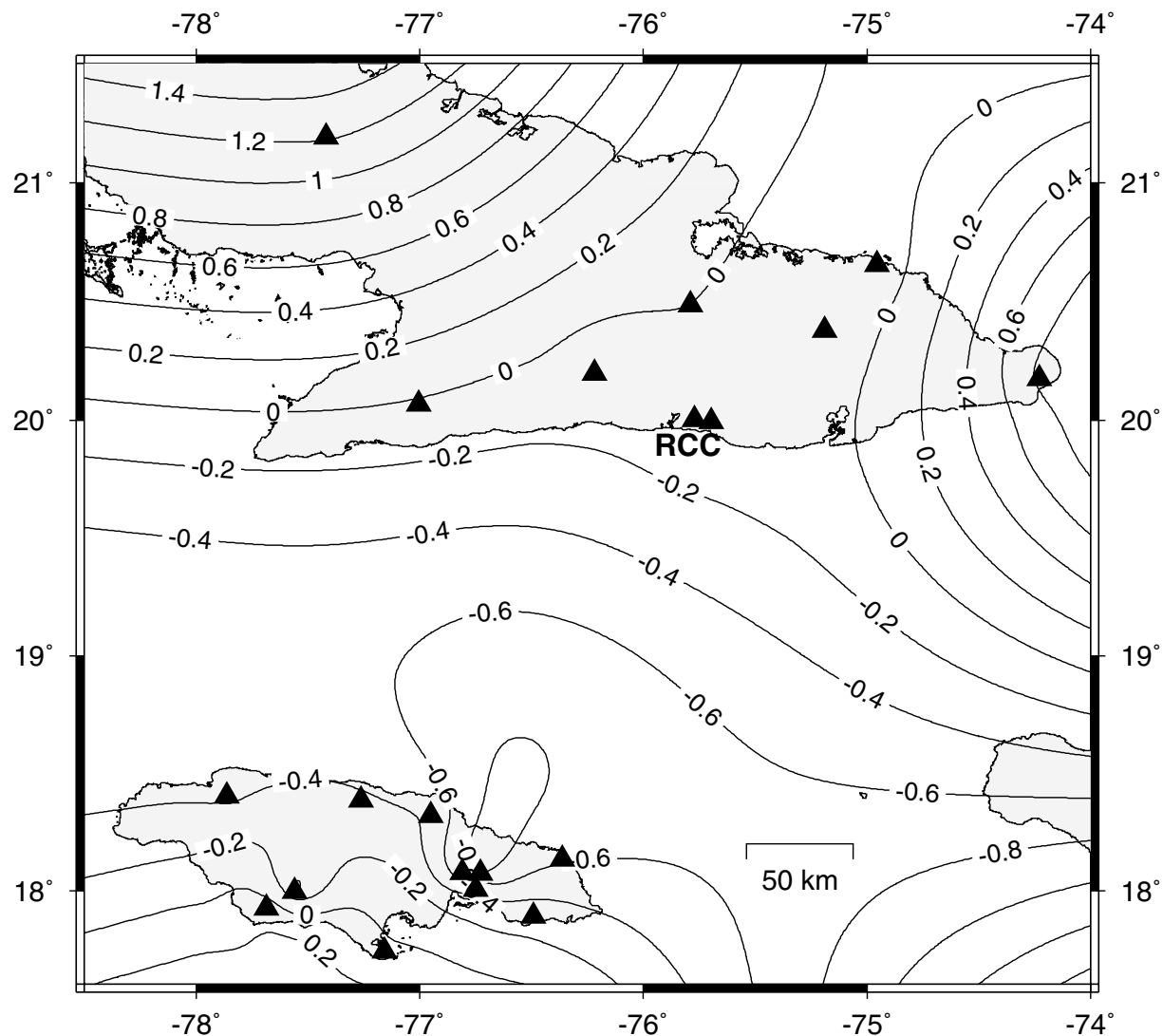
Figure 4. Contour lines showing delay times of *P* waves for each station (station corrections). The station corrections were calculated with respect to the reference station (RCC).

Snoke *et al.* (1984). The fault-plane solutions presented have nodal planes that have been resolved to within ±15°. Although each solution was constrained by seven or more polarities of the *P* wave, we categorize each solution with a quality factor based on the distribution of polarities in all quadrants and the focal-depth error. Combining these two criteria we obtain nine possible quality factors (Table 6).

4.1.1 The Cabo Cruz Basin

The CCB is a narrow E–W-trending depression, bordered on the north and south by two segments of the Oriente Fault and divided by normal faults into a series of oblique horsts and grabens (Calais & Mercier de Lépinay 1991). The discontinuous trace of the Oriente fault with left-stepping offsets generates local tensional strain and causes pull-apart subsidence (Cotilla 1993; Perrot *et al.* 1997). According to the new merged Cuba–Jamaica catalogue, the seismicity in the CCB is shallow. Note that the set of epicentres defines very well the western part of the basin (Fig. 1). We performed depth

cross-sections of the hypocentres located in this zone, but no clear trend was found.

The observed focal mechanisms are consistent with E–W extension in this area (Table 7). Most fault planes are trending N55°–58°E and dipping 38°–45° to the north, which are in good agreement with the normal faults mapped by Calais & Mercier de Lépinay (1991). Small earthquakes occurring in the CCB are generated by normal faults. However, strong earthquakes should be expected along the northern and southern borders of the CCB where the major OFZ segments are located. This was the case with the last strong earthquake that occurred in this area (Perrot *et al.* 1997). The earthquake is labelled as P1 in Fig. 7 and is detailed in Table 7. The rose diagram in Fig. 7 represents the orientation of the maximum horizontal compressive stress (σ_h) obtained from the *P*, *B* and *T* axes according to Zoback (1992). Earthquakes with an unknown (U) stress regime (Tables 7 and 8) are not represented in the rose diagram. The diagram shows clear N15°E horizontal compression, in agreement with the expected W–E horizontal extension in this pull-apart zone. The lower inset in Fig. 7 shows the result of the stress inversion but this is discussed in Section 4.2.
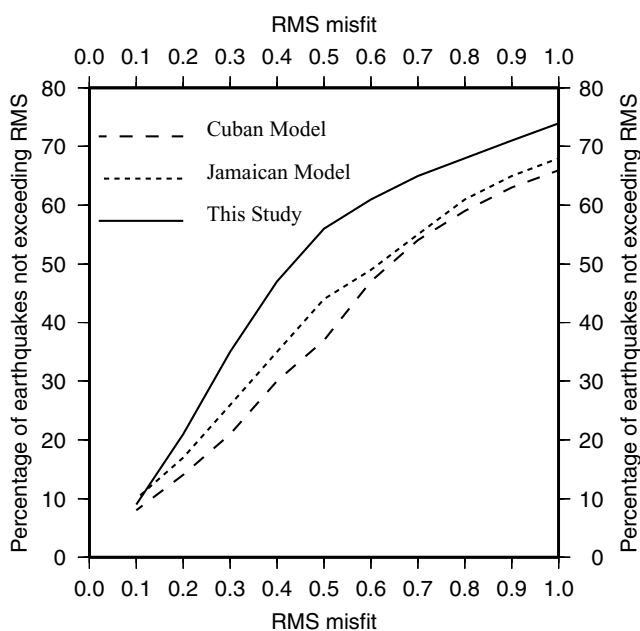
Figure 5. Percentage of the cumulative number of earthquakes having rms misfit lower than the upper limit values defining the *x*-axis. The earthquake locations (569 earthquakes) were calculated using three different models. The new velocity model shows 56 per cent of the earthquakes with an rms misfit of less than 0.5.

4.1.2 The Santiago deformed belt

The SDB was described for the first time by Calais & Mercier de Lépinay (1990, 1991). It is a narrow submarine mountain range extending over 300 km along the OFZ with folds and thrust faults showing clear evidence of transpressional deformation (Calais & Mercier de Lépinay 1990, 1991; Calais *et al.* 1998). The dashed line in Fig. 6 crossing zone 'c' represents the line of a depth cross-section (inset to Fig. 6) of earthquakes with an error in depth of less than 15 km. The depth section shows shallow and relatively deeper seismicity (deeper than 30 km). Shallow seismicity in the first 30 km measured from the north is associated with inland faults and the northern segment of the OFZ. Beyond 30 km the earthquakes are generated by thrust faults in the SDB. Deep seismicity, on the other hand, seems to be generated by reverse faults. Earthquake focal mechanisms (Fig. 8 and Table 8) in this zone show evidence of reverse faulting at depths below 30 km. It is unlikely that shallow thrust faults in SDB can be responsible for earthquakes at such depths in an oceanic crust. Another process, perhaps crustal thickening might be occurring there (see the discussion).

The focal mechanisms shown in Fig. 8 are not restricted only to the SDB; we include the segment of the OFZ (that we define as OFS), which connects the northern border of the CCB and continues eastwards along the southern Cuban margin. The events labelled as C1, C2, C3 and C4 are taken from the Harvard CMT Catalogue. Two groups of fault regimes are dominant in the area: (1) left-lateral strike-slip and (2) reverse faulting. The first group corresponds to the transition area from CCB to SDB occurring along the OFZ. The fault planes follow the trend of the OFZ and dip at 65°–80° to the north. The earthquakes located in the vicinity of the CCB (3, 13–15) have a minor normal component. However, once we move eastward the earthquakes (1, 2, 4, 5) begin to exhibit a minor reverse component. This pattern shows evidence of the transition from transtension to transpression along the OFZ. Note that the earthquakes labelled

as 1, 2, 4 and 5 are not located on the mapped segment of the OFZ. The possibility that they are shifted north is low owing to the small errors in their locations. Since the resolution of seismic reflection, gravimetric and magnetic measurement throughout the area was not high enough to map the entire OFZ trace, one of the segments bordering the north side of the SDB might continue to the west. If so, then earthquakes 1, 2, 4 and 5 could be associated with one of the OFZ fault segments. The rose diagram on the upper left-hand corner plots maximum horizontal compressive stress for the events labelled as 1–5 and 13–15. It shows a clear N45°E maximum horizontal compressive stress orientation. The second group corresponds to earthquakes located in the SDB and the surrounding area, which are mainly the result of reverse faulting with variable fault plane orientations. Solutions 9 and 16 might be associated with cross-cutting compressional faults trending N100°E and caused by a discontinuity of the major Oriente transcurrent fault. In this area the trace of the Oriente fault was assumed to be caused by inadequate geophysical information and, therefore it was mapped as a dashed line. Furthermore, the assumed cross-cutting segment indicating the discontinuity might be located more to the west of where it was mapped. Note that the deformation in the coastal Cuban margins surrounding this area supports this assumption. Earthquakes with relatively deeper hypocentres such as 0 and 7 (Table 8) are unlikely to be associated with the mapped shallow thrust faults of SDB. They must be the result of another process (see the discussion). The rose diagram on the lower right-hand corner plots maximum horizontal compressive stress for the events, which belong to this group (0, 6–12, 16–20 and C1–C4). It exhibits a scattered σ_h orientation with a small tendency to be oriented in a N65°E direction. The scatter σ_h orientations might be associated with the irregular alignment of the thrust faults mapped in SDB.

4.2 Stress inversion of earthquake focal mechanisms

It has been suggested that most of the stress accumulated by the Caribbean–North American plate motion is released seismically along the northern Cuban margin during a relatively few but strong earthquakes (Perrot *et al.* 1997; Van Dusen & Doser 2000). This sparse occurrence of strong and moderate earthquakes makes it difficult to use earthquake focal mechanisms for mapping the crustal stress field in this area. The focal mechanism solutions presented in this study offer a good opportunity to estimate the principal stress orientations in this part of the Caribbean–North American plate boundary. For this purpose, we use the FMSI (Focal Mechanism Stress Inversion) software (Gephart 1990) based on procedures described in Gephart & Forsyth (1984). The modelled stress tensors and the corresponding misfit values are determined through a grid search and the misfit for a given mechanism is defined as the minimum rotation about any arbitrary axis that brings each nodal plane into compliance with the stress model being tested. The data set used in the inversion was weighted from 1 (worst) to 4 (best). We assigned weight 4 to the earthquakes labelled as P1 and C1–C4. The rest of the earthquakes were weighted from 1 to 3 according to the quality factor described in Table 6. We performed the inversion for each zone and the entire region calculating the misfit value at 5° intervals for a total of over 150 000 input models.

The results of the stress inversion for each zone are shown as the lower inset in Figs 7 and 8. Given the fact that a set of identical or nearly identical focal mechanisms cannot constrain the stress tensor (Hardebeck & Hauksson 2001), the principal stress axes for the CCB and OFS may not be well constrained by the inversion process and therefore should not be used in our interpretation. The
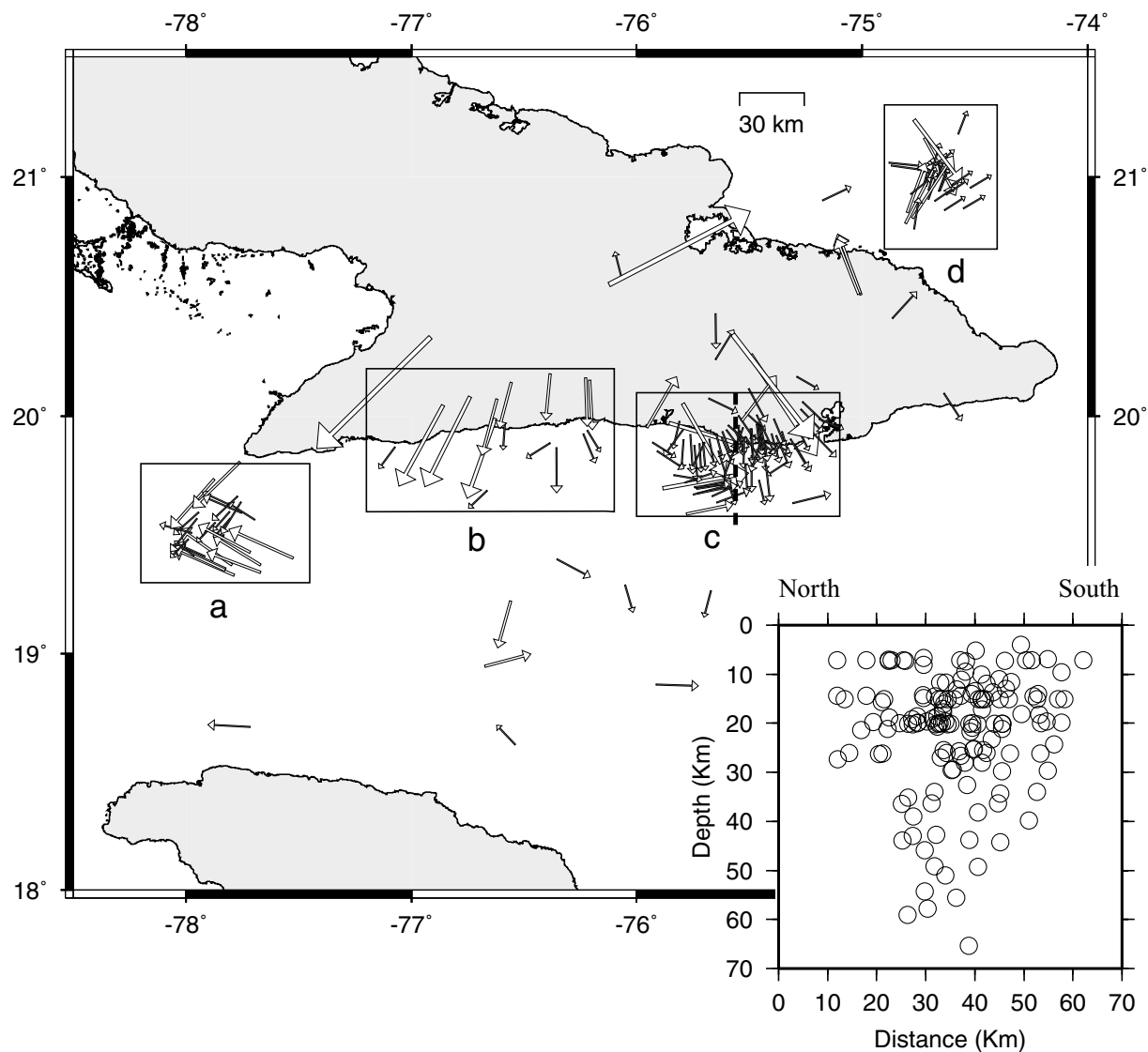
Figure 6. Epicentral changes with differences larger than 10 km between the original and the new locations. The arrows point from the original to the new locations, calculated with the velocity model obtained in this study. The original locations were computed with the Cuban velocity model without station corrections. Boxes indicate zones with distinct clustering towards significant structural features; (a) Cabo Cruz basin; (b) segments of the OFZ; (c) Santiago deformed belt; (d) junction of the NCFS and CNF. The dashed line crossing zone c represents the location of a depth cross-section (see inset) across the Santiago deformed Belt. The plotted points in the depth cross-section correspond to earthquakes having errors in depth less than 15 km.

SDB, on the other hand, shows a dissimilar focal mechanism and gives a more reliable estimation of the stress tensor. The solution shows a horizontal σ_1 (oriented ENE–WSW) with nearly vertical σ_3, indicating a thrust faulting regime.

Table 5. Number of earthquakes with error in location less than 10 km for the entire dataset (569 earthquakes) using different velocity models.

Error less than 10 km	Cuban model	Jamaica model	This study
Epicentre error radius	130	151	187
Hypocentre error radius	72	73	82
Latitude error	177	188	223
Longitude error	241	240	285
Depth error	112	111	112

Hardebeck & Hauksson (2001) proposed that a given focal mechanism data set is adequately diverse for use in stress inversions if the rms difference from the average mechanism is greater than 40°–45°. Furthermore, we have inverted only those focal mechanisms satisfying the required criteria for estimating the stress field of the entire region. In this sense, we used 28 focal mechanisms from all three data sets having sufficient levels of diversity. The resulting σ_1 is nearly horizontal in an ENE–WSW direction with near vertical σ_3, which corresponds to a thrust faulting regime (Fig. 9). This result seems to indicate that the plate boundary along the OFZ enters into a thrust faulting regime within the SDB, showing that this area is undergoing active transpressional deformation along a major transcurrent fault. This pattern is probably a result of a regional oblique motion along the OFZ (Calais & Mercier de Lépinay 1990, 1991). The orientation of the principal stress axes seems to be induced by an oblique WSW–ENE convergence of
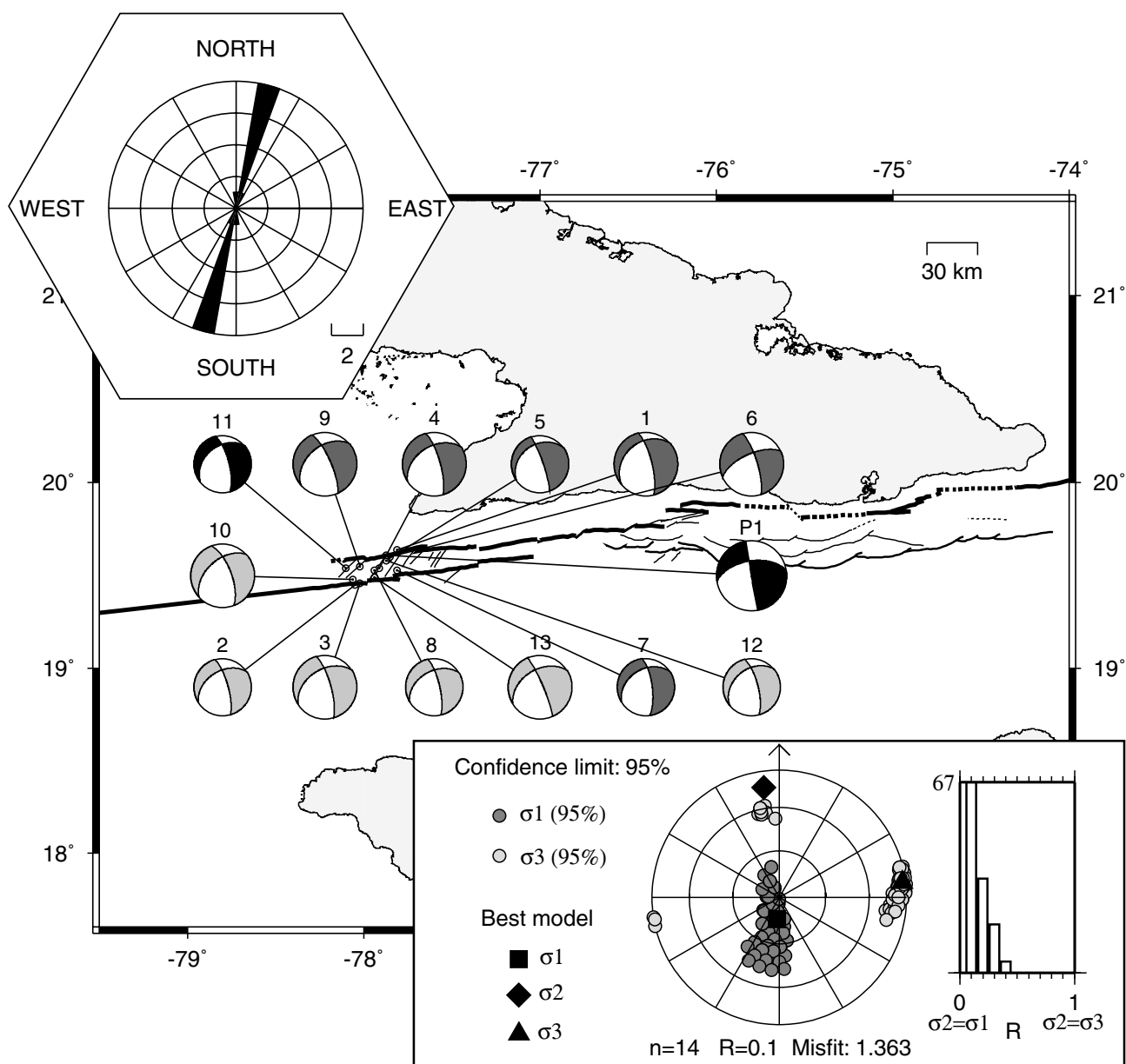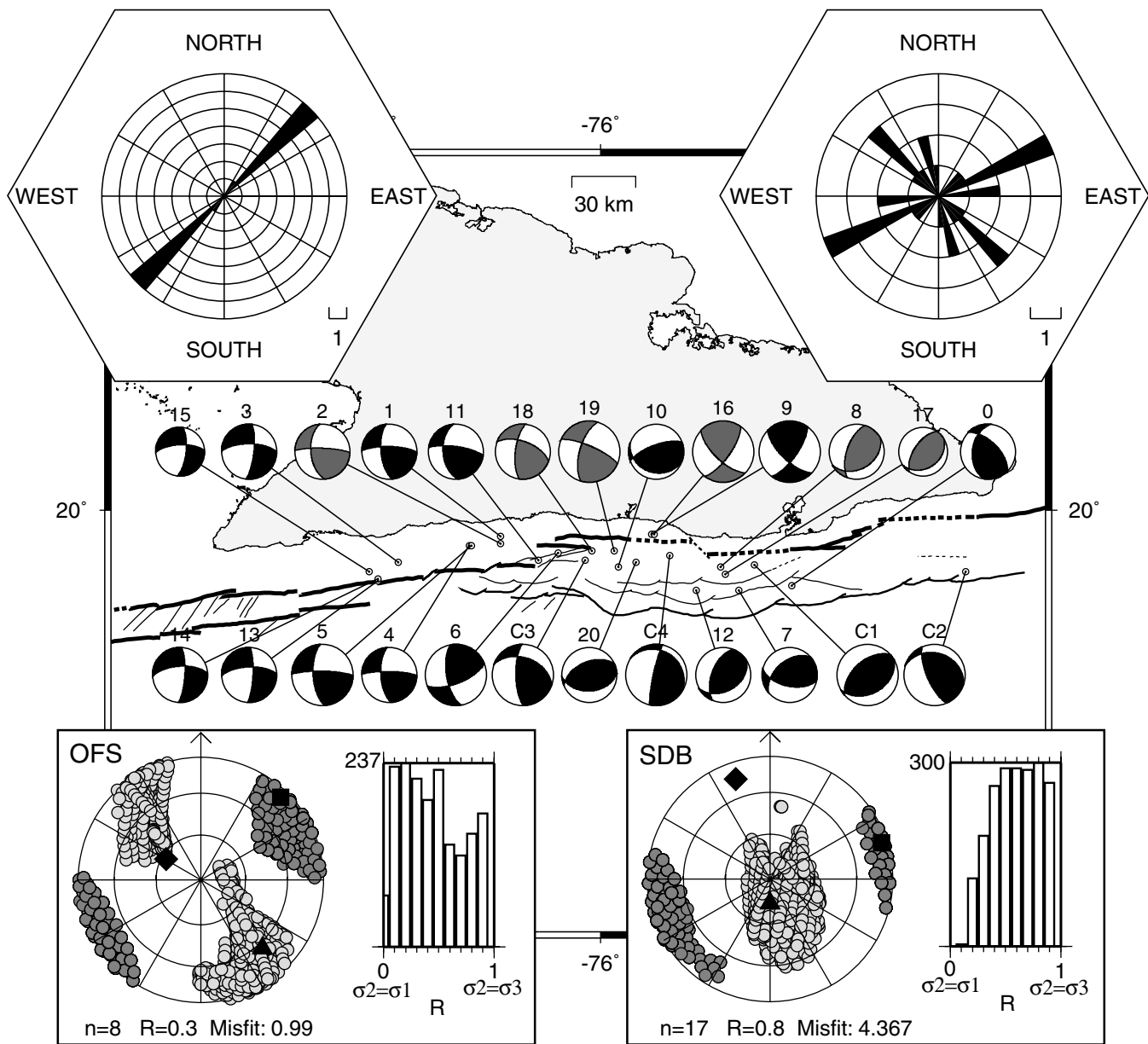
Figure 7. Earthquake focal mechanisms in the Cabo Cruz basin. The rose diagram in the upper left-hand corner shows the orientation of the maximum horizontal compressive stress ($\sigma_{\rm h}$). The $\sigma_{\rm h}$ orientations were computed according to Zoback (1992). The earthquake labelled as P1 is from Perrot *et al.* (1997). The compressional quadrants are shaded according to the first quality index (Table 6), darkest = best and lightest = worst. The circles are sized according to the second quality index (Table 6), biggest = best and smallest = worst. The lower inset shows the result of the stress inversion (Gephart 1990) for σ_1 and σ_3 at a 95 per cent confidence level and the best model fitting the observation. The histogram shows the distribution of R defined by $R = (\sigma_2 - \sigma_1)/(\sigma_3 - \sigma_1)$ for all the models fitting the observation within a 95 per cent confidence limit.

the GM with the NAP. A summary of the stress inversion results for the three individual zones and the entire region is shown in Table 9.

5 DISCUSSION

The process of microplate formation described by several authors in previous studies seems to explain the present-day tectonic regime in this area. Oblique plate motions along strike-slip faults, rather than orthogonal plate convergence, may play an important role in the possible formation of microplates (Karig *et al.* 1986; Mann

et al. 1995). In the case of the Gonave Microplate (GM), the development of the transpressive structure of the SDB is associated with a regional oblique relative motion of two blocks involved in strike-slip movements (Calais & Mercier de Lépinay 1991). Mullins *et al.* (1992) suggested that the northeastern corner of the Caribbean Plate (an area of the present-day Gonave Microplate) became impeded in a strike-slip restraining bend setting adjacent to the southeast extension of the Bahama carbonate platform. The GM is essentially being 'left behind' and being accreted to the North American Plate (NAP) as its eastward progress is impeded by the Bahama Platform (Mullins *et al.* 1992; Dolan & Wald 1994; Mann *et al.* 1995).

Figure 8. Earthquake focal mechanisms along the eastern part of the OFZ. Rose diagrams show the orientation of the maximum horizontal compressive stress (σ_h). The Rose diagram in the upper left-hand corner corresponds to the earthquakes 1–5 and 13–15 (OFS). The Rose diagram in the upper right-hand corner corresponds to the earthquakes 0, 6–12, 16–20 and C1–C4 (SDB). Earthquakes labelled as C1–C4 are from Harvard CMT catalogue. The lower insets show the result of the stress inversion for the two groups with symbols as in Fig. 7.

The characterization of seismicity at depth is the bottleneck for different seismotectonic interpretations in this area. Seismic reflection studies have been unable to map structures deeper than 12 km. In previous studies, Goreau (1983) noticed a high negative gravity

Table 6. Quality factor definition for earthquake focal mechanisms determined from first-motion polarities. The combination of any two quality indices result in nine possible quality factors.

First quality index	Polarities distribution (strike-slip case)	Second quality index	Error in depth (less than)
A	Four quadrants	a	5 km
B	Three quadrants	b	10 km
C	Two quadrants	c	15 km

anomaly under the deformed sediments of the Oriente Deep (the west part of SDB) and proposed the existence of a major north-dipping thrust along the southern Cuban margin. However, this structural interpretation, based on only six profiles, relies mainly on extrapolation as pointed out by Calais & Mercier de Lépinay (1991). Recent GPS measurements (De Mets *et al.* 2000) have estimated 3 ± 3 mm yr^{-1} of boundary normal convergence south of eastern Cuba, which suggest a small oblique motion (WSW–ENE) of the GM with respect to the NAP. The apparent north-dipping trend in the depth cross-section in the SDB (inset in Fig. 6) is weakly supported, taking into account the errors in depth (<15 km) of the plotted earthquakes. Bearing in mind this error, the deepest earthquakes shown in the depth cross-section may be as shallow as 30–35 km. However, previous studies (Ewing *et al.* 1960; Case *et al.*

Table 7. Earthquake focal mechanism solutions for the Cabo Cruz Basin. *P*-trn, *P*-plg, *T*-trn and *T*-plg are the trend and the plunge of the *P* (compression) and *T* (tension) axes, respectively. σ_h (maximum horizontal compressive stress) directions and Reg. (faulting regime) according to Zoback (1992). *Q* (quality factor), explained in Table 6.

No	Date	Time	Lat. (N)	Lon. (W)	Dep.	Mag. (Ml)	P trn	P plg	T trn	T plg	σ_h	Reg.	Q.
1	20/05/98	1531	19.64	77.81	19	3.6	223	52	98	24	354	NF	Bb
2	29/05/98	2050	19.45	78.05	13	3.4	213	44	104	19	194	NS	Cc
3	31/05/98	0908	19.46	78.02	11	3.5	213	44	104	19	194	NS	Cb
4	02/06/98	1034	19.54	77.91	13	3.4	213	44	104	19	194	NS	Bb
5	26/06/98	1326	19.59	77.86	14	3.4	220	45	95	30	–	U	Bc
6	30/06/98	0756	19.60	77.85	15	2.9	207	29	113	8	203	SS	Bb
7	17/08/98	1748	19.53	77.81	12	3.4	224	51	107	20	197	NS	Bc
8	02/09/98	0718	19.53	77.94	26	3.2	216	44	107	19	197	NS	Cc
9	23/11/98	0523	19.55	78.02	10	3.0	205	44	96	19	186	NS	Bb
10	24/11/98	0943	19.48	78.06	26	3.4	203	48	100	11	190	NS	Cb
11	27/11/98	0131	19.54	78.10	18	3.4	217	51	100	20	190	NS	Ac
12	13/01/99	1550	19.58	77.87	26	3.3	217	51	100	20	190	NS	Cc
13	14/05/99	0529	19.49	77.94	9	3.4	209	37	99	24	–	U	Cb
P1	25/05/92	1655	19.61	77.87	19	6.9 M_s	221	23	120	25	–	U	A

Table 8. Earthquake focal mechanism solutions for the eastern part of the OFZ and Santiago deformed belt. *P*-trn, *P*-plg, *T*-trn and *T*-plg are the trend and the plunge of the *P* (compression) and *T* (tension) axes, respectively. σ_h (maximum horizontal compressive stress) directions and Reg. (faulting regime) according to Zoback (1992). *Q* (quality factor), explained in Table 6.

| No	Date	Time	Lat. (N)	Lon. (W)	Dep.	Mag. (Ml)	P trn	P plg	T trn	T plg	σ_h	Reg.	Q.
0	25/04/98	1751	19.68	75.14	34	3.2	67	9	173	59	67	TF	Ab
1	17/05/98	1954	19.89	76.45	15	3.9	41	6	134	28	41	SS	Ab
2	17/05/98	2033	19.86	76.45	15	3.3	39	16	139	31	39	SS	Bb
3	18/06/98	1454	19.78	76.91	13	2.7	230	27	137	6	227	SS	Ab
4	23/07/98	2217	19.85	76.59	16	3.3	42	10	136	25	42	SS	Ab
5	23/07/98	2319	19.85	76.58	17	3.2	42	10	136	25	42	SS	Aa
6	08/09/98	1837	19.82	76.19	18	3.3	120	2	29	35	120	SS	Aa
7	01/11/98	0408	19.66	75.38	44	3.0	167	4	70	60	167	TF	Ab
8	05/01/99	0146	19.76	75.46	32	3.2	305	14	68	65	305	TF	Bb
9	19/01/99	1503	19.90	75.77	32	3.4	86	2	354	30	86	SS	Aa
10	04/02/99	0933	19.76	75.92	17	3.2	352	24	136	61	352	TF	Ab
11	05/02/99	0246	19.79	76.28	20	3.1	42	15	144	38	42	SS	Ab
12	13/02/99	2042	19.66	75.57	30	3.2	308	9	62	68	308	TF	Ab
13	29/03/99	0859	19.70	77.00	8	3.3	227	25	133	8	223	SS	Ab
14	29/03/99	1135	19.71	77.00	12	3.4	227	29	133	7	223	SS	Ab
15	20/04/99	0031	19.74	77.04	9	3.4	228	31	137	1	227	SS	Ac
16	28/05/99	1136	19.90	75.76	32	3.4	86	2	354	30	86	SS	Ba
17	15/06/99	0730	19.73	75.44	21	3.4	313	15	97	72	313	TF	Bc
18	22/09/99	1933	19.83	76.04	26	3.3	240	5	146	38	240	SS	Bb
19	26/09/99	1338	19.83	75.94	26	3.4	63	7	157	29	63	SS	Ba
20	16/12/99	0322	19.78	75.84	16	4.4	346	5	102	79	346	TF	Ab
C1	01/09/85	0101	19.77	75.31	10	5.0Mw	324	7	104	80	324	TF	?
C2	12/02/89	1426	19.74	74.36	25	5.2Mw	230	23	97	58	230	TF	?
C3	05/22/90	2035	19.79	76.07	15	5.3Mw	241	17	131	47	241	TS	?
C4	09/04/90	0803	19.81	75.69	15	5.2Mw	265	35	123	49	–	U	?

1990) have estimated a Moho depth of 10–21 km in this area. Therefore, the observed deep seismicity suggests that there may be a significant increase in the crustal thickness around the SDB. The focal mechanism of the deepest earthquake in Fig. 8 (event number 7), with a depth of 44 km (Table 8), shows reverse faulting with a small strike-slip component, which may support an underthrusting of the GM beneath the Cuban block in the SDB area as was suggested by Enman *et al.* (1997).

Another important feature is the earthquake activity in the interior part of the GM (Fig. 1). Geophysical investigations of the Caribbean crust have revealed several scarps, mostly NE–SW-oriented, on the seafloor in the interior part of the GM (Donnelly 1994), which suggest that the GM is undergoing in-

ternal deformation. Continued movement along both the northern and southern strike-slip boundaries of the GM has resulted in internal deformation of the microplate (Mann *et al.* 1995), with NE–SW-oriented structures probably being reactivated in normal faulting.

6 CONCLUSIONS

The combined Cuban and Jamaican catalogues over a period of 2 years allowed us to obtain for the first time a 1-D *P*-wave velocity model based on local seismic data. The model represents a significant improvement in the earthquake locations and can be used as an initial reference model for seismic tomography.
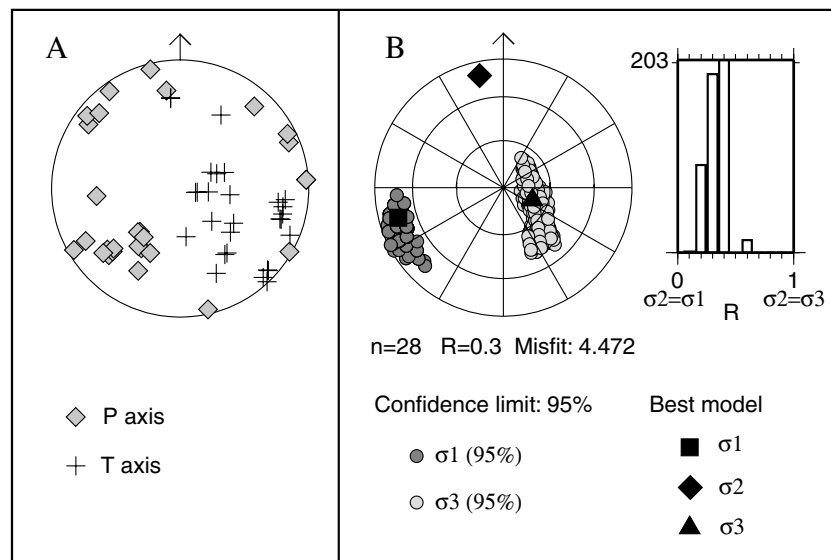
Figure 9. Stress inversion result for the entire region. (a) The *P* and *T* axes of the focal mechanisms used in the inversion. (b) The obtained principal stress axes within a 95 per cent confidence limit and the best model fitting the observation.

Table 9. Earthquake focal mechanism stress inversion results for the three areas and the entire region. *R* is defined by $R = (\sigma_2 - \sigma_1)/(\sigma_3 - \sigma_1)$.

Area	No of F.M.	FMSI misfit	R	σ_1		σ_2		σ_3	
				trn	plg	trn	plg	trn	plg
CCB	14	1.363	0.1	186	76	352	14	83	3
OFS	8	0.99	0.3	44	7	301	63	138	26
SDB	17	4.367	0.8	72	5	341	15	180	74
Entire region	28	4.472	0.3	254	16	348	12	113	70

The seismicity along the plate boundary is shallow in the west but increases in depth eastward. It is concentrated along two local structures: (1) the CCB and (2) the SDB. Deep seismicity seems to be restricted only to the SDB.

Despite the limited data set, recorded over only 2 years, the new earthquake locations permit us to identify and characterize the tectonic regime along the OFZ. The CCB is dominated by transtension and the SDB by transpression. The earthquake focal mechanisms along these structures show evidence that transtension and transpression are occurring at the same time and at short distances along a major transcurrent fault, the Oriente fault.

The stress field for the entire region is suggested to be transpressional, which is in agreement with the dominant structural trend associated with the SDB. The principal stress axes are well constrained from the inversion of focal mechanisms within a 95 per cent confidence level. They have a near horizontal σ_1 (ENE–WSW-oriented) and a nearly vertical σ_3, indicating a thrust faulting regime.

The deep seismicity in the SDB and the thrust faulting regime obtained from the stress inversion seem to support the previously suggested underthrusting of the GM beneath the Cuban block (Enman *et al.* 1997), which probably causes a crustal thickening in the SDB area.

ACKNOWLEDGMENTS

REFERENCES

Alvarez, J., Blanco, P., Medvedev, S.V., Menende, L. & Shteynberg, V.V., 1973. The seismic conditions of Santiago de Cuba, *Bull. (Izv.) Acad. Sci. USSR, Earth Phys.,* **5,** 320–324.

Arden, D.D., 1975. Geology of Jamaica and the Nicaragua Rise, in *The Ocean Basins and Margins,* Vol. 3, pp. 617–661, eds Nairn, A.E.M. & Stehli, F.G., Plenum, New York.

Bush, V.A. & Shcherbakova, I.N., 1986. New data on the deep tectonics of Cuba, *Geotectonics,* **20,** 192–203.

Calais, E. & Mercier de Lépinay, B., 1990. A natural model of active transpressional tectonics: the *en échelon* structures of the Oriente deep along the northern Caribbean transcurrent plate boundary (Southern Cuban margin), *Rev. Inst. Fr. Pét.,* **45,** 147–160.

Calais, E. & Mercier de Lépinay, B., 1991. From transtension to transpression along the Southern Caribbean plate boundary off Cuba: implications for the recent motion of the Caribbean plate, *Tectonophysics,* **186,** 329–350.

Calais, E., Perrot, J. & Mercier de Lépinay, B., 1998. Strike-slip tectonics and seismicity along the Northern Caribbean plate boundary from Cuba to Hispaniola, in *Active Strike-slip and Collisional Tectonics of the Northern Caribbean Plate Boundary Zone,* Vol. 326, pp. 125–142, eds Dolan, J.F. & Mann, P., Geol. Soc. Am. Special Paper, Boulder, CO.

Case, J.E., MacDonald, W.D. & Fox, P.J., 1990. Caribbean crustal provinces; seismic and gravity evidence, in *The Geology of North America, The Caribbean Region,* Vol. H, pp. 15–36, eds Dengo, G. & Case, J.E., Geol. Soc. Am., Boulder, CO.

Cotilla, M., 1993. A seismotectonic characterization of Cuba, *PhD thesis,* Inst. of Geophysics and Astronomy, Acad. of Sciences of Cuba, Havana, p. 200.

Cotilla, M., 1998. An overview on the seismicity of Cuba, *J. Seismol., 2,* 323–335.

De Mets, C., Gordon, R.G., Argus, D.F. & Stein, S., 1990. Current plate motions, *Geophys. J. R. astr. Soc.,* **101,** 425–478.

De Mets, C., Jansma, P.E., Mattioli, G.S., Dixon, T., Farina, P., Bilham, R., Calais, E. & Mann, P., 2000. GPS geodetic constraints on Caribbean–North American Plate motion, *Geophys. Res. Lett.,* **27,** 437–440.

Deng, J. & Sykes, L.R., 1995. Determination of Euler pole for contemporary relative motion of the Caribbean and North American plates using slip vectors of interplate earthquakes, *Tectonics,* **14,** 39–53.

Dixon, T.H., Farina, F., Demets, C., Jansma, P., Mann, P. & Calais, E., 1998. Relative motion between the Caribbean and North American plates and related boundary zone deformation from a decade of GPS observations, *J. geophys. Res.,* **103,** 15 157–15 182.

Donnelly, T.W., 1994. The Caribbean Sea floor, in *Caribbean Geology: an Introduction,* pp. 41–63, UWI Publishers' Association, Kingston.

Dolan, J.F. & Wald, D.J., 1994. Consequences of time-transgressive, oblique underthrusting of the southeastern Bahamas: localization of large thrust earthquakes and controls on large-scale forearc subsidence events, *Geol. Soc. Am., Abstr. Programs,* **26,** A–251.

Edgar, N.T., Ewing, J.I. & Hennion, J., 1971. Seismic refraction and reflection in the Caribbean Sea, *Am. Assoc. Petr. Geol. Bull.,* **55,** 833–870.

Enman, S.V., Belousov, T.P., Marquez, M.E., Rueda, J.S. & Jorge, G.D., 1997. Recent crustal movements and morphostructural pattern of Southeastern Cuba: Santiago de Cuba Geodynamic Research Site, *Izvest. Phys. Solid Earth,* **1,** 55–69.

Ewing, J., Antoine, J. & Ewing, M., 1960. Geophysical measurements in the western Caribbean Sea and in the Gulf of Mexico, *J. geophys. Res.,* **65,** 4087–4126.

Gephart, J.W., 1990. FMSI: a FORTRAN program for inverting fault/slickenside and earthquake focal mechanism data to obtain the regional stress tensor, *Comp. Geosci.,* **16,** 953–989.

Gephart, J.W. & Forsyth, D.W., 1984. An improved method for determining the regional stress tensor using earthquake focal mechanism data: application to the San Fernando earthquake sequence, *J. geophys. Res.,* **89,** 9305–9320.

Goreau, P.D.E., 1983. The tectonic evolution of the north-central Caribbean plate margin, *PhD thesis,* Woods Hole Oceanographic Institution, WHOI83–84, p. 245.

Hardebeck, J.L. & Hauksson, E., 2001. Crustal stress field in southern California and its implications for fault mechanics, *J. geophys. Res.,* **106,** 21 859–21 882.

Havskov, J. & Otemöller, L., 1999. SEISAN: the earthquake analysis software, Version 7.0, Institute of Solid Earth Physics, University of Bergen, Norway, p. 226.

Karig, D.E., Sarewitz, D.R. & Haeck, G.D., 1986. Role of strike-slip faulting in the evolution of allochthonous terranes in the Philippines, *Geology,* **14,** 852–855.

Kissling, E., 1988. Geotomography with local earthquake data, *Rev. Geophys.,* **26,** 659–698.

Kissling, E., Ellsworth, W.L., Eberhart Phillips, D. & Kradolfer, U., 1994. Initial reference models in local earthquake tomography, *J. geophys. Res.,* **99,** 19 635–19 646.

Kissling, E., Kradolfer, U. & Maurer, H., 1995. VELEST user's guide—short introduction, Institute of Geophysics and Swiss Seismological Service, ETH Zürich, p. 25.

Lay, T. & Wallace, T.C., 1995. *Modern Global Seismology,* pp. 80–86, Academic, New York.

Lienert, B.R. & Havskov, J., 1995. A computer program for locating earthquakes both locally and globally, *Seism. Res. Lett.,* **66,** 26–36.

Mann, P., Taylor, F.W., Lawrence Edwards, R. & Teh-Lung, Ku., 1995. Actively evolving microplate formation by oblique collision and sideways motion along strike-slip faults: an example from the northeastern Caribbean plate margin, *Tectonophysics,* **246,** 1–69.

Moreno, B., 2002. The new Cuban Seismograph Network, *Seism. Res. Lett.,* **73,** 505–518.

Mullins, H.T. *et al.*, 1992. Carbonate platforms along the southeast Bahamas–Hispaniola collision zone, *Mar. Geol.,* **105,** 169–209.

Perrot, J., Calais, E. & Mercier de Lépinay, B., 1997. Tectonic and kinematic regime along the Northern Caribbean Plate Boundary: new insights from broad-band modeling of the May 25, 1992, $M_s = 6.9$ Cabo Cruz, Cuba, earthquake, *Pure appl. Geophys.,* **147,** 475–487.

Snoke, J.A., Munsey, J.W., Teague, A.G. & Bollinger G.A., 1984. A program for focal mechanism determination by combined use of polarity and $SV-P$ amplitude ratio data, *Earthquake Notes,* **55,** 1–15.

Sykes, L.R., McCann, W.R. & Kafka, A.L., 1982. Motion of the Caribbean plate during the last 7 million years and implications for earlier Cenozoic movements, *J. geophys. Res.,* **13,** 10 656–10 676.

Van Dusen, S. & Doser, D., 2000. Faulting processes of historic (1917–1962) $M \geq 6.0$ earthquakes along the north-central Caribbean Margin, *Pure appl. Geophys.,* **157,** 719–736.

Wiggins-Grandison, M., 2001. Preliminary results from the new Jamaican seismograph network, *Seism. Res. Lett.,* **72,** 525–537.

Zoback, M.L., 1992. First and second-order lithospheric stress patterns, *J. geophys. Res.,* **97,** 11 703–11 728.

SAFE-Tools: A Web-based application for identification of active faults.

B. Moreno[1,2], K. Atakan[1], K. A. Furuløkken[1], S. Temel[3] and O. J. Berland[1]

(1) Institute of Solid Earth Physics, University of Bergen. Allegt. 41, 5007 Bergen, Norway.

(2) Centro Nacional de Investigaciones Sismológicas, Calle 17 No. 61 e/ 4 y 6 Vista Alegre, Santiago de Cuba, Cuba

(3) Bea Systems Inc., 140 Allen Road Liberty Corner, NJ 07938

INTRODUCTION

Recognition of active faults, particularly in low seismicity regions such as Western Europe, has been a challenging task for earth scientist for many years. These regions are generally characterized by low hazard but high risk, due to the concentration of population and material properties with high-vulnerability. Detection of tectonic deformation that may lead to destructive earthquakes in such areas requires innovative research strategies appropriate to the climate, slowly deformation rates, and heavy human modification of areas.

The variety and amount of information involved in the characterization of slowly deforming faults, which we defined as slow active faults, are in general distributed between several institutions and are difficult to access. This information such as earthquake data, paleoseismic trench, geophysical cross-section, etc., should be gathered, parameterized and stored in a way that make them more accessable for use in seismic hazard studies. Within the framework of the European project SAFE (Slow Active Faults in Europe), a software (SAFE-T) for identifying slow active faults is being developed. The system is a Web-based application with data visualization and user interaction occurring through Internet.

1

The information relevant to fault identification by nature consists of geospatial data with several parameters or properties attached. Geographical Information Systems (GIS) are commonly used for the management and visualization of spatially referenced data. However, commercially available GIS software are usually expensive, mainly operating as stand-alone (client-side) applications. An effort to integrate GIS into client-server architecture is being carried out by the Open GIS Consortium (http://www.opengis.org/index.htm). This is an association of companies, government agencies and universities that are developing open interface, standard protocols and specifications to make geospatial data accessible to the public. For example, Web Map Service is one of the well established achievements of the Open GIS Consortium. CubeServ, Cadcorp SIS and DEMIS (URL references in Table 1) are examples of server interfaces based on this technology.

Several Internet-based applications have been developed using Web Map Service interfaces; e.g. NASA Web Map Viewer, Geode, IMA (Table 1). Here maps are dynamically generated on the server side and transmitted as images to the client. Other Web-based tools (e.g. Faults of southern California, J.V. Voyager, FAUST) use static images of maps which have been created in advance and stored in the server side. In SAFE-T we use the facilities of the Web Map Service interface to dynamically generate maps with background information and then plot our geospatial data on it. The data consist of geological and geomorphic maps, paleoseismological, historical or instrumental earthquake data, geophysical anomalies, faults etc., which have been interpreted, parameterized and stored in a relational database. In this report we focus a description of the database structure and the Graphical User Interface (GUI) implementation. In addition some technical aspects of the system is presented. Since we use some technical terminology, which in some cases readers may not be familiar with, a list of technical terms with a brief explanation is included in the glossary.

BASIC DESIGN

SAFE-T is based on a client-server architecture, with data communication and visualization occurring through the Web (Figure 1a). The processing module on the server side interacts with a relational database while client access the server through the Internet. A distinctive feature of the system in comparison to existing GIS software, which stores raw data (e.g. grid data such as digital elevation model), is that the database contains mainly interpreted data. On the client-side, as part of the GUI, three interfaces are operating: (1) Editing, (2) Query and (3) Visualization. The editing interface allows data entry and maintenance of the database. The query interface gives the user the possibility of requesting data and launching the processing. The visualization interface displays requested data and processing results. The relevant data may be distributed in several database servers, which are connected on Internet (Figure 1b). Once the user (client) connects to SAFE-T system, he has access to several databases located at different institutions. To ensure portability, by which we mean a system independent of different computer platforms, Java programming language was used for developing the system.

APPLICATION ARCHITECTURE

The application architecture is based on 3-Tier architecture (Mukhar et al., 2001; Birnam, 2001). The application is divided into three layers: (1) The presentation, which is the graphical user interface (GUI), (2) the processing-logic and (3) the database (Figure 2a). These three layers may be seen as the view, the controller, and the model. The view (GUI) has access to the model (database) only through the controller (processing-logic). This model-

view-controller framework makes the application flexible in terms of extensibility and reusability, which means that additional functionality can easily be added to the application and the processing-logic can be generalized and reused in other applications.

Normally, to deploy the system components involved in the model-view-controller framework additional applications are needed, which we call here "Containers" (Figure 2a). For example, the relational database management system (RDBMS) provides the basic function to access the database. An application server is needed to deploy EJB/JSP/Servlet (Monson-Haefel, 2002; Hall, 2002) on the server side and, in the client side a Browser is needed to show the HTML documents (Powell, 2000). SAFE-T is using MySQL (http://www.mysql.com) as RDBMS and WebLogic (Girdley et al., 2002) as application server. Figure 2b shows the communication framework between components. On the client side the GUI, which comprise HTML forms and a Java Applet, is interacting with the server through a Servlet or Java Server Page (JSP) (see Glossary). The Servlet gets the information through the Enterprise Java Beans (EJB) (see Glossary), which map the database, and send it back to the GUI either as a HTML document or directly to the Java applet.

THE DATABASE

Relational database: Basic concepts.

The first step in designing a relational database (RDB) is the classification of the information to be stored. The information is classified as different types of entities or objects according to the processing logic and the nature of the data. Each entity has a set of attributes or properties that describe its nature. Classes of entities are collected in a table where each column is associated with one of their attributes. A relational database is a set of tables connected to

each other by logical relationships. The relationship between tables can be (1) one-to-one, when one row of a table is related with one row of another table; (2) one-to-many, when one row of a table is related with many rows of another table and (3) many-to-many.

Preservation of the data integrity is a basic guiding principle during the database design process. The attributes of the entities have to be organized in a way that each piece of data is stored once and in the correct place. To design entities with data integrity a technique known as normalization process is used. This technique consists of applying several rules to the tables to make sure that there is not redundancy of information or failure in their logical relationships. In general the data normalization can be summarized in three basic steps (Mukhar et al., 2001): (1) Eliminating of redundant attributes and/or redundant rows, (2) Removing of derived data and (3) Making certain that each table represents only one single logical entity.

RDB Tables

In SAFE-T, broad types of information have to be considered for diagnosing slow active faults. Such information can be categorized into six main groups: (1) seismologic, (2) paleoseismic, (3) geophysical, (4) geological, (5) geochemical and (6) geomorphic. These data are stored in tables with appropriate logical relationships (Figure 3). Four main tables are identified: (1) earthquakes, (2) maps, (3) faults and (4) cross-sections. These tables are considered as "parent" tables with a set of sub-tables describing particular cases within the corresponding type of data. The data are geographically referenced either as a point (e.g. earthquakes), a poly-line (e.g. fault segments), a line (e.g. cross-sections) or a polygon (e.g. fault zones, geological units) (Figure 4a). Maps are stored as individual images and cannot be used by the processing module. However, the components of the maps can be parameterized

and stored in the RDB to be used in a meaningful way. For example, in the case of "map of stress field" we stored in the database the region (polygon) in which the stress field is applicable and the corresponding parameters describing the principal stresses.

There are some types of information, such as geophysical anomalies and geological units, which are represented both on the surface as a map and in vertical projections (cross-sections). For example, maps of geophysical anomalies or geological units are parameterized as a set of polygons enclosing the area corresponding to the extent of the anomaly or geological unit. On the other hand cross-sections are geographically referenced as lines and the associated anomalies have relative locations (distance and depth) to the first point of the coordinates of the cross-section (Figure 4b). In either case, each anomaly or geological unit represents a row in the table.

Four examples of the data parameterization (tables) are listed below. The first two examples, MAP and CROSS-SECTION, are parent tables whereas the second two are daughter tables, which include the specified information. The description of the complete list of tables used in the system can be found at: http://www.ifjf.uib.no/seismo/safe-t/tables.html

MAP (Parent table for grouping different type of maps)

- MapID (unique identification or key)

- Providing institution

- Type (e.g. geological map, topographic map, geophysical map etc.)

- TwoPointWindow: Coordinates of the map (two points defining a box that covers the map area, that is the longitude and latitude of the upper left corner and lower right corner)

- Projection

- URL-link-ImageFile

- Relevant Links

- References

- Comments

MapGeophyAnomaly (Map of geophysical anomaly)

- MapID (link to the Map table)

- Coordinates of the polygon defining the area where the information is applicable

- Anomaly type (e.g. gravity, magnetic, Moho depth, cover thickness etc)

- Anomaly polarity (if magnetic anomaly: normal or reverse)

- Anomaly value (value with its sign: in case of gravity positive or negative)

- Quality Factor (to indicate an uncertainty of the information): Very good, Good, Poor

  and Bad)

CROSS-SECTION (Parent table for grouping different type of cross-section)

- CrossID (unique identification or key)

- Providing institution

- Coordinates of the line defining the position

- Type (e.g. seismic line, borehole, geophysical cross-section, geological cross-section,

  paleoseismic trench etc.)

- Length of the line in meters

- Depth to the surface in meters

- URL-link-ImageFile

- Relevant Links

- References

- Comments

CrossGeophyAnomaly (Cross-section of geophysical anomaly)

- CrossID (link to the Cross-Section table)

- Anomaly type (e.g. gravity, magnetic, Moho depth, cover thickness etc)

- Distance in meters from the first point coordinates of the cross-section

- Depth in meters from the first point coordinates of the cross-section (min and max)

- Dip angle from horizontal (i.e. up to 180 degrees)

- Width of the anomaly gradient change in meters (to indicate how well the anomaly (fault) is defined by the change in the gradient)

- Quality Factor (to indicate an uncertainty of the information): Very good, Good, Poor and Bad)

In addition all of the tables include three more properties: the user who entered the information, an access level, and a time stamp. These properties are designed for internal use.

Open geosciences data retrieval

One of the objectives within the design of SAFE-T is to create data formats and protocols that allow interoperability between web-based applications which are retrieving geosciences data. Toward this end, we are developing server-side applications (URL-based commands) to retrieve different types of data (objects) through Internet. These objects can be used for other

web-based applications by calling a URL address (a server side application) followed by several input parameters. The information should be retrieved in a well-defined structured format. The Extensible Markup Language (XML) (White et al., 2001; Laurent and Cerami, 1999) provides a sophisticated text format that is easily read and manipulated by both people and computers. For example, to get a list of earthquakes located in a specific region within a given magnitude range, the following URL-based command could be called:

http://www.safe-tools.net/getEarthquakes?bbox=6.0,42.0,8.0,45.0&maginterval=6,9

where "getEarthquakes" is a Servlet (see Glossary), which can receive different parameters such as the bounding box of the area selected (bbox=minLong,minLat,maxLong,maxLat). The command will return a list of earthquakes in XML format. For example:

```
- <SAFE_DATA>
  - <EARTHQUAKE>
      <NAME>1356 BASEL EARTHQUAKE</NAME>
      <PROVIDING_INST>IPG</PROVIDING_INST>
      <CATALOG_AGENCY>ISC</CATALOG_AGENCY>
      <EVIDENCE>HISTORICAL</EVIDENCE>
      <YEAR>1356</YEAR>
      <MONTH>10</MONTH>
      <DAY>18</DAY>
      <HOUR></HOUR>
      <MINUTE></MINUTE>
      <SECOND></SECOND>
      <LATITUDE>43.8</LATITUDE>
      <LONGITUDE>7.5</LONGITUDE>
      <DEPTH></DEPTH>
```

```
        <MB></MB>

        <MS>6.5</MS>

        <MC></MC>

        <ML></ML>

        <MW></MW>

        <ME></ME>

        <MT></MT>

        <RMS></RMS>

        <LATITUDE_ERR></LATITUDE_ERR>

        <LONGITUDE_ERR></LONGITUDE_ERR>

        <DEPTH_ERR></DEPTH_ERR>

        <NUM_STATIONS></NUM_STATIONS>

        <IMAGE_URL>HTTP://WWW.IMG.COM/PIC1.JPG</IMAGE_URL>

        <RELEVANT_LINKS>HTTP://WWW.DOC.COM/D1.DOC</RELEVANT_LINKS>

        <REFERENCES></REFERENCES>

        <COMMENTS></COMMENTS>

    </EARTHQUAKE>

  - <EARTHQUAKE>

        …

        …

    </EARTHQUAKE>

 </SAFE_DATA>
```

Here, we intend to propose specifications and data formats that could become the standard way to exchange geosciences-related data associated with active faulting and earthquakes through the Internet. Examples of XML files for different types of information used in the system can be seen at http://www.ifjf.uib.no/seismo/safe-t/XMLfiles.html.

THE GRAPHICAL USER INTERFACE

The graphical user interface consists of HTML forms and a "Navigation Map" which is a Java Applet (Figure 5). HTML forms are used for the main layout of the system and specific functions such as adding new objects into the database, removing and visualizing parametric information of a particular object, launching the "Diagnostics Wizard" (see "Processing Module" section), etc. Only an authorized user can add and remove objects from the database. The identification of users is achieved through a user's login and password using a secure Internet connection. The database can also be populated with XML files containing one or several objects. In this sense, authorized users submit XML files to the server side. The server-side application validates the information and replies to the user whether the transaction succeeded or not.

The "Navigation Map" allows the user to perform four main functions: (1) Select an area on the map by a zoom-in/zoom-out action, (2) Choose type of objects to be plotted in the selected area, (3) Pick a particular object to see detailed information about it, and (4) Filter the data by different properties. The objects plotted on the map are also shown in a list (Figure 5). There is a direct link between the list and the map. Picking an object in the map will highlight the corresponding item in the list and vice versa. The background maps in which objects are plotted are transmitted as images to the client side. The user has the choice to select several background maps (Figure 5), which are generated by different Web-Map-Servers over Internet. Most of these Web-Map-Servers belong to the Open GIS Consortium, which dynamically generate images with different layers of information (e.g. country boundaries, topography, etc.). In this case there is no limit for zooming and the quality of the map depends on the resolution of the raw data stored.

PROCESSING MODULE

The criteria for diagnosing slow active faults are being defined by a multidisciplinary group of scientists (Sebrier and Siame, 2001). In the first version of the system we implemented a "Diagnostics Wizard", or a quiz, to highlight the most important factors involved in the identification of slow active faults. Through the "Diagnostics Wizard" the users follow a logical sequence of questions. The main objective is to search for evidence or types of information relevant to deciding if the fault is active or not. This process is performed at regional, local and site scales considering space, time and dynamic properties of the data. At the end of the quiz the user receives an indication whether the fault is active or not. The present implementation of the Diagnostic Wizard is an interactive tool aiming to assist the scientist in evaluating the relevant data for identifying active faults. The user is guided through a set of questions which systematically search for diagnostic criteria in the existing data. In order to assess the reliability and the importance of the information, a multi-step weighting procedure is applied.

In the future implementations the diagnostic criteria will be automatically applied to the data stored in the database. The algorithm for automatic processing is similar to the "Diagnostics Wizard". The only difference is that the evidence used to decide if the fault is active is obtained directly from the database.

CONCLUDING REMARKS

In this study, we have presented a software tool for recognizing active faults, designed especially for slowly deforming areas such as Europe. This effort is the first attempt at classifying and gathering a wide range of geospatial data for the European area into a

distributed relational database, which can be accessed directly by a web-based application. Furthermore, we have investigated the possibility of implementing a processing module that will help seismologists and earthquake geologists identify active faults in a given area. The flexible design of the system and the large variety of information considered in the database structure provide the opportunity to add other types of processing modules associated with active faulting and earthquakes, such as seismic hazard analysis, orientation of regional principal stress, etc. The use of distributed database technology reduces the amount of work required to maintain a large database, which can be problematic for a single institution. With the development of the information technologies, web-based applications can also easily be moved to other communication devices such as mobile phones, increasing both the usability and public interest.

HOW TO USE THE SYSTEM

The system can be accessed at the Web site: http://www.safe-tools.net/ at the Institute of Solid Earth Physics, University of Bergen.

ACKNOWLEDGEMENTS

for his comments and suggestions. Susan Hough improved the overall quality of the manuscript.

GLOSSARY

Class: Type of data with properties and methods/operators.

Entity/Object: Instance of the Class.

Relational Database: Set of tables related each other where one row represents an entity and the columns are the properties.

Relational Database Management System (RDMS): Software providing basic functions to access a relational database.

Java Applet: Java program running in an Internet browser. The applet, which is stored in the server side, is downloaded and executed on the client side when the HTML document is downloaded.

Servlet: Java program running on the server side and interacting with the client.

Java Server Page (JSP): HyperText Markup Language (HTML) document embedding Java code, which is running on the server side.

Enterprise Java Beans (EJB): Network-aware Java classes mapping the database. They provide services (session bean) and hold information (entity bean).

Application Server: Software for deploying Java components of the Web application on the server side, which include EJB, JSP, Servlet, etc.

Extensible Markup Language (XML): Document holding information in text format (i.e. data from the database). Standard way to exchanges structured textual data between computer programs.

REFERENCES

Birnam S., 2001, *Distributed Java platform Database Development*, Java Series, Sun Microsystems Press

Hall, M., 2002, *More Servlets and JavaServer Pages*, Java^{TM} 2 Platform, Enterprise Edition Series, Sun Microsystems Press.

Girdley, M., Woollen, R. and Emerson, S. L., 2002, J2EE Applications and BEA WebLogic Server, Prentice Hall PTR, United States of America

Laurent, S. St., and Cerami, E., 1999, *Building XML Applications*, McGraw-Hill

Monson-Haefel, R., 2002, *Enterprise JavaBeans^{TM}, Second Edition*, O'Reilly & Associates, Inc.

Mukhar, K., Lauinger T., Carnell J., and eight others, 2001, *Beginning Java Databases*, Wrox Press

Sebrier, M and Siame, L. 2001, Criteria for characterizing slow active faults and standardization of paleoseismological analyses: Determination of a basic set of diagnostic criteria. SAFE-Project Internal Report Deliverable.9.1, CNRS, Paris VI, France, 18p.

Powell, T. A., 2000, *HTML: The complete reference, Third Edition*, Osborne McGraw-Hill

White C., Quin, L., and Burman, L., 2001, *Mastering XML*[TM]*, Premium Edition*, Sybex.

TABLES

Name	URL	Description
CubeServ	http://www.cubewerx.com/	World Web-Map-Server
Cadcorp SIS	http://www.cadcorp.com/	World Web-Map-Server
DEMIS	http://www.demis.nl/DEMIS_UK/	World Web-Map-Server
FAUST	http://www.ingv.it/~roma/banche/catalogo_europeo/	Database of potential Sources for Earthquakes larger than M 5.5 in Europe
Faults of southern California	http://www.scecdc.scec.org/faultmap.html	Faults of southern California
Geode	http://dss1.er.usgs.gov/	Geo-data Explorer (USGS)
IMA	http://atlas.geo.cornell.edu/ima.html	Interactive Mapping and data analysis
J.V. Voyager	http://jules.unavco.ucar.edu/VoyagerJr/Earth	Jules Verne Voyager, Jr. Interactive Map Tool
NASA Web Map Viewer	http://viewer.digitalearth.gov/	Interactive Map Tool

Table 1. URL references of Web Map Servers and Interactive Map tools

FIGURE CAPTIONS

Figure 1. Basic design of the system. (a) Client-server architecture. (b) Communication between database servers.

Figure 2. (a) Model-View-Controller framework. The view (GUI) has access to the model (database) only through the controller (processing-logic). (b) Interaction between components. On the client side the GUI, which comprise HTML forms and a Java Applet, is interacting with the server through a Servlet or Java Server Page (JSP).

Figure 3. Information included into the database. It is categorized into six main groups: (1) seismologic, (2) paleoseismic, (3) geophysical, (4) geological, (5) geochemical and (6) geomorphic.

Figure 4. (a) The data is visualized through four categories of symbols, which are geographically referenced either as a point (e.g. earthquakes), lines (e.g. cross-sections), poly-lines (e.g. fault segments) or polygons (e.g. fault zones). (b) Example of a cross-section geophysical anomaly images (CrossGeophyAnomaly). The arrow points to the anomaly, which is parameterized and stored in the database. The examples of images shown are with the courtesy of Kris Vanneste, Royal Observatory of Belgium.

Figure 5. Main layout of the system. The HTML document has the "Navigation Map" (Java Applet) embedded. HTML forms are used for specific functions such as adding new objects into the database, removing and visualizing parametric information of a particular object, etc.

The "Navigation Map" allows the user to select an area on the map by a zoom-in/zoom-out

action, choose type of objects to be plotted in the selected area, pick a particular object to see

detailed information about it, and filter the data by different properties.
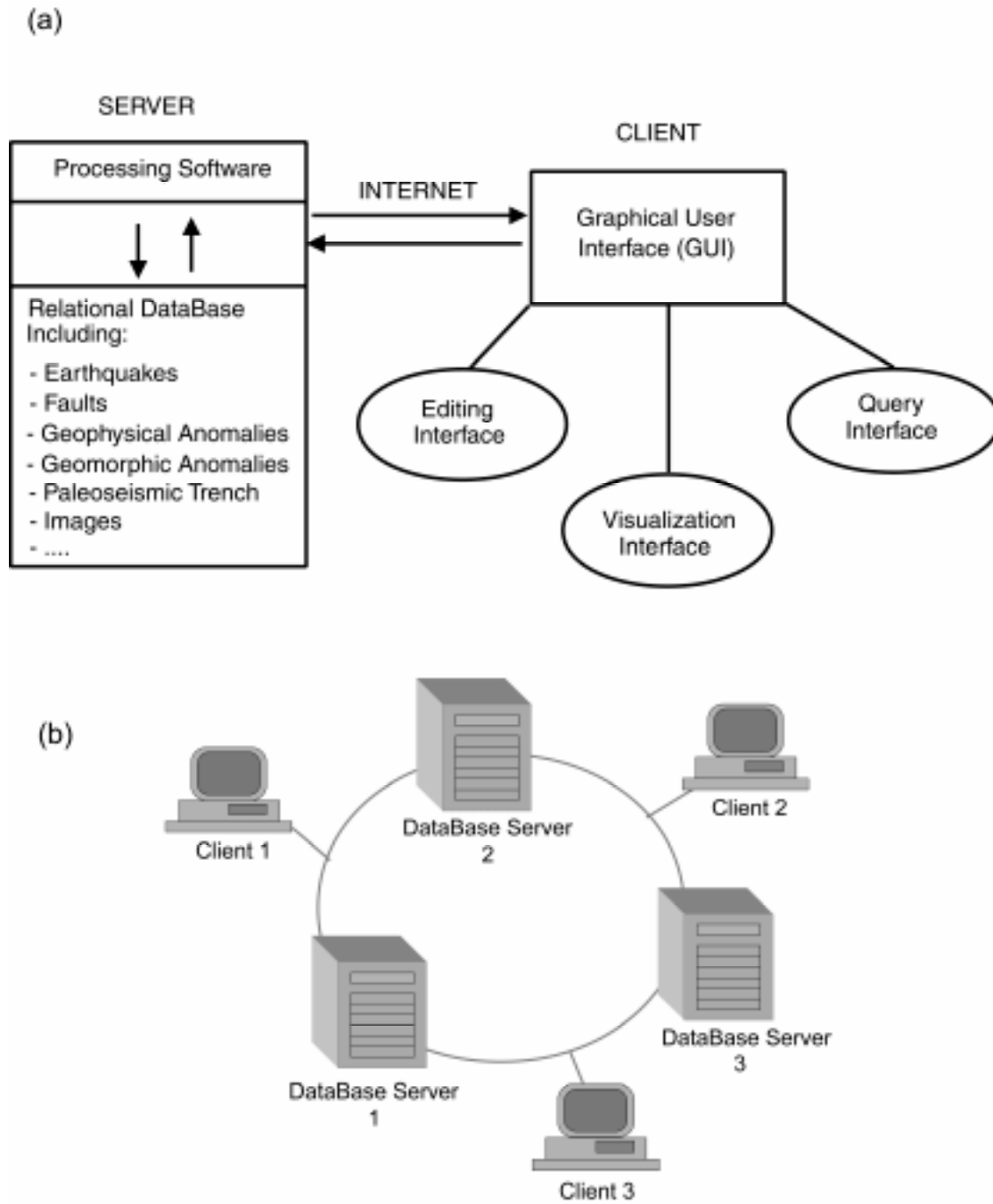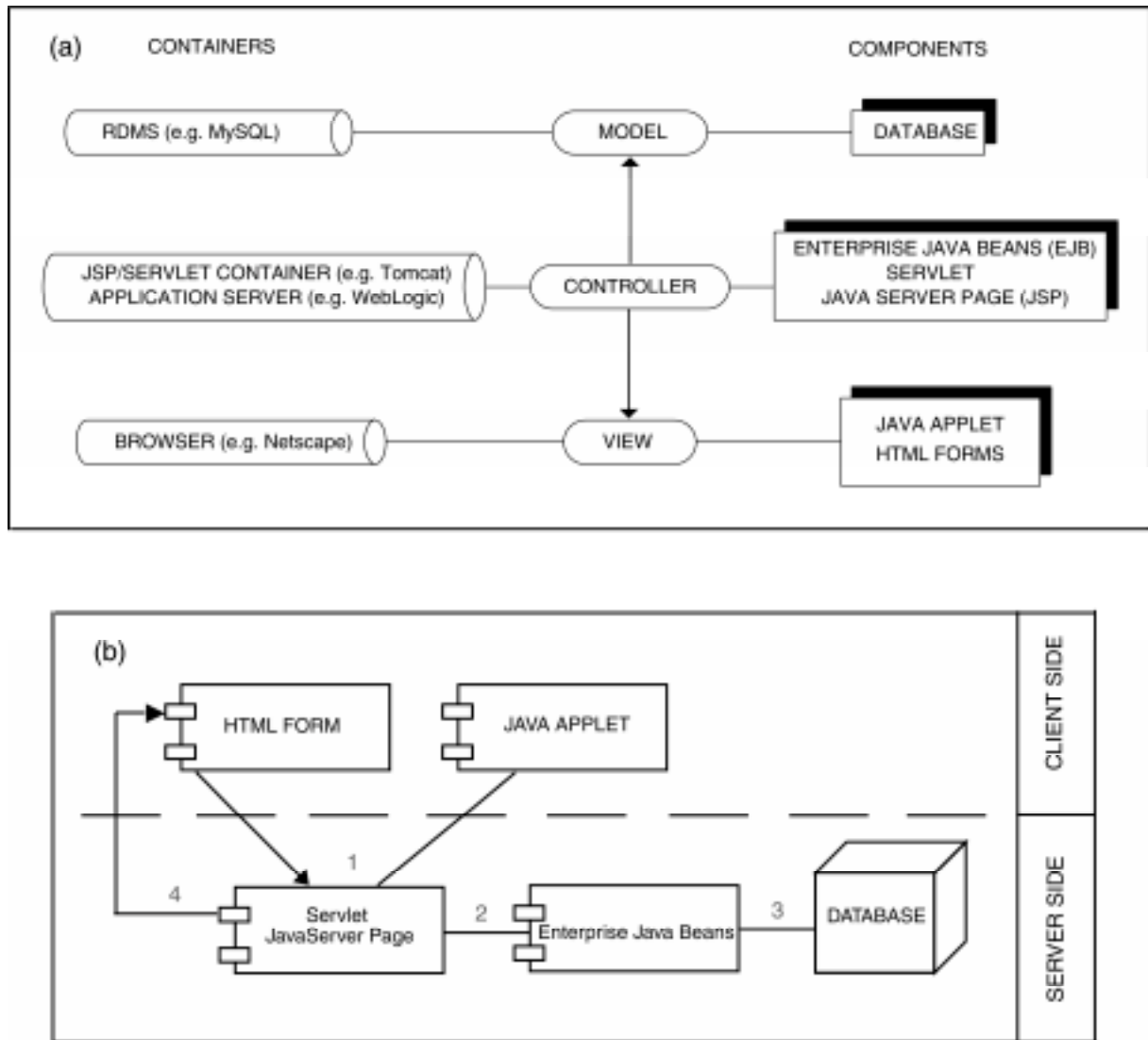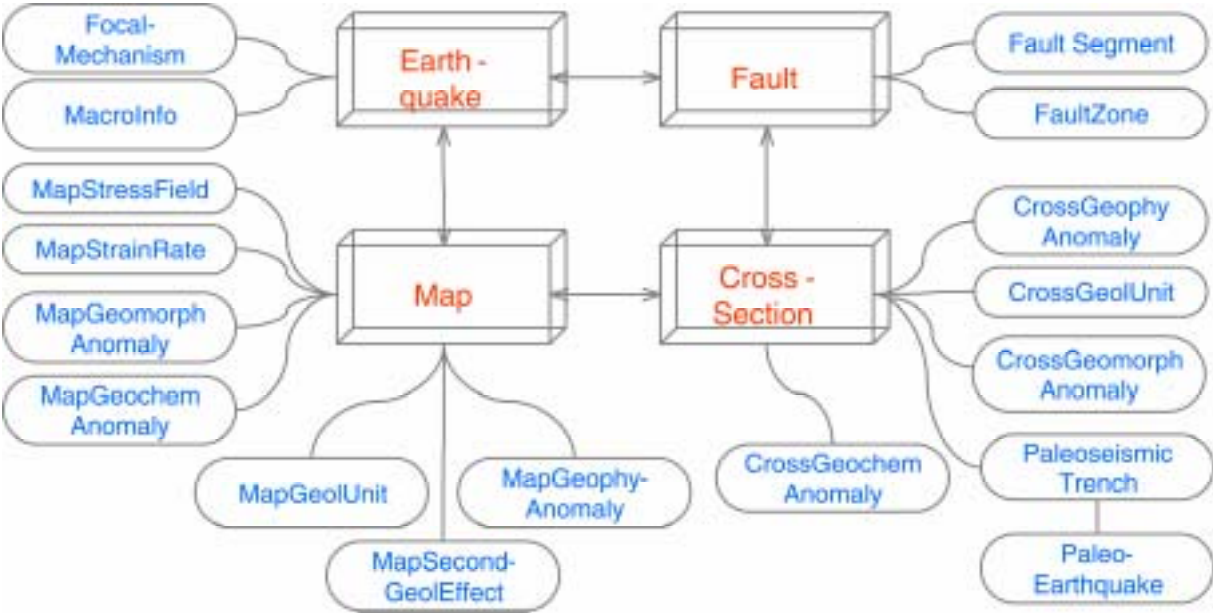
(a)

SERVER

Processing Software

CLIENT

INTERNET

Graphical User
Interface (GUI)

Relational DataBase
Including:

- Earthquakes
- Faults
- Geophysical Anomalies
- Geomorphic Anomalies
- Paleoseismic Trench
- Images
- ....

Editing
Interface

Query
Interface

Visualization
Interface

(b)

DataBase Server
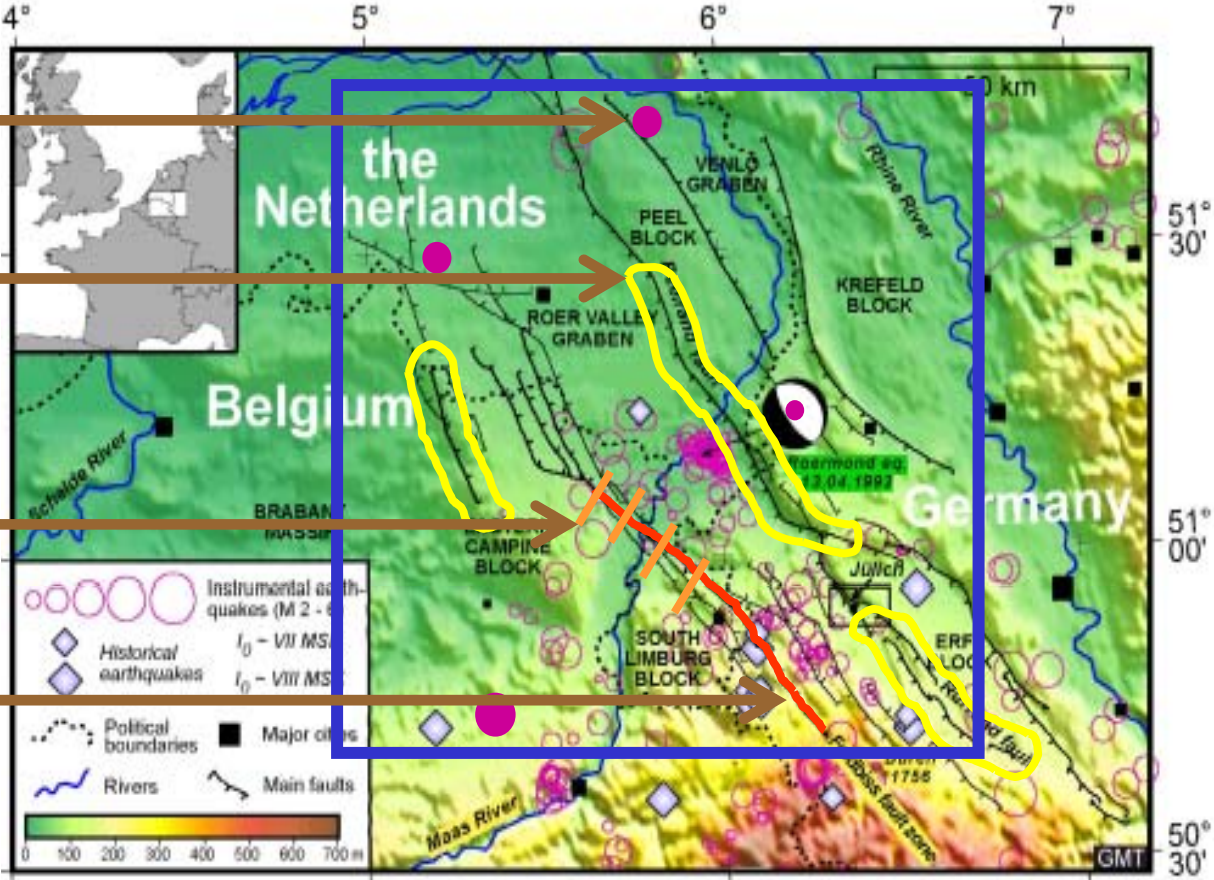2

Client 1

Client 2

DataBase Server
1

DataBase Server
3

Client 3

Figure 1

Figure 2

Figure 3

Figure 4a

Figure 4b

Figure 5